

0402699564





***Reprocessing of Tungsten Alloy Swarf by Oxidation
Reduction Pressing and Sintering***

By

Abdulsalam A. Alhazza

***A Doctoral Thesis Submitted In Partial Fulfilment of the Requirement
for the Award of the Doctor of Philosophy of
Loughborough University***

October 2009

© Abdulsalam A. Alhazza (2009)

Abstract

Tungsten and the tungsten alloy group materials have a wide range of uses extending from everyday ones, e.g. the coil of an incandescent lamp or the contact tip of an electrical switch or an automobile horn, to components of nuclear fusion reactors or ion drive motors in space probes. The reason for this range of uses lies in the many outstanding properties of tungsten, in particular its high melting point, low vapor pressure, high atomic number, good electrical and thermal conductivity.

In the Tungsten Oxygen system (W-O), there are not only the stoichiometric oxides WO_3 , $WO_{2.9}$, $WO_{2.7}$, WO_2 , but also non stoichiometric structures that represent the ordered or partially ordered defect structures of the oxygen-rich oxide, in which the central W atom is octahedrally surrounded by six oxygen atoms. In WO_3 , neighboring octahedra are in contact only at the corners. With increased oxygen deficiency (reduction, conversion to lower oxides), common edges and surfaces are progressively formed.

The aim of this work was to produce a homogeneous powder for recycling from "heavy metal swarf". The process route envisaged was a controlled oxidation, to breakdown the swarf. In the first step the microstructure of the swarf was to be characterized using optical metallography, Scanning electron microscope (SEM), and X-ray diffraction (XRD). This characterization was followed by the oxidation to achieve the mechanical breakdown and to give a friable oxide. In this step a Thermogravimetry (TG) was used to determine the temperatures for oxidation and to give some idea of the kinetics of the process. SEM and XRD were used to determine the morphology and the type of the oxide. According to the TG results, temperatures could be selected for oxide manufacture.

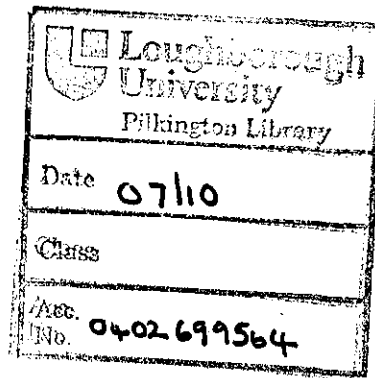
Different temperatures were used for oxidation processes which were determined from the TG oxidation curve. The oxidation process was run for different temperatures to achieve the best oxidation powder for subsequent reduction in further processing. A reduction by

Abstract

hydrogen was carried out for a selected oxide powder to produce a friable metal powder.

Time and temperature for the reduction process was determined and a characterization analysis was run to prove the fully reduced powder for the next pressing and sintering step.

Finally, pressing and sintering of the reduced powder was processed to complete the recycling procedure and to produce the final heavy metal alloy. The powder was pressed using a pressure instrument with a small metallic die to hold the powder. The final tungsten alloy pellet was sintered in a high temperature furnace to produce the final recycled metal. Furthermore, microscopic analysis of the recycled metal was characterized to compare the microstructure to the first heavy alloy.



Acknowledgements

This report would not have been possible without the help of God (Allah) and support of many people.

First and foremost, I would like to express my sincere and deepest gratitude to Prof. Nassehi for his dedicated and excellent supervision which includes the invaluable advice, discussion, co-operation, guidance and most of all for being very understanding for my situation as student and a father at the same time.

I would like to take this opportunity to show my appreciation and deep thanks to Prof. Wakeman who has been supportive and helpful. And also I would like to extend my thanks to all the staff in the Chemical Engineering and IPTME Departments for their help and support.

I also wish to extend my gratitude to the Kuwait Institute for Scientific Research, for granting me the scholarship to pursue my PhD.

I would also like to thank my parents and last but not least ,my deepest gratitude and indebted to my wife and my children who gave me the love, encouragement and support throughout the years of my study.

Table of Contents

Page

ABSTRACT	I
ACKNOWLEDGEMENTS	III
CHAPTER 1 INTRODUCTION	1
1.1 INTRODUCTION	2
1.2 RECYCLING	2
THERE ARE MANY METHODS USE IN RECYCLING PROCESSES:	5
1.3 OBJECTIVE	6
2 CHAPTER 2 LITERATURE REVIEW	8
2.1 INTRODUCTION	9
2.2 GEOLOGY OF TUNGSTEN ORE	10
2.3 TUNGSTEN COMPOSITE	10
2.4 TUNGSTEN HEAVY METAL ALLOY	11
2.5 PROPERTIES	12
2.2.1 Introduction	12
2.2.2 Mechanical Properties	14
2.2.3 Chemical Properties	14
2.6 IMPURITIES	15
2.7 TUNGSTEN REACTIONS	16
2.7.1 Reaction with non-metal Compound	16
2.7.2 Reaction with Metal Compound	17
2.8 OXIDATION /REDUCTION OF TUNGSTEN	18
2.8.1 Oxidation	18
2.5.2 Oxidation of Tungsten Metal Powder	18
2.8.3 Oxidation by air	19
2.8.4 Reaction of Tungsten with Water	19
2.8.5 Tungsten and Oxygen	21
2.8.6 Reduction of Tungsten Oxide by Hydrogen	23
2.8.7 The Reduction Sequence	24
2.8.8 Chemical Reaction	25
2.8.9 Reduction Mechanism	27
2.8.10 General reduction behaviour of Tungstates	28
2.8.11 Iron Tungstate	29
2.8.12 Cobalt Tungstate	30
2.8.13 Nickel Tungstate	32
2.8.14 Silver Tungstate	33
2.8.15 Copper tungstate	34
2.8.16 Nucleation and Crystal Growth	36
2.9 PRESSING AND SINTERING	37
2.9.1 Compacting	37
2.9.2 Sintering	38
2.9.3 Sintering Stages	41
2.10 ANNEALING OF W-ALLOY DURING PRESSING AND SINTERING	43
3 CHAPTER 3 APPARATUS & METHODOLOGY	44
3.1 INTRODUCTION	45
3.2 APPARATUS	45
3.2.1 Thermogravometry Analysis (TGA)	45
3.2.2 X-Ray Diffraction Analysis (XRD)	46

3.2.3 Scanning Electron Microscope (SEM).....	47
3.2.4 Carbolite Furnace	48
3.3 MATERIALS	48
3.3.1 W-Oxide	49
3.3.2 Tungsten Powder	49
3.3.3 Tungsten Pellet	51
3.4 METHODOLOGY	51
3.4.1 Experimental Procedure.....	51
3.4.2 Materials Characterisation	53
3.4.3 X-Ray Diffraction analysis	53
3.4.4 Scanning Electron Microscopy (SEM).....	53
3.4.5 Thermogravimetric Analysis (TGA).....	54
3.4.6 Furnace.....	54
3.4.7 Oxidation Experiments.....	54
3.4.8 Reduction Experiments	55
3.4.9 Pressing and Sintering	56
3.4.10 Microstructural Examination	57
4 CHAPTER 4 RESULTS AND DISCUSSION	58
4.1 INTRODUCTION	59
4.2 STARTING MATERIAL	59
4.3 OXIDATION PROCESS	64
4.3.1 TGA and Furnace.....	64
4.3.2 X-ray diffraction	79
4.3.3 Friability	83
4.4 REDUCTION PROCESS	83
4.4.1 Furnace.....	83
4.4.2 X-ray Diffraction	84
4.4.3 Scanning Electron Microscopy	87
4.4.4 Reduction Behaviour.....	87
4.5 PRESSING AND SINTERING	89
4.6 FAILURE ANALYSIS	92
5 CHAPTER 5 MATHEMATICAL CORRELATION AND MODELING	95
5.1 INTRODUCTION	96
5.2 Mathematical Correlation.....	96
6 CHAPTER 6 CONCLUSION AND RECOMMENDATIONS FOR FUTURE WORK ...	121
6.1 CONCLUSIONS	122
6.2 RECOMMENDATIONS FOR FUTURE WORK	124
REFERENCES	126

List of Figures

FIGURE 1: OPTICAL MICROGRAPH OF A 95 WT% TUNGSTEN HEAVY METAL ALLOY WITH 3.2 WT% NI AND 1.8 WT% CU (YIH AND WANG, 1979).....12

FIGURE 2: SURVEY OF TUNGSTEN-OXYGEN COMPOUND (LASSNER AND SCHUBERT, 1999).22

FIGURE 3 REDUCTION PATHS ASSOCIATED WITH THE REDUCTION OF PURE WO₃, MAIN TRANSITIONS ARE MARKED WITH THICKER LINES (SCHUBERT 1991).....26

FIGURE 4: CHEMICAL VAPOUR TRANSPORT OF TUNGSTEN VIA VOLATILE WO₂(OH)₂ (LASSNER AND SCHUBERT, 1999).....29

FIGURE 5 SHIMADZU TGA.....45

FIGURE 6 PHILIPS XRD.46

FIGURE 7 JEOL SEM JXA 3600.47

FIGURE 8 ELECTRIC FURNACE.48

FIGURE 9 THE STARTING MATERIAL (SWARF).....49

FIGURE 10 OXIDE POWDER AT 900°C.....50

FIGURE 11 TUNGSTEN POWDER AFTER REDUCTION OF THE W OXIDE ×200.....50

FIGURE 12 TUNGSTEN PELLET AFTER PRESSING AND SINTERING.51

FIGURE 13 SWARF MOUNTED AND POLISHED UP TO 6 MICRONS52

FIGURE 14 CERAMIC BOATS.....55

FIGURE 15 DRAPER PRESS AND 3.5 MM DIE.....57

FIGURE 16 TUNGSTEN ALLOY (SWARF).60

FIGURE 17 HEAVY METAL SWARF MATERIAL MAGNIFIED ×2020.....60

FIGURE 18 COMPOSITE MATERIAL CONTAIN 95.4% W.....61

FIGURE 19 ELONGATED GRAINS ×1010.61

FIGURE 20 EDS ANALYSIS OF THE GRAINS IN THE SWARF (STARTING MATERIAL).62

FIGURE 21 EDS ANALYSIS OF THE MATRIX IN THE SWARF (STARTING MATERIAL).63

FIGURE 22 XRD ANALYSIS FOR THE TUNGSTEN ALLOY SWARF (STARTING MATERIAL).64

FIGURE 23 OXIDATION OF TUNGSTEN ALLOY IN NATURAL AIR.66

FIGURE 24 OXIDATION OF TUNGSTEN ALLOY AT 750°C FOR 3 HRS.67

FIGURE 25 OXIDE POWDER AT 800°C.....69

FIGURE 26 OXIDE POWDER AT 850°C.....69

FIGURE 27 OXIDATION OF TUNGSTEN ALLOY AT 800°C FOR 3 HRS.71

FIGURE 28 OXIDATION OF TUNGSTEN ALLOY AT 850°C FOR 3 HRS.72

FIGURE 29 OXIDATION OF TUNGSTEN ALLOY AT 900°C FOR 3 HRS.76

FIGURE 30 OXIDATION OF TUNGSTEN ALLOY AT 950°C FOR 1.5 HRS.77

FIGURE 31 OXIDATION OF TUNGSTEN ALLOY AT 1000°C FOR 1 HRS.78

FIGURE 32 EDAX ANALYSIS FOR THE W-OXIDE AFTER OXIDATION AT 1000°C.....79

FIGURE 33 XRD ANALYSIS FOR THE TUNGSTEN OXIDE AT 900°C.....80

FIGURE 34 XRD FOR THE OXIDE AT 950°C.80

FIGURE 35 XRD ANALYSIS FOR THE OXIDE AT 1000°C81

FIGURE 36 SEM IMAGE FOR THE OXIDE AFTER OXIDATION AT 900°C.81

FIGURE 37 SEM IMAGE FOR THE OXIDE AFTER OXIDATION AT 950°C.....82

FIGURE 38 SEM IMAGE FOR THE OXIDE AFTER OXIDATION AT 1000°C.82

FIGURE 39 SEM IMAGE FOR THE OXIDE POWDER AT 1000°C.83

FIGURE 40 XRD FOR NOT FULLY REDUCED POWDER.....85

FIGURE 41 FULLY REDUCED POWDER.....86

FIGURE 42 EDS ANALYSIS FOR THE REDUCED POWDER.88

FIGURE 43 MICROGRAPH FOR THE COMPACTED PELLET ×1000.....90

Table of Content

FIGURE 44 MICROGRAPH FOR THE COMPACTED PELLET $\times 400$	90
FIGURE 45 ENLARGED GRAINS IN SOME REGION $\times 400$	91
FIGURE 46 EDS ANALYSIS FOR THE FINAL REDUCED PELLET.....	92
FIGURE 47 NOT FULLY OXIDIZED TUNGSTEN ALLOY.	93
FIGURE 48 NOT FULLY OXIDIZED TUNGSTEN ALLOY.	94
FIGURE 49 CURVE FIT FOR OXIDATION AT 750°C	97
FIGURE 50 CURVE FIT FOR OXIDATION AT 800°C	97
FIGURE 51 CURVE FIT FOR OXIDATION AT 850°C	98
FIGURE 52 CURVE FIT FOR OXIDATION AT 900°C	98
FIGURE 53 CURVE FIT FOR OXIDATION AT 950°C	99
FIGURE 54 CURVE FIT FOR OXIDATION AT 1000°C	99
FIGURE 55 C-FACTOR VS TEMPERATURE.	104
FIGURE 56 OXIDATION TIME VS TEMPERATURE.	105
FIGURE 57 MAX. MASS (MG) VS TEMPERATURE ($^{\circ}\text{C}$).	106
FIGURE 58 MASS (MG) VS TEMPERATURE ($^{\circ}\text{C}$).	106
FIGURE 59 C FACTOR (MG/MIN) VS TEMPERATURE ($^{\circ}\text{C}$).	107
FIGURE 60 OXIDATION TIME VS TEMPERATURE ($^{\circ}\text{C}$).	107
FIGURE 61 THREE DIMENSION CURVE FITTING FOR THE OXIDATION PROCESS.....	109
FIGURE 62 THE EXPERIMENTAL DATA FOR TUNGSTEN OXIDATION EXPRESSED AS PARABOLIC RATE	110
FIGURE 63 A SCHEMATIC DIAGRAM FOR SMALL PIECE OF TUNGSTEN	112
FIGURE 64 THE PARABOLIC RATE CONSTANT FOR TUNGSTEN OXIDATION	117
FIGURE 65 AN ARRHENIUS TYPE PLOT FOR DIFFUSION COEFFICIENTS FOR OXYGEN FOR TUNGSTEN CORROSION.....	119
FIGURE 66 DIFFUSION COEFFICIENT IN THE CORE AND PRODUCT LAYER VERSUS THE PARABOLIC RATE CONSTANT FOR TUNGSTEN	120

Chapter 1 Introduction

1.1 Introduction

Due to the brittle behaviour of tungsten metal and most of its alloys at room temperature, intense effort has been made to search for other means to better utilize the density and high temperature properties of the metal. The result is the emergence of a class of tungsten-based composites, which may be described as heavy alloys, infiltrated tungsten or other composites.

The term “Tungsten heavy metals” means two-phase tungsten alloys of the type W-Ni-Fe and W-Ni-Cu which contain tungsten grains within a transition metal alloy matrix. The density varies depending on tungsten content.

1.2 Recycling

Recycling is the processing of used materials into new products in order to prevent waste of potentially useful materials. In addition, it reduces the consumption of fresh raw materials, reduces energy usage, and reduces air and water pollution.

There are many kinds of recyclable materials, starting from ones used domestically like different kinds of glasses, paper, plastic, textiles, and electronics, ending with the big factories' waste like batteries, electronic components, steels, aluminum and different kinds of metals.

Materials recycling would produce a fresh supply of the same material, like the conversion of office paper to more office paper, or polystyrene to more polystyrene. However, this is often difficult or too expensive compared with producing the same product from raw materials. Another form of recycling is the extraction of certain materials from a group of products due to their hazardous nature or to their intrinsic value.

In the world, recycling facilities earn billions of pounds a year and growth has exceeded 7% per year in the past five years (from 2003 to 2008) (Organization for Economic co-operation

and Development, 2008).

The Technical University of Denmark conducted a study and found that in 83% of cases recycling is the most efficient method to dispose the household waste [‘The price of virtue’, *The Economist* (June 7, 2007), ‘The truth about recycling’, *The Economist* (June 7, 2007)].

Economic analysis of recycling has an important feasibility as cost and benefits, that’s includes reduce hazardous waste leaching from landfills, decreased air pollution and greenhouse gases from incineration, reduce energy consumption, and reduce waste and resource consumption, which leads to a reduction in environmentally damaging mining and timber activity. In the United Kingdom, the Waste and Resources Action Programme stated that Great Britain’s recycling efforts reduce CO₂ emissions by 10-15 million tonnes a year, while in the United State the Environmental Protection Agency (EPA) has concluded that the recycling effort reduce the countries carbon emission by a net 49 million metric tonnes in 2005 [*The Economist* (June 7, 2007)].

There are many different recyclable materials like concrete aggregate, batteries, clothing, glass, paper, plastic, textiles, timber, electronics, ferrous and non-ferrous metals, but each type requires a different recyclable technique.

Metal recycling is a £4.5 billion UK industry and employs over 8000 people, processing ferrous and non ferrous metal scrap into vital secondary raw material for the smelting of new metals.

All metals can be recycled into high quality new metal, and generally produces metals of equivalent quality, for example in steelmaking, copper and aluminium the recycling process uses the scrap metals as a major raw material.

Metal recycling supply major worldwide industry. Manufacturing of metals is one of the largest UK manufacturing sectors, employing many people, and contributing more value to the UK economy than motor and aerospace combined (Barbier, 1971).

The UK produces considerably more scrap than is required for domestic markets. In 2005, 13 million tonnes of metals was recycled in the UK. Around 40% of this was used in the UK, and the remaining 60% exported worldwide.

The worldwide market for ferrous scrap is predicted to continue its growth, and has averaged 5% per annum over the past 12 years. 4.6 million tonnes of iron and steel and stainless steel scrap were supplied to steelworks in the UK, and 0.9 million tonnes to UK foundries; 6.1 million tonnes was exported. The major export market was other Europe countries, and Asia, particularly India. Furthermore, over one million tonnes of non-ferrous metals was processed. Approximately 45% of this was aluminium, 31% copper, and significant quantities of nickel, brass, zinc, and lead. UK exports topped 800,000 tons of non ferrous metal in 2005 with Europe, China and India as the main destinations.

Recently, recycling is an important aspect in metal industry. One of the recent examples of metal recycling is the navy ship which was established in New York from the world trade centre wreck. 24 tons of scrap steel was melted down in a foundry in Amite, then it was poured into the molds on September 9, 2003 and launched in December 20, 2007, and has been called never forget.

A most important scrap recycling in most industrialized countries is scrap containing tungsten. The reason is that most tungsten ores contain less than 1wt% WO_3 and very seldom higher concentrations. It is evident that the least valuable scrap contains about 15 times more tungsten than an average ore.

Due to the low abundance of tungsten, which requires the mining of a huge ore tonnage to gain a small amount, it was always a valuable metal. Consequently, it is the high intrinsic value in anything containing tungsten which makes tungsten scrap an interesting and worthy material for reuse. Also, the tungsten world market was decisive in increasing the recycle percentage of the total tungsten production recently.

There are many methods use in recycling processes:

- 1- Hydrometallurgy: most tungsten scraps can be processed by this method. However, it is an expensive, high energy consuming and chemical waste producing procedure. The scrap must be oxidized by air, chemicals or electrical energy, in order to transfer tungsten to the hexavalent state, which is soluble in alkaline solution.
- 2- Melting metallurgy: Certain scrap materials are recyclable in this method. Super alloys, Menstruum WC, Stellites, and cast eutectic carbides require very pure scrap while, for steel products impure scrap can also be used. Furthermore, any tungsten processed by this method cannot be recycled again by other methods, with the exception of re-melting.
- 3- Direct recycling: supplied material is transformed to powder of the same composition by either chemical or physical treatment, or a combination of both. Consequently, the composition of the scrap must be the same as for the final product and it should offer the possibility of converting the scrap to a powder in a metallurgically acceptable form. Finally, the direct recycling is combined with a minimum of energy consumption, chemical waste, and lowest production cost.
- 4- Semi direct recycling: This method can be applied to the binary or ternary phase alloys. One component is dissolved chemically, leaving the other phases intact. The integrity of the structure is lowered by dissolution and the attrition can take place.

Finally, scrap should always kept as pure as possible, not only in regard to contamination by foreign materials, but also in regard to the grade of purity (Lassner and Schubert, 1999). In this research work the method used is the direct recycling due to the possible intensive advantages mentioned above.

The aim in this work is to break down the heavy metal swarf to an oxide powder, followed by a reduction process to return the actual metal in a powder form for subsequent pressing and sintering. In this work the recycling process aimed to complete in the lowest cost.

Consequently, the goal in the oxidation and reduction study is to find the shortest time and lowest possible temperature. Finally, at the end of the recycling process a heavy alloy metal is aimed to produce with a good metallic microstructure compared with the start material.

1.3 Objective

The main theme of this thesis is to understand and describe the recycling process of the heavy metal tungsten alloy 'swarf' taken from the machining waste. The specific objectives are as follows:

1. In the first step the aim is to break down the swarf to obtain a powder for further recycling process.
2. In the oxidation process the aim is to obtain the shortest oxidation time, the lowest possible oxidation temperature, and the best oxide product. The oxide powder obtained from oxidation process with lowest cost is the target in this stage.
3. After the oxidation process is completed, a mathematical equation is needed to find the relation between the time and weight and to support the experimental work.
4. In the reduction process the aim is to return the powder to its original material in powder form to be ready for pressing.
5. The reduction of tungsten alloy by hydrogen is a dangerous since the hydrogen is a highly flammable element. It is more safe to find another element to use in this work other than hydrogen.
6. The reduction process is an important stage in this work, the aim in this stage is to find the full reduction for the oxide powder and the best reduced powder to enhance the metallic property of the microstructure.

7. The final experimental stage in this work is pressing and sintering. In this stage the aim is to complete the recycle process and to produce a metal alloy with a metallic microstructure for further reuse.

8. The aim of optical examination for the final product is to find the differences between the first and final material and to study the microstructure for both materials.

2 Chapter **2** Literature Review

2.1 Introduction

Tungsten contains 74 protons in its nucleus and 84 to 116 neutrons. The electron configuration of the unexcited tungsten atom is defined by $4f^{14} 5d^4 6s^2$. The term symbol is 5D_0 , which means that the K, L, M, and N shells are complete while the O and P shells are incomplete. The neutral atom contains 74 electrons. The electron configuration, especially the $5d^4$ shell, is responsible for the typical tungsten-related physical and chemical properties.

Tungsten is a metastable phase and converts to α -tungsten when heated above 600 to 700°C. α -tungsten (body-centred cubic structure) forms at least partially during low temperature hydrogen reduction of tungsten oxides, tungsten bronze, or ammonium paratungstate. Several foreign elements, such as P, As, Al, and K, promote its formation and also have a stabilising effect at higher temperatures. Moreover, β -tungsten (body-centred cubic structure) forms during electrolytic reduction of WO_3 in phosphate metals and in thin films, produced by evaporation, sputtering, or chemical vapour deposition. γ -tungsten (face-centred cubic structure of the A1 type) is only found in thin, sputtered layers and amorphous tungsten at the very beginning of sputtering. γ -tungsten will transform to the α modification when heated above 700°C.

The density of tungsten is amongst the highest of all metals (Bailar et al., 1973) and is equal to that of gold. Measured densities of sintered materials may vary significantly, since the full density ($19.25 \text{ g}\cdot\text{cm}^{-3}$) is only achieved after heavy working.

The mechanical properties of tungsten are intrinsic only when a high percentage of single crystals is present. Polycrystalline tungsten is the most important form, and the majority of the metal used is of this form. The mechanical properties are also strongly influenced by two main factors: microstructure and the presence, concentration, and combination of

impurity elements.

The microstructure of a tungsten sample, which influences the mechanical properties over a wide range, depends on the type of preparation (powder metallurgy, arc cast, electron beam melted, zone refined, chemical vapour deposition) and the subsequent working (deformation, annealing, recrystallisation).

In the case of powder metallurgical processing (P/M tungsten), the crystal size and shape can be regulated by the sintering conditions, the type and degree of deformation, and the intermediate and final annealing processes. In this way, it becomes possible to produce material with the desired mechanical properties (Yih and Wang, 1979).

2.2 Geology of tungsten ore

Geological tungsten is divided into two main categories: Wolframite and Scheelite. Wolframite is a mixture of iron tungstate and manganese tungstate, whereas Scheelite consists of calcium tungstate (Barbier, 1971).

Wolframite occurs in monoclinic crystals and has a dark colour ranging from reddish brown to black, while Scheelite crystallisation is tetragonal, and is generally a whitish ore.

The most important deposits of Wolframite are mostly found in quartz veins. China holds approximately 77% of the world reserves, followed by the United States with only 5% (Barbier, 1971).

2.3 Tungsten Composite

Due to the outstanding thermal properties of tungsten metal, it is used for many

applications. However, there are some limitations, like sensitivity towards oxidation and poor workability. Two main alloying systems have been developed to improve the thermal and mechanical properties of tungsten metal.

The two alloys are summarised below:

1. A heavy metal alloy that depends on either tungsten, nickel, and iron (W-Ni-Fe) or tungsten, nickel, copper, and iron (W-Cu-Ni-Fe). These alloys are used in high density applications and when outstanding mechanical properties are required.

Tungsten copper and tungsten silver alloys (W-Cu and W-Ag), in which the good thermal and electrical conductivity of (copper and silver) are combined with high solidity and corrosion resistance of tungsten.

2.4 Tungsten Heavy Metal Alloy

As mentioned previously, the two-phase composite material exhibits a high density and a combination of strength and ductility. These two-phase materials (W-Ni-Fe and W-Ni-Cu) are called tungsten heavy metal alloys.

The alloying elements help the tungsten grains hold together to improve the workability of the alloy. These alloys exist in the range of 2-10 wt%. Figure 1 shows an optical micrograph of 95 wt% tungsten heavy metal alloy with 3.2 wt% nickel and 1.8 wt% copper. The graph shows spherical tungsten grains with diameters from 20 to 60 μm and a binder matrix containing about 20 wt% tungsten (Lassner and Schubert, 1999).

There is a wide range of uses for the heavy metal alloys. They are used as rigid tools for machining, as X-ray and γ -ray radiation shields, and for defence purposes.

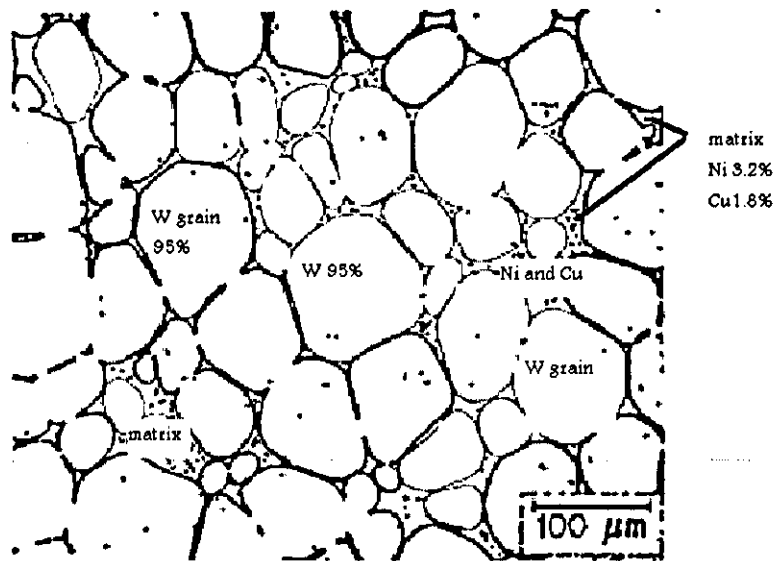


Figure 1: Optical micrograph of a 95 wt% tungsten heavy metal alloy with 3.2 wt% Ni and 1.8 wt% Cu (Yih and Wang, 1979).

2.5 Properties

2.2.1 Introduction

Mechanical properties are very sensitive to processing conditions, impurities, and microstructure. Problems with controlling porosity, impurities, and microstructural homogeneity are therefore common in heavy alloy fabrication. Residual sinter porosity and the formation of interface precipitates are the main reasons for inferior material properties. Ultimate tensile strengths (660-1350 MPa), yield strengths (565-300 MPa), and fracture elongations (5-30%) can vary widely (Cheney, 1984).

With increasing tungsten content, the contiguity (i.e., the W-W interfacial area as a fraction of the total interface area) of the tungsten grains increases, and both the strength and ductility decrease (Danninger and Lux, 1997). While the trend is most pronounced for

fracture elongation, the tensile strength exhibits a maximum at about 85 volume% W (93 wt%) before it significantly decreases. At 99 wt% W, the elongation is zero, and the tensile strength is about 400 MPa (German, 1992).

Besides their high density and the unique combination of high strength and ductility, there are other attributes that make heavy metals a versatile product:

- the high modulus of elasticity (much higher than that of steel),
- excellent vibration damping characteristics (for chatter-free heavy machining),
- good machinability,
- the high absorption ability for X-rays and γ -rays,
- good thermal and electrical conductivity,
- low electrical erosion and welding tendency,
- good corrosion resistance.

Research in tungsten heavy metal alloys has previously been boosted by its ballistic application as an anti-armour kinetic energy penetrator. Many papers and reviews on this have been published (Cai et al., 1995, Dowding et al. 1994, and Magness and Kapoor 1995). Although the basic requirements are the same for civil and defence applications (i.e., high density, strength, and elongation), there are two more important factors that must be considered for this specific application: the behaviour of the material under high strain rate conditions and their ballistic performance (i.e., their penetration ability).

In particular, the latter aspect (penetration ability) is of critical importance and is still a weak point of heavy metals. Their ballistic performance is inferior to that of depleted uranium, which is still used as a standard penetrator material (Cai et al, 1995). Nevertheless, recent environmental considerations have put a strong emphasis on substituting depleted uranium with heavy metals due to the radioactivity of the former. Efforts to improve the ballistic performance through proper processing and compositional modifications have failed (Cai et al, 1995, Dowding et al, 1995). Recent research has therefore focused on

alternative matrix alloys, such as tungsten-hafnium, tungsten-uranium composites (Cai et al, 1995, German and Chum, 1984), and heavy metal alloys with a speculating core of WC (Ekbohm et al, 1992).

2.2.2 Mechanical Properties

The outstanding mechanical properties of polycrystalline tungsten include its high strength and yield point at elevated temperatures and its high creep resistance. In addition, the indication of absolute values for the mechanical properties of polycrystalline tungsten is not appropriate as long as the related structure, structural history, type of impurity elements, their concentration, and distribution cannot be precisely defined. However, for technical samples, this is especially difficult, due to the high cost and time required for analysis.

2.2.3 Chemical Properties

Although the main properties of interest for tungsten applications are of a purely physical nature (for example, high melting point, high density, and low vapour pressure), the chemical properties are also of special importance because they determine and limit applications of the metal in diverse environments.

On the one hand, tungsten can be considered to be a rather inert metal that is resistant to many elements and compounds. It is compatible with most ceramics and glasses up to high temperatures and shows good resistance to many molten metals. Tungsten is stable in mineral acids at low temperatures and is only slightly attacked at higher temperatures. On the other hand, it reacts with numerous agents, as well as elements and chemical compounds. For example, at room temperature, it is strongly attacked by fluorine. Below 100°C, it dissolves in hydrofluoric-nitric acid mixtures and alkali solutions containing oxidising agents (Koch-Bienemann, 1989).

2.6 Impurities

Impurities in tungsten distribute randomly in the solid solution. A foreign element in the interstitial position (e.g., hydrogen, nitrogen, oxygen, silicon, or carbon) has a very low solubility in tungsten (less than 0.1 $\mu\text{g/g}$), which is between 100 to 1000 $\mu\text{g/g}$ at eutectic temperatures.

The foreign elements in tungsten are located at grain boundaries or within the crystals. When impurities melts during high temperature treatments, these elements improve the ductility and strength, while the concentration difference between the bulk and the atoms that are distributed to the grain boundaries weaken the grain boundary strength. In addition, the heavy working of tungsten forms low energy sites called dislocation tangles (Koch-Bienemann, 1989).

Analysis of the distribution of foreign elements in tungsten at low concentration requires complicated preparation and sophisticated equipment. More research work is needed to improve the knowledge in this field by using more advanced equipment.

Particles of foreign matter present in raw materials often combine within diffusion zones, causing voids. The size and concentration of these impurities play an important role in the mechanical properties. These impurities, located in the crystal lattice, can cause structural defects ranging in size from the order of atomic distances to several microns. In addition, the mechanical properties or ductility could be changed completely if a combination of impurities is present.

2.7 Tungsten Reactions

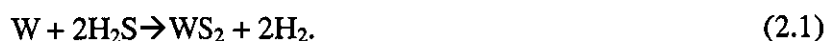
2.7.1 Reaction with non-metal Compound

The reaction of tungsten with non-metal compounds occurs mainly by oxidation. The oxidation of tungsten by water starts at room temperature and accelerates at higher temperatures up to 2000°C. The reaction depends on the ratio of tungsten and oxygen (O:W) and the partial pressure ratio (p_{H_2O}/p_{H_2}). The presence of hydrogen (H_2) indicates a reaction product. The volatility of tungsten oxides increases in water by the formation of the volatile oxide hydrate $WO_2(OH)_2$ (Rieck, 1967).

Tungsten is an efficient catalyst for both the synthesis and decomposition of ammonia. At elevated temperatures, partial or complete dissociation of NH_3 occurs, and hydrogen and nitrogen are released in the gas phase. Nitrogen oxides (N_2O , NO , and NO_2) form tungsten oxides at high temperatures and release nitrogen during oxidation reactions.

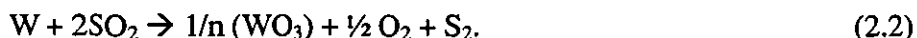
The reaction of tungsten powder with different non-metal compounds varies according to the compound and temperature. Tungsten powder reacts only slightly with hydrogen fluoride (HF) at 300°C, and the reaction product is undefined. Up to 600°C, there is little corrosion. The oxidic passivation layer on tungsten converts into low-valent, non-volatile fluoride, which protects the surface. At higher temperatures, they disproportionately form volatile fluorides, and the corrosion rate is markedly increased.

Hydrogen sulphide (H_2S) reacts with tungsten powder at 350-500°C according to the following equation:

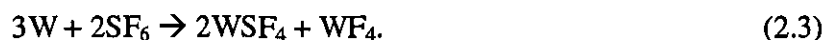


At low temperatures, the hexagonal modification forms.

Sulphur oxide (SO₂) reacts with tungsten and behaves as an oxidant to form sulphur during the following reaction:



For sulphur hexafluoride (SF₆), the reaction occurs at temperatures between 500-700°C, and WSF₄ and tungsten tetrafluoride are formed:

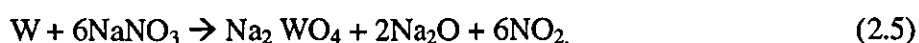
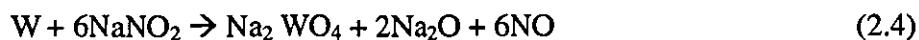


2.7.2 Reaction with Metal Compound

The alkali hydroxide metal compounds do not attack tungsten as long as all oxidising material (including air) is excluded. Any oxidic material on the tungsten metal surface will be dissolved. The presence of oxidising agents like nitrates, nitrites, chlorates, etc. leads to a vigorous attack.

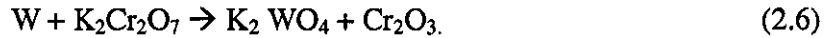
The reaction of tungsten with metal compounds occurs only in the presence of oxidising materials and oxidising agents such as nitrates, nitrites, and chlorates.

The hydroxide metals attack tungsten aggressively, and the metal dissolves. The dissociation of tungsten scrap in a mixture of sodium hydroxide (NaOH) with sodium nitrate (NaNO₂) or sodium nitride (NaNO₃) has been used for different purposes. The reaction occurs according to the following equations:



A mixture of 20-90% W with potassium dichromate burns easily at temperatures from 650 to

660°C, and little change in weight is detected:



No reaction of uranium dioxide (UO₂) with tungsten occurs, even at high temperatures, where the oxide reacts with tungsten around the grain boundaries. Other compounds react with tungsten at different temperatures in different ways (Wittenauer et al., 1992).

2.8 Oxidation /Reduction of Tungsten

2.8.1 Oxidation

X-ray photoelectron spectroscopy (XPS) analysis shows that the oxidation process of tungsten metal starts at room temperature and increases with high temperatures. The oxidation rate increases rapidly with increasing humidity and above 200°C. The oxide formed is always tungsten trioxide (WO₃) (Warren et al., 1996).

The formation of WO₃ starts at 750°C, and above 900°C, it becomes substantial. At very high temperatures (above 1300°C), WO₃ formation follows the linear oxidation rate, and the surface remains free of oxide (Ong and Fassel 1962).

The reaction rate is highly affected by the oxygen pressure at high temperatures, and tungsten is fully oxidised between 700°C and 1300°C. Increasing the temperature to 1817°C with a low oxygen partial pressure causes WO₂ to form faster than WO₃. Above 2227°C, metal volatilisation occurs.

2.5.2 Oxidation of Tungsten Metal Powder

The reaction of tungsten powder depends on the grain size and the preparation method

employed. Tungsten powder, with an average grain size $> 1 \mu\text{m}$, reacts like bulk tungsten. Finer powders can be pyrophoric. Tungsten powder that is reduced by hydrogen at low temperatures from tungstic acid-derived WO_3 contains large concentrations of $\beta\text{-W}$ and burns spontaneously when in contact with air. If such a powder is saturated by an inert gas containing only a low concentration of oxygen, it is no longer pyrophoric. It is assumed that a high density of lattice defects is responsible for the pyrophoricity.

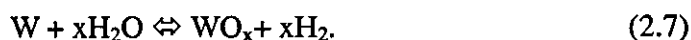
2.8.3 Oxidation by air

Oxygen is adsorbed on clean tungsten surfaces in a variety of atomic and molecular states. It is adsorbed molecularly at low temperatures ($<0^\circ\text{C}$), but at room temperature, this adsorption is a precursor state to atomic adsorption. A covered surface shows an ordered oxygen superstructure. If the temperature is increased, a more extensive coverage occurs and oxide-like structures are formed. The surface layer can be described as adsorbed oxide (Schmidbaur, 1987, Yih and Wang, 1979, Warren et al, 1996).

Oxygen diffuses from the surface into the crystal lattice forming a bcc (α) solid solution. The solubility is very low. Calculated diffusion coefficients at 1700°C are given as 10^{-7} and 3×10^{-8} to $5 \times 10^{-8} \text{ cm}^2 \text{ s}^{-1}$ for polycrystalline tungsten (Lee, 1964 and Aitken et al., 1967) and 7×10^{-8} to $5 \times 10^{-8} \text{ cm}^2 \text{ s}^{-1}$ for monocrystalline tungsten (Lee, 1964).

2.8.4 Reaction of Tungsten with Water

Tungsten reacts with water below the boiling point according to the following equation:



XPS analysis shows that the reaction of tungsten with water forms WO_2 , WO_3 , and oxide hydrate, where water acts as an oxidising agent (Warren et al., 1996):

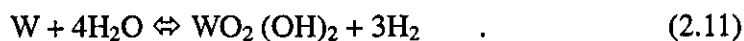


The corrosion rate of tungsten in water is 3.8 μg of tungsten per m^2 per hour at 38°C. An oxide film is formed slowly on the tungsten surface during the reaction. The corrosion rate increases with higher temperature and pressure; at 150-360°C and 70-80 atm, the corrosion rate is 1.6 g of tungsten per m^2 per hour.

The reaction of tungsten with water vapour or humid air (60-95% relative humidity) leads to the formation of WO_3 . The reaction depends on temperature and the partial pressure ratio of $\text{PH}_2\text{O}/\text{PH}_2$. An oxide layer is formed. The thickness of the oxide layer increases with increasing humidity, and the increase is more rapid than in liquid water. The reaction starts at the surface, where the water molecules are adsorbed and dissociate. The oxygen atoms diffuse into the tungsten grain, forming tungsten oxide, and the hydrogen escapes as an element.

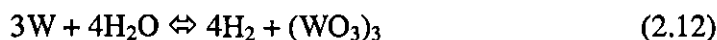
The formation of tungsten oxide depends on temperature and the partial pressure ratio $\text{PH}_2\text{O}/\text{PH}_2$. At low concentrations, WO_2 is formed. At higher concentrations, higher oxides form: $\text{WO}_{2.72}$, $\text{WO}_{2.9}$, and WO_3 .

An earlier study on the tungsten-oxygen system by Pierre et al. showed that above 600°C, gaseous $\text{WO}_3 \cdot \text{H}_2\text{O} = \text{WO}_2(\text{OH})_2$ is the most volatile compound formed in the W-O-H system. This compound is responsible for all processes of vapour phase transport at that temperature:



At high temperatures, tungsten filament reacts with water between 1307°C and 2927°C, and

the following oxides form: WO, WO₂, WO₃, (WO₃)₂, (WO₃)₃, and (WO₃)₄ (Yuehui et al., 2003). Above 2250°C, the water molecules dissociate and the oxygen reacts with the tungsten. Between 2200-3200°C, the trimetric and quadratic series form according to the following equations:



These reactions with water show the oxidation of tungsten when in contact with water at high temperatures. This reaction could be very destructive to the metal at high temperatures, especially because tungsten is used for heaters and cathodes in high temperature applications and as a filament in incandescent lamps. The water could increase the burning or corrosion of the metal (Schmidbaur, 1987).

2.8.5 Tungsten and Oxygen

A survey of tungsten-oxygen compounds published by Lassner and Schubert, 1999 is shown in Figure 2. The survey shows the stable stoichiometric binary oxides (WO₃, WO_{2.9}, WO_{2.72}, and WO₂), and the stoichiometric tungstates and acids. Additionally, nonstoichiometric, fully oxidised, and reduced compounds are presented.

The tungsten-oxygen bonding behaves differently in each compound. When the compound is fully oxidised, the tungsten atoms are situated at the centre of octahedrons and are surrounded by six oxygen atoms arranged at the corners to form WO₆.

In the reduction process, the octahedron becomes more complicated and the oxygen atoms are situated at the corner and face-sharing edges. The loss of each oxygen atom from the oxide lattice leads to the addition of two electrons to the conduction band.

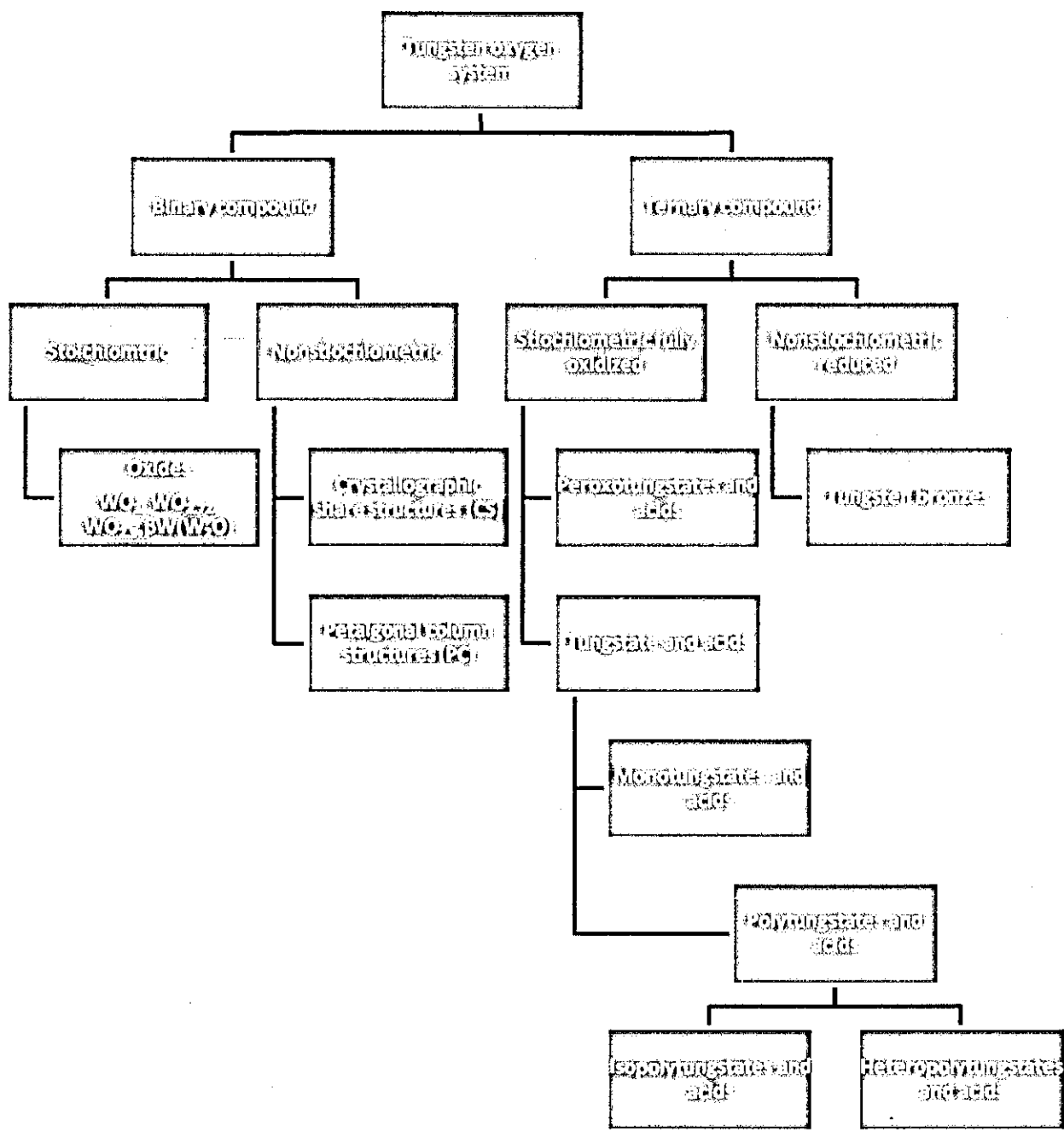


Figure 2: Survey of tungsten-oxygen compound (Lassner and Schubert, 1999).

Within the fully oxidised compounds, which are also called tungstates, the tetrahedral WO_4 and the pentagonal bipyramid WO_7 are also found beside the octahedral in the reduced compound.

Much is known about ternary and quaternary tungsten oxides. Some have been described in the literature, and some can be found in relevant compilations (Ekstrom and Tilley, 1980; Haase et al, 1979 and 1984; Yih and Wang, 1979). The crystal chemistry of tungsten is one of the most complex and richest fields in structural chemistry, where many compounds can be formed with a large combination of elements (Parsons, 1965. Yih and Wang, 1979. Mullendore, 1989. Haase et al, 1979).

2.8.6 Reduction of Tungsten Oxide by Hydrogen

This reaction works in the direction opposite to the reaction of tungsten with water. In this reaction, hydrogen is the reducing agent, and is usually applied in excess; accordingly, the partial pressure is higher. Haubner et al. (1983) showed that the hydrogen reduction of tungsten powder produced from tungsten oxides proceeds according to the following equation:



In the reduction of tungsten oxides by hydrogen at temperatures between 600 to 1100°C, tungsten blue oxide (WO_{3-x}), tungstic acid (H_2WO_4), and tungsten trioxide (WO_3) can be used as starting materials.

The chemical reaction in the reduction process is a combination of chemical vapour transport (CVT) and a chemical conversion to tungsten metal. This combination is responsible for the final powder properties. The reduction process can regulate the powder properties by changing the reduction parameters. The powder properties, such as the

average grain size, grain shape, and grain distribution, are very important in the final tungsten metal processed.

During the reduction process and chemical vapour transport (CVT), some of the trace impurities present in the oxide may evaporate, which cleans the tungsten powder of some trace impurities. Additionally, a foreign phase can be present during the CVT growth of tungsten, leading to its inclusion in the tungsten powder particles. This process plays an important role in the production of “non-sag” tungsten wire used for incandescent lamps (Schubert, 1991).

Basu and Sale (1979) reduced blue tungsten oxide in controlled H₂-H₂O atmospheres at different temperatures. They found that the reduction of some oxides (e.g., W₁₈O₄₉) proceeded more rapidly than that of blue oxide under the same experimental conditions.

The reduction of WO₃ to W, as described by the simple equation:



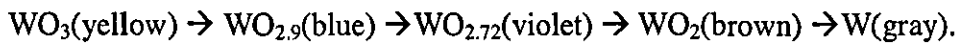
is in reality a rather complex process. Parsons (1965) conducted some research to describe the relation between density, diffusion, temperature, and time in the reduction process using a theoretical model equation. Industrially, this model is not used due to the complexity of the parameter interactions. The reduction process is still based on basic aspects and some experimental methods in the industry.

2.8.7 The Reduction Sequence

The reduction process depends on several parameters such as temperature, time, and humidity. Consequently, any increase in the layer height will result in an increase in the diffusion resistance and an increase in reduction time (“transport control reaction”). The fast reduction

process from tungsten trioxide to tungsten is diminished when the layer height is increased, due to the humidity increase in the layer.

A number of stable oxide stages form during this stage:



During the hydrogen reduction of pure tungsten oxide (WO), oxygen reacts thermally with hydrogen to form water. The water reduction curve can be represented in four steps according to the reduction process procedure.

The lengthening of the reduction time caused by increasing the oxide layer can be helpful in chemical- and transport-controlled processes (Haubner et al., 1983).

2.8.8 Chemical Reaction

At low reduction temperatures (500-750°C), the reduction of tungsten oxide is controlled by reducing the powder layer (less than 1 mm) and increasing the hydrogen flow (i.e., optimal material exchange). Under these conditions, the formation of α -W or β -W metals can be observed:



Furthermore, different phases of powder layers can occur simultaneously during low temperature reduction. These layers indicate differences in the oxygen partial pressure (humidity) within the reacting particles, as well as the nucleation and growth rates of the different phases.

The reduction sequence given in Figure 3 is the experimentally proven reduction path

associated with the reduction of pure WO_3 ; the main transitions are marked with thicker connected lines (Schubert, 1991)

The formation of metastable β -W from $WO_{2.9}$ and $WO_{2.72}$ and that of α -W from WO_2 during low temperature reduction indicate that the structural relationships between the individual phases are important in the formation of the final metal phase

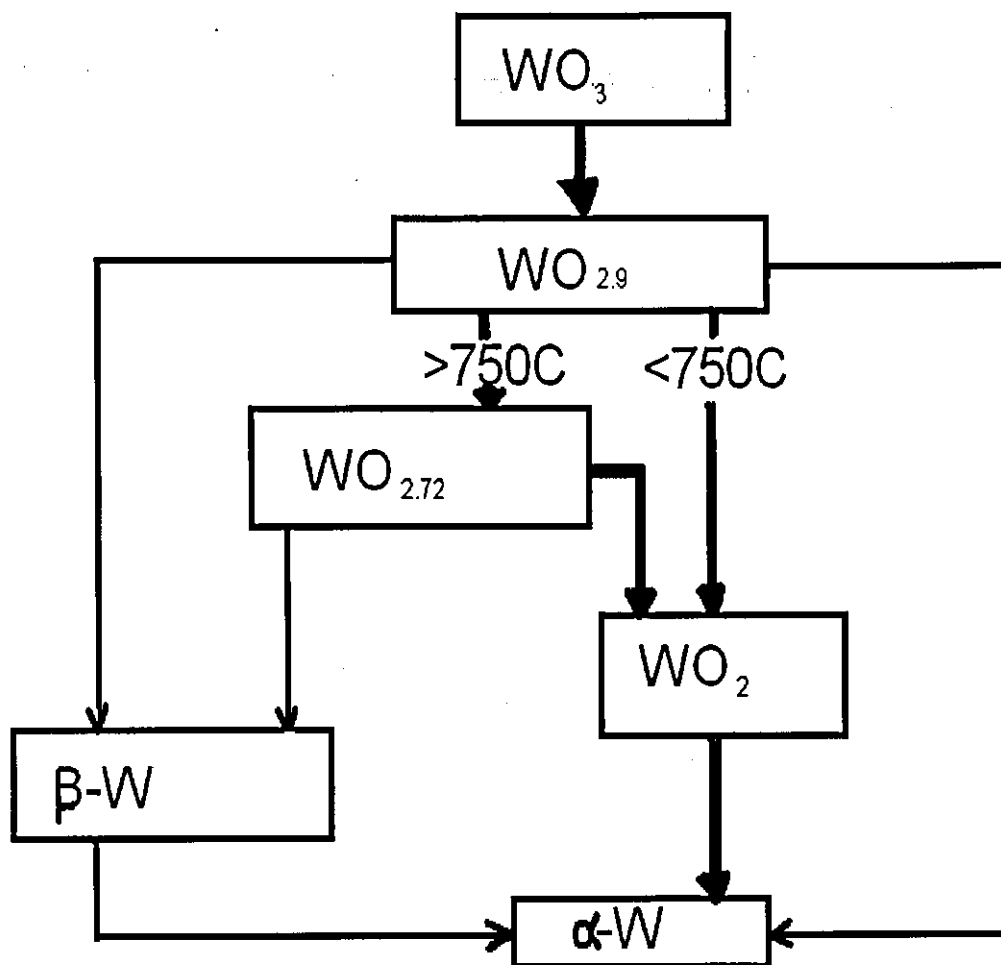


Figure 3 Reduction paths associated with the reduction of pure WO_3 , main transitions are marked with thicker lines (Schubert 1991).

2.8.9 Reduction Mechanism

There are two fundamentally different reduction mechanisms that can be postulated for the reduction process:

1- Diffusion in the solid state (oxygen transport)

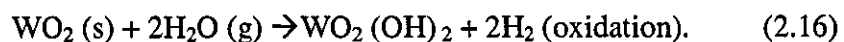
The basic mechanism in this reduction process is known. The reduction starts by direct oxygen removal from the solid oxide and varies for different phase transitions. At the end of the process, the metal powder forms a polycrystalline structure.

These reactions mainly occur at low reduction temperatures between 500- 750°C and are characteristic for the first oxidation process $WO_3 \rightarrow WO_{2.9}$ transition ("crystallographic shear" transition).

2- Chemical vapour transport (CVT) (tungsten transport)

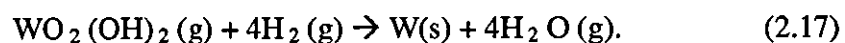
The basic mechanism is the transfer of tungsten via the volatile $WO_2(OH)_2$, which is separated into three sequential stages:

Stage 1 Reaction of the oxide surface with water vapour to form a volatile oxide hydrate:



Stage 2: Transport of $WO_2(OH)_2$ from the higher to the lower oxide (respectively, to W metal).

Stage 3: Reduction of the volatile $WO_2(OH)_2$ at the surface of the growing oxide (respectively, to W metal)



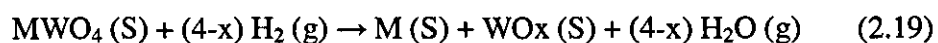
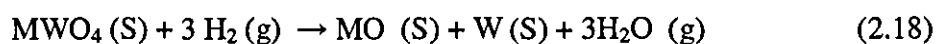
All phase nucleation processes and grain growth in this reduction stage are governed by the solid state reactions. Equation 2.17 shows an important example of this phase mechanism where α -W grains are formed from the WO_2 matrix in the presence of temperature and humidity during the reduction sequence (Hellmer et al., 1985).

In the reduction process using CVT, the reduction sequence can be controlled to modify the morphology of the intermediate and final reduction products.

During the reduction, the oxide reacts with water to form $WO_2(OH)_2$. The reaction of WO_2 with water vapour at high pressure builds $WO_2(OH)_2$ during the formation of α -W. The difference in the vapour pressure enables the driving force for CTV of tungsten to oxidise the WO_2 to form $WO_2(OH)_2$ and to reduce the phase $WO_2(OH)_2$ to form tungsten metal. This CVT process is shown schematically in Figure 4 for the $WO_2 \rightarrow W$ transition.

2.8.10 General reduction behaviour of Tungstates

The reduction behaviours of various bivalent metal tungstates with H_2/H_2O gas mixtures up to a temperature of $1100^\circ C$ were studied by Basu and Sale (1978). They concluded that the reduction process might be classified into two types:



In the first type, metal tungstate is reduced to form a metal oxide and tungsten. In the second type, the metal is formed along with a tungsten oxide in the initial stages of reduction, and then the tungsten oxide is subsequently reduced to tungsten as the reduction proceeds. A mixture of tungsten and alloy or tungsten alloy and tungsten oxides is produced when an intermediate behaviour between these two extremes occurs.

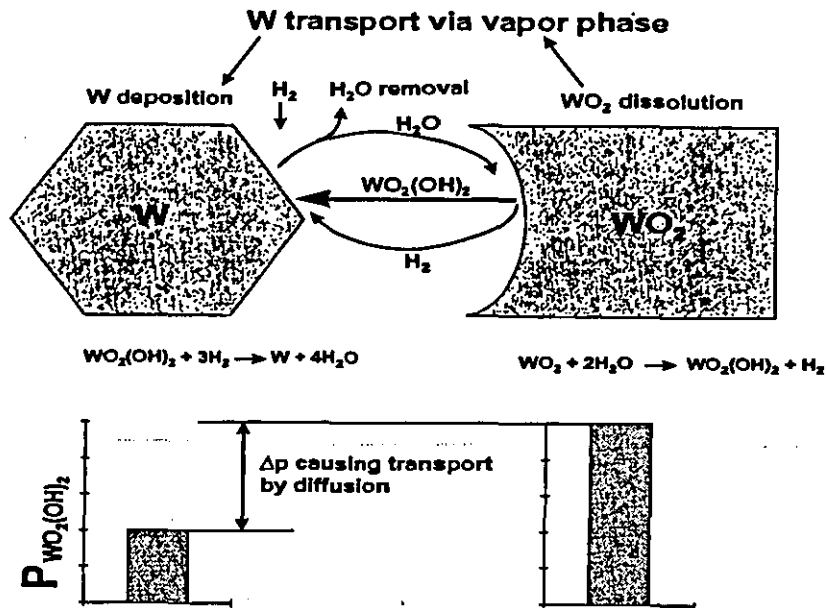


Figure 4: Chemical vapour transport of tungsten via volatile $WO_2(OH)_2$ (Lassner and Schubert, 1999).

Metals such as magnesium, strontium, barium, and manganese that have a high affinity for oxygen behave according to one extreme, while metals such as copper, cadmium, and lead that have a low affinity for oxygen behave according to the opposite extreme. Other metals, such as iron, cobalt, and nickel, are found to behave in an intermediate manner between the two extremes. These tungstates produce mixtures of tungsten alloys via their reduction.

2.8.11 Iron Tungstate

A series of iron tungstate salts occur as the minerals ferberite, hubnirite and wolframite. By fusing a mixture of ferrous oxide with tungsten trioxide between 480°C and 700°C, ferrous tungstate, ($FeWO_4$), may be produced whereas when a mixture of sodium tungstate and ferrous chloride (1:2:2) is fused monoclinic crystals of artificial ferberite are formed. The trihydrate, $FeWO_4 \cdot 3H_2O$, may be obtained as a light brown powder by adding a solution of ferrous salt to one of sodium tungstate.

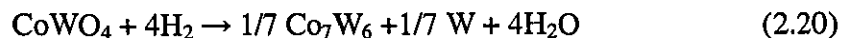
Trihydrate is dissolved by boiling acids, with separation of tungsten trioxide. (Li and Wang, 1955). However, it is not dissolved by cold hydrochloric, sulphuric or nitric acid and not soluble in water.

Basu and Sale (1978) noticed that ferrous tungstate crystallized with wolframite structure and suggested that FeWO_4 shows intermediate reduction behaviour which eventually produces a mixture of tungsten and tungsten alloys.

Gellar et al (1977) studied the Fe-O-W system they found that in the data of their XRD study the intermetallic compound between Fe-W were hard to interpret because only weak reflections were observed. However they showed that the intermetallic phase Fe_2W is homogenous from 66.66 %Fe – 33.33%W to 63.5%Fe – 36.5%W. A phase Fe_3W_2 is homogenous from 57.5 to 58.0%Fe and actually has the mean composition Fe_{11}W_8 . Furthermore, Fe was found to be soluble in W up to 2% and W in Fe up to 2%.

2.8.12 Cobalt Tungstate

Reduction of cobalt tungstate (CoWO_4) by hydrogen gas has been studied by Basu and Sale (1978) in the temperature range 900°C to 1100°C. He found that the reduction of CoWO_4 behaves in an intermediate manner between the two extreme behaviours discussed previously, and followed the equation:

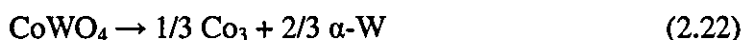


Later work by Bracconi and Dufour (1976) and Halliday (1979) has confirmed this observation. Bracconi and Dufour (1976), studied the reaction of CoWO_4 over the temperature range 440-1100°C, also found that the reduction mechanism varies with temperature, i.e.

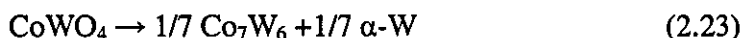
at 425-550°C:



at 700-800°C:



above 800°C:



It was found that at low temperature (below 550°C), the intermediate phase $\text{CoW}_{2.5}\text{O}$ formed first along with $\beta\text{-W}$. This intermediate phase was then reduced to form an amorphous ϕ phase, which did not give an X-ray diffraction pattern. Co_3W only began to crystallize at a substantial rate from this phase to temperature above 700°C. By this temperature all β -tungsten had transformed to α -tungsten. The Co_7W_6 phase was found to form only by reaction of Co_3W and α -tungsten at temperatures in excess of 800°C.

French and Sale (1985) also studied the reduction of CoWO_4 with hydrogen and found that the reduction process occurred via the formation of an amorphous phase which contains cobalt, tungsten and oxygen. The amorphous phase becomes unstable at low oxygen potentials and (depending on the degree of cobalt enrichment of the amorphous phase) precipitate either, or both Co_3W and Co_7W_6 . Furthermore, they studied the XRD analysis of the product obtained at various times and temperatures of the reaction and did not detect any cobalt-containing phase (other than residual CoWO_4) until greater than 50% reduction had occurred.

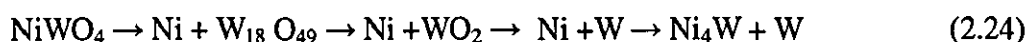
However, after very short reduction periods, β or α -tungsten were detected in the product, with a commensurate decrease in the amount of CoWO_4 present. This observation was explained such that it appears that cobalt is either retained in a non-crystalline amorphous phase or it is disappeared in such a fine particle that it does not produce a diffraction pattern. They found that Co_3W is produced at low temperatures whereas at higher temperatures the amount of Co_3W decreased as the amount of Co_7W_6 increased. They also

found that Co_7W_6 and α -tungsten are the only reaction products identified by XRD at temperatures greater than 800°C .

2.8.13 Nickel Tungstate

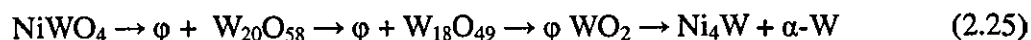
The reduction of nickel tungstate NiWO_4 has been studied by Basu and Sale (1978). He found that nickel tungstate behaves in a complicated manner at temperatures in the range of 900 - 1100°C . This first stage of the reduction process was found to produce a mixture of nickel and $\text{WO}_{2.72}$. Subsequent reduction was found to lead to the formation of WO_2 and ultimately tungsten metal which then reacted with the nickel to form an alloy based on the formula Ni_4W .

Furthermore, he found that at 700°C , Ni and $\text{W}_{18}\text{O}_{49}$ reduced successively into WO_2 and W. Then W combined with metallic nickel to form the intermetallic compound Ni_4W , i.e.



Weber and Egli (1981) established a phase diagram for the NiO-WO_3 system and gave the presence of only one ternary compound NiWO_4 , which melts at 1420°C .

Albiston and Sale (1986) studied the reduction behaviour of NiWO_4 in dry hydrogen over the temperature 200 - 900°C . They found that the reduction behaviour was similar to that of cobalt tungstate which was studied by French and Sale (1985). They found the full sequence of reduction was obtained at 700°C and above this their XRD results showed the formation of the intermetallic compound in the final reduction product, i.e. at 600 - 900°C



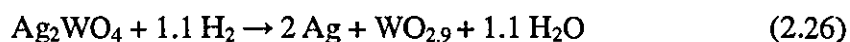
(They used ϕ to represent an amorphous nickel-containing phase).

2.8.14 Silver Tungstate

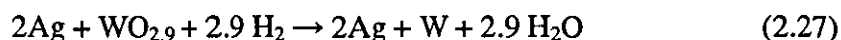
Silver tungsten alloys are not found to exist in the ternary silver tungsten-oxygen system, because silver and tungsten have no mutual solubility in the molten and solid state (Hansen, 1958). However, only one stable ternary compound is known to exist, based on the formula Ag_2WO_4 , while the binary W-O and Ag-O systems are both known to contain stable oxides.

Lassner and Schubert (1999) studied the reduction behaviour of Ag_2WO_4 in controlled CO/CO_2 gas mixtures and found that tungsten is first reduced to give metallic silver and tungsten oxide which could be reduced to tungsten metal. This reduction behaviour is identical to that copper tungstate.

Walkden and Sale (1982) studied the preparation and hydrogen reduction of silver tungstate. The reduction mechanism at 500°C can be summarized as :



Followed by



They found that β -tungsten was present in the fully reduced powder at temperatures above 500°C , whilst at 600°C and above silver and α -tungsten were produced. The rate of reduction was found to double approximately for every hundred degree rise in reduction temperature from 500 to 900°C .

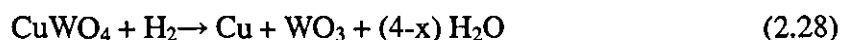
Walkden and Sale (1982) showed that the morphologies of reduced powders changed with

increase in reduction temperature from 500 to 900°C. At low temperatures, with the resultant low rates of reduction, gross segregation of phases was found in the totally reduced powders, which consisted of agglomerates giving silver rich areas and tungsten rich interiors of very fine particles. If these materials were held for longer periods of time at these temperatures, the silver rich cluster were seen to densify in order to produce large silver particles.

At high temperatures little segregation of phases was observed and gross sintering of silver was absent as reduction was very rapid. A two stage reduction process was devised to minimize segregation whilst still obtaining fine tungsten particles. The first stage was carried out at 300°C such that the silver tungstate was allowed to reduce metallic silver and $WO_{2.9}$ in order to reduce the migration and segregation of the silver. In the second stage a high temperature reduction process in the region 700°C to 900°C was carried out such that tungsten oxide reduced quickly and gave little time for coalescence of the silver phase.

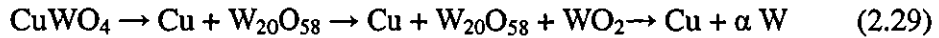
2.8.15 Copper tungstate

Basu and Sale (1978) suggested that the reduction of copper in dry H_2 tungstate proceed initially according to:



The reaction then proceeds by the reduction of the WO_3 . A more detailed investigation was conducted by Basu and Sale (1978). In this study the reduction of $CuWO_4$ in hydrogen, in the temperature range 500 to 700°C was investigated. This work supports Basu and Sale (1978) and gives a more detailed account of both the kinetics and mechanisms of reduction.

At 500°C the following reduction sequence was observed:



The detection of WO_2 in this sequence was not in agreement with other work on the reduction of WO_3 at those temperatures and may be the result of the presence of H_2O from the dehydration of tungstate.

At 700°C the reduction of CuWO_4 was shown to be



Where it is evident that the immiscibility of the two elements allowed the reduction of copper tungstate to be the same as the reduction of WO_3 one the metallic copper has been liberated.

During later work, Basu and Sale (1979) investigated the reduction of copper tungstate in the $\text{H}/\text{H}_2\text{O}$ gas mixtures. They observed several important features in the reduction of copper tungstate. Firstly, it was observed that widely varying morphologies could be obtained by controlling $\text{H}/\text{H}_2\text{O}$ ratio in the reducing gas and these could lead to the production of various copper tungsten powders of usual morphologies for the ultimate manufacture of Cu-W electrical contact. Secondly, they also noticed that the copper particles in the final powders were of deferent sizes. At low temperatures a large proportion of the metallic copper particles sintered together to produce a large globules, whilst the tungsten remained in the finally disseminated form. As the temperatures of reduction was increased the copper particle size appeared to be reduced, presumably due to the much shorter reduction times. Consequently, Basu and Sale (1979) concluded that in order to produce a fine dispersion of the two phases as short as possible reduction period is required.

2.8.16 Nucleation and Crystal Growth

During the reduction process when a new phase forms, the first step is phase nucleation. If the structure of the new phase does not match the host matrix, phase nucleation problems can occur (incoherent nucleation). The formation of W from WO_2 is a good example for this aspect. When WO_2 is reduced by wet hydrogen, the reaction comes to a standstill at comparatively low humidity.

Although from a thermodynamic point of view the reaction should proceed even at much higher humidity, under these wet conditions no W nucleation takes place. However, tungsten growth by CVT is possible, which can be demonstrated by adding nucleation aids, such as metallic tungsten. In this case, a slow further overall reduction occurs, but the W is deposited mainly on already present W particles. Similar reactions take place on the walls of the reduction boats, where W is readily deposited on the wall surface.

The strong influence of the humidity on the nucleation rate of the metal has an important consequence for the technical process. Besides the reduction temperature, it is the dynamic humidity within the layer which determines the nucleation and growth conditions. The lower the humidity during the $\text{WO}_2 \rightarrow \text{W}$ transition (i.e. the lower the powder layer and the closer to the top of the layer), the higher the nucleation rate and hence the lower the growth of the individual grains, resulting in smaller average grain sizes. The reverse is true for high humidity, where only few nuclei form, leading to a coarse powder.

Due to the varying growth conditions for the individual particles the powder always exhibits a certain grain size distribution. Grain growth of the metal occurs by CVT through the formation of $\text{WO}_2(\text{OH})_2$.

2.9 Pressing and Sintering

2.9.1 Compacting

There are two main routes for tungsten powder to be consolidated into a compact: pressing in rigid dies (uniaxial pressing) and isostatic pressing in flexible moulds (compaction under hydrostatic pressure). Other techniques, such as powder rolling, cold extrusion, explosive compaction, slip casting, vibratory compaction, or metal injection moulding, have gained no industrial importance.

Due to its relatively high hardness and difficult deformation tungsten powder is not easy to compact. Nevertheless, in most cases compaction is performed without lubricant to avoid any contamination by the additive. The resulting compacts are generally sufficiently strong so that they can be handled without breaking. For machining the part, it must be pre-sintered beforehand (Koch-Beinemann et al., 1989).

Pressing of powders in rigid dies is carried out either in mechanical or hydraulic presses. The pressure is applied from the top, or from the top and bottom (double action presses). Die and punches are made of high-speed tool steel or (more rarely) hard metal. Mechanical presses (pressing forces up to 1 MN) are used for small parts and high production rates. They allow a higher degree of dimensional precision and are well suited for process automation. Hydraulic presses are mainly used for simple forms. Large presses with up to 30 MN pressing force are used for pressing of plates which are to be rolled to sheet metal. The size and shape of the compact are limited by the capacity of the press and also by the geometry of the part.

The pressing density is not the same all over the compact due to the friction between the powder and the die wall and the nature of the load distribution inside the die. This is more pronounced for large parts and large part heights and can lead to crack formation or

distortion of the pressed compact during sintering. Large and critical parts are therefore commonly pressed isostatically.

The compaction pressures can reach 1000 MPa (using hard metal dies and punches). but the typical pressure are in range of 200-400 MPa (2-4 t/cm²). The compact density is in the range of 55-65% of the theoretical density (75% at most) and it depends upon the applied pressure, particle size, size distribution, particle shape, and size of the compact. There are several theoretical equations relating compact density and applied pressure, but in practice empirical relations are commonly used (Yih and Wang, 1979).

Although the compact density increases as average particle size varies from 1 to 9 μm , the compressive strength exhibits a maximum between 3 and 6 μm . This maximum corresponds to the preferred particle size range for most tungsten compacts.

2.9.2 Sintering

Sintering is a heat treatment to increase the strength of the green compacts. The main aim of sintering is densification in order to provide the metal with the necessary physical and mechanical properties and a density which is suitable for subsequent thermomechanical processing (Pink and Eck, 1991).

Sintering of tungsten is commonly carried out in a temperature range of 2000 up to 3050°C, under flowing hydrogen to prevent oxidation, either by direct sintering (self-resistance heating) or indirect sintering (resistance element heating systems). The density obtained should be a minimum of 90% of the theoretical density, but is commonly in the range between 92 to 98% (Cheney, 1984)

Sintering is commonly carried out in molybdenum wire resistance heated furnaces under hydrogen or nitrogen mixtures (dissociated ammonia) but can also be performed in vacuum

units. The use of wet hydrogen has become industrial practice to suppress hydrogen embrittlement (water vapour porosity) (Cai et al, 1995). The temperature/time program of the sintering cycle must be adjusted to the composition and size of the sintered parts. A cleaning step in hydrogen at 1000°C is commonly performed to render the outgassing of volatile compounds. High purity powder grades must be used for sintering. Otherwise, blistering will occur on liquid phase sintering, and interface precipitations will occur on cooling.

Isothermal sintering is carried out above the eutectic temperature, typically between 1440 and 1500 °C, but can be as high as 1600 °C. The higher the tungsten content of the alloy, the higher the temperature. Tungsten-nickel-copper alloys are sintered at somewhat lower temperatures than tungsten-nickel-iron alloys. Sintering times are between 30 minutes and two hours. Prolonged sintering under dry hydrogen leads to swelling of the parts and significant embrittlement due to pore coarsening by ripening and coalescence. Residual porosities larger than 0.5% drastically reduce the ductility (German and Chum, 1984; German, 1985).

On cooling, a significant amount of tungsten remains in solid solution, depending on the binder composition and the cooling rate. The solubility is highest in binary W-Ni alloys (up to 40 wt%; resulting in low ductility), but additions of Fe and Cu depress it to lower values (typically 20 to 25 wt% W), providing a tough and ductile binder matrix. Shrinkage porosity can form on cooling, in particular in W-Ni-Cu alloys and at high cooling rates; furthermore, impurities (P, S, C) segregate at the tungsten matrix interface. Both effects must be controlled by proper manufacturing conditions, since they significantly lower the ductility.

Optimal mechanical properties require subsequent heat treatment of the alloys. Solution annealing at 900 to 1300°C and subsequent quenching to avoid impurity segregation and formation of intermetallic phases significantly improves ductility (Hogwood and Bentey, 1994).

To increase hardness and strength, heavy metals can be cold worked (swaged, rolled) at the expense of elongation and toughness. Aging at 500 °C after 25% deformation (cold work) is a compromise to achieve both high ultimate tensile strength and elongation. Conventional procedure is a double swaging heat treatment cycle (deformation 25-30%) (German, 1997).

Although a considerable amount of densification already occurs during solid state heating, isothermal liquid phase sintering is a prerequisite to obtain near theoretical density and a high degree of microstructural homogeneity. Rapid final densification occurs on formation of the liquid phase under the action of capillary forces. Particle rearrangements, solution or re-precipitation processes (Ostwald ripening), and coalescence contribute to a higher packing density and a significant grain coarsening during sintering.

The original tungsten powder grain size, of 3-5 μm is transformed during sintering to rounded tungsten particles (spheroids) of at least 10 times the original grain diameter. Shape accommodation (formation of polyhedra with rounded corners) plays an important role in high tungsten alloys, where only a small quantity of liquid is available for achieving full density depending on the binder composition heavy metals can be classified into two main groups (Yih and Wang, 1979; Cheney, 1990):

(a) W-Ni-Fe (Ni: 1-7 wt%, Fe: 0.8-3 wt%, Mo: 0-4 wt%)

This group is ferromagnetic. Typical nickel-to-iron ratios range between 1: 1 and 4: 1. The preferred ratio is 7:3, since this composition avoids the formation of intermetallic phases (Penrice, 1984). W-Ni-Fe alloys exhibit excellent strength and ductility combinations and can be cold-worked to a reduction of 60% without intermediate annealing. Molybdenum acts as grain refiner. Higher additions of iron or additions of molybdenum cause a significant matrix-strengthening effect and improve high-temperature strength (Yih and Wang, 1979)

Other additives, such as Co, Ta, and Re, act as grain refiners and increase hardness and strength, but lower the ductility (Cai et al, 1995). Rhenium additions are of interest in net-shape production, since their high strength in the as-sintered condition (1180 MPa) does not require any post-sintering treatment. Bose et al (1989).

(b) W-Ni-Cu (Ni: 1-7wt%, Cu: 0.5-3 wt%, Fe: 0-7 wt%)

Members of this group are nonmagnetic and exhibit a higher electrical conductivity. The nickel-to-copper ratio ranges from 3:2 to 4:1. W-Ni-Cu alloys exhibit lower strength and ductility than comparable W-Ni-Fe alloys. Due to the low melting point of copper, low heating rates are required to obtain full density .

2.9.3 Sintering Stages

Pink and Eck (1991) and Bewlay and Briant (1995) studied the sintering behaviour of tungsten alloys and stated that it commonly takes place in three stages

First, during the early stage, the formation of necks takes place between the individual particles and grows by diffusion, increasing the inter-particle contact area. The powder aggregate shrinks, involving centre to centre approach of the particles. In this stage, the degree of densification is still low and the pore structure is open and fully connected.

Second, with increasing neck formation (intermediate stage), the necks become blunted and lose their identity. The pores radii (which are assumed to be cylindrical) vary along their lengths and, with increasing shrinkage, the pore channels break up into small still partly interconnected segments. During this stage (channel closure stage), pronounced densification occurs and significant grain growth occurs concurrent with shrinkage.

Finally, in the last stage (isolated pore stage), the pore segments further break up into chains of discrete, isolated pores of more or less spherical symmetry. This stage occurs when about 90% of the theoretical density is achieved. The sintering density then approaches asymptotically the practical limit of 92-98%. Investigations by Bewlay and Briant (1995) have shown that the densification is controlled by grain boundary diffusion over most of the densification range, unless at very high densities it becomes controlled by lattice diffusion. At 2400°C, the time necessary to obtain high densities decreases to 1-2 hours and, at 3000°C, 20-30 minutes. The finer the starting tungsten powder, the more rapid the densification at a given temperature (Yih and Wang, 1979)

Swinkels and Ashby (1981) estimated the influence of temperature and time on densification by using so-called density diagrams (sintering maps) which are based on approximate sintering models. Nevertheless, empirical rate equations are used for industrial purposes to calculate the necessary sintering times at different temperatures.

Metallic elements, such as Fe, Ni, Cr, Nb, etc., are evaporated but remain partly in the ingot, forming solid solutions. If Fe or Ni is present in the form of large, heterogeneous contaminations (such as iron particles stemming from reduction boats), these can lead to local melt formation and subsequent formation of large voids, which do not close during sintering. Elements which have practically no solubility in tungsten, such as alkali or earth-alkali metals, are volatilized. Grain boundary diffusion and carrier distillation effects most likely play an important role in "cleaning" the grain boundaries.

The sintering of tungsten can be enhanced by the addition of small amounts of alloying elements (0.5-1%), such as Ni or Pd. This phenomenon is called "activated sintering." It is explained by the enhancement of grain-boundary diffusion in tungsten due to the presence of the respective element in the grain boundary. High densities (up to 99%) can be obtained even at 1100°C (at this temperature, tungsten compacts are commonly pre-sintered). This agrees with Albiston and Sale (1985) who concluded that Ni activates the sintering of the

composite powder in a similar manner to that achieved for W alone.

2.10 Annealing of W-alloy during Pressing and Sintering

The effects of temperature on cold worked material are divided into three regions according to the temperature increase, recovery, recrystallization and grain growth.

Recovery takes place in the temperature range just below recrystallization. Hardness and strength do not change greatly, but corrosion resistance is improved.

Recrystallization takes place when the temperature rises above the recovery range. In this higher temperature range the formation of new stress free and equiaxed crystals lead to lower strength and higher ductility. With less cold work there are fewer nuclei for the new grains, and the resulting grain size is larger.

As the temperature is raised further, the grains continue to grow. This is because the large grains have less surface area per unit of volume. There are fewer atoms leaving a unit grain boundary area in a large grain than in a small grain and the larger one grows at the expense of the smaller. The temperature required for recrystallization varies with the metal. It is approximately one third to one half the melting temperature of the pure metal. Also, the greater the amount of cold work, the lower the recrystallization temperature.

The recrystallization temperature increases with increased alloying. However, it decreases with increased cold work, finer grain size, and longer holding times. The atom motion is required in recrystallization and the presence of foreign atoms (alloying elements) makes atom motion more difficult. Similarly, longer holding times give atoms more time to move, and so recrystallization can occur at a lower temperature. Therefore, it is common to use 1 hour at temperature to determine the recrystallization temperature.

3 Chapter 3 Apparatus & Methodology

3.1 Introduction

This chapter presents the main apparatus used in this work starting with the material examination, the analysis of the raw metal alloy and then the oxide powder process, and analysis of the oxide powder, ending with the last experiment to recycle the final material. After the recycle process , a microscopic analysis of the resultant metal is done.

The methodology of the research work can be divided into three parts. First, the oxidation process where the swarf is oxidized at different elevated temperatures to produce a homogenous powder. Second, the reduction process where the oxide powder is reduced by hydrogen to return the original in a powder form. Finally, pressing and sintering where the metal powder is returned to the metal form in readiness for further analysis.

3.2 Apparatus

3.2.1 Thermogravimetry Analysis (TGA)



Figure 5 Shimadzu TGA.

This instrument provides a continuous recording of mass changes of a sample of material, as a function of a combination of temperature with time and of pressure and gas composition.

The sample of material is placed on an arm of a recording microbalance, where that arm and the sample are placed in a furnace. The furnace temperature is controlled in a pre-programmed temperature-time profile (most commonly), or in a rate controlled mode, where the pre-programmed value of the weight changes imposes the temperature change in the way necessary to achieve and maintain the desired weight change rate.

3.2.2 X-Ray Diffraction Analysis (XRD)



Figure 6 Philips XRD.

X-ray diffraction (XRD) analysis of the heavy metal swarf was carried out with a “PHILIPS” (Figure 6) diffractometer using Cu-K α radiation ($\lambda= 1.54 \text{ \AA}$), generator voltage 50 kV and a generator current 40 mA. The diffractometer was fitted with a diffractometer control system type “PW3710”. The sample was placed in a small square recess in the holder and was pressed in the holder to be flat. All the samples were scanned over the range of 10° to 100° at a scan rate of 4°/min in a continuous scan. The measurements took about one hour. The x-ray diffraction data were automatically matched to data in the Joint Committee on Powder Diffraction International Centre (JCPDS) diffraction file.

3.2.3 Scanning Electron Microscope (SEM)



Figure 7 Jeol SEM JXA 3600.

The scanning electron microscope used to characterize the samples was “JEOL” JXA 3600 (Figure 7) equipped with a 35 mm camera. The microscope was operated in the range of 15 to 25 keV which is the energy range for the sample prepared. The instrument has the ability to take graphs photo at different magnifications, and is equipped with energy dispersive analysis of x-rays (EDAX) to perform chemical analysis for most of the solid samples.

The powder samples are usually spread onto adhesive carbon tape to be prepared for analysis. The powder was vacuum coated with carbon once it was attached to the tape, to prevent charging of the oxide powder sample and to improve the high magnification photos.

3.2.4 Carbolite Furnace



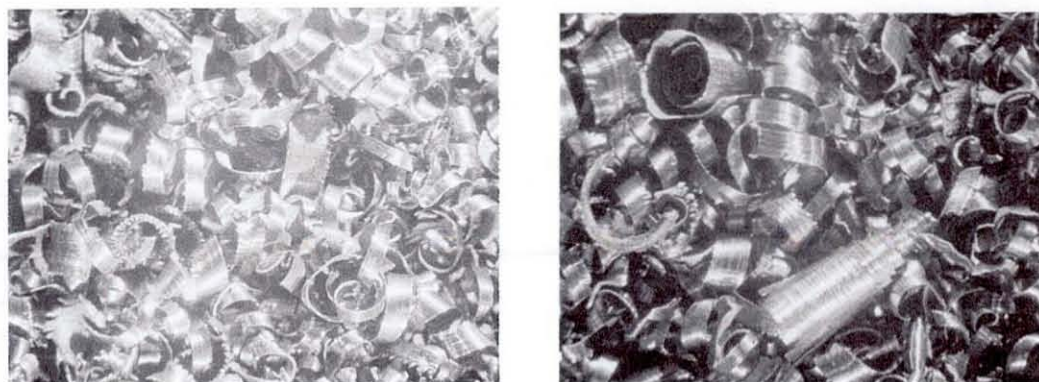
Figure 8 Electric furnace.

The furnace used in this research work was an electric carbolite furnace (Figure 8) with a temperature range up to 1500°C. The chamber size is big enough (5" W×4.25"H×6"D) to enable a large amount of oxide (20 grams) to be produced. The stability of the furnace is $\pm 2^{\circ}\text{C}$ at 1000°C and the uniformity is $\pm 5^{\circ}\text{C}$.

3.3 Materials

The material used in this work was tungsten alloy swarf which was taken from the machining waste after the cutting process of the alloys. The waste was contaminated with cooling oil, which was used for cooling while the metal was being cut. The residual metal

takes a spiral shape with different sizes; part of the metal is thin, whilst other part are wide and long (Figure 9 a and b). The material is treated and cleaned before the analysis and will be discussed in the experimental procedure section.



(a) (b)
Figure 9 The starting material (Swarf).

3.3.1 W-Oxide

The oxide powder obtained from the oxidation of the tungsten alloy used in this work varies according to oxidation process. Different oxidation temperature-time leads to different oxide powders. There are different types of tungsten powder according to friability, colour, and particle size. A sample of oxidation powder at 900°C is shown in Figure 10. The oxide powder will be discussed in details in the result and discussion chapter.

3.3.2 Tungsten Powder

The tungsten powder is the powder obtained after the reduction of the tungsten oxide in a hydrogen atmosphere. The metal powder has a gray colour with very fine particles (1-3 μ m). Figure 11 shows a compact powder after reduction at 800°C.

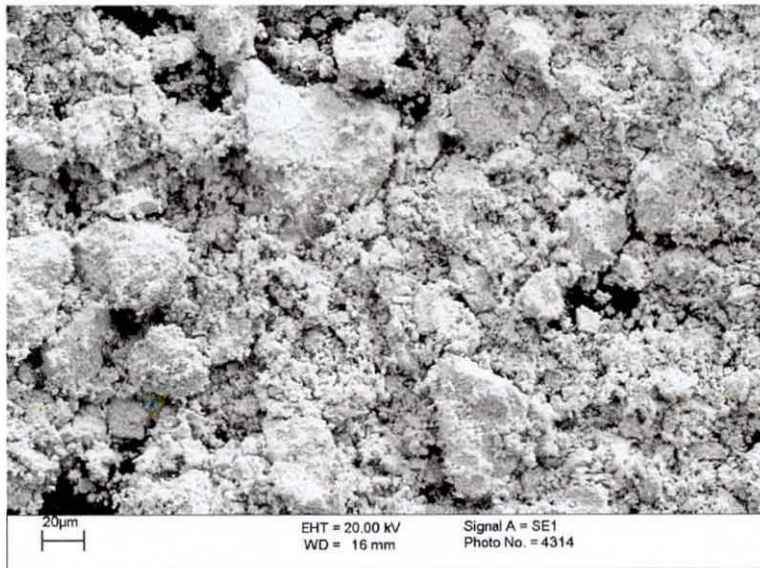


Figure 10 Oxide powder at 900°C.



Figure 11 Tungsten powder after reduction of the W oxide ×200.

3.3.3 Tungsten Pellet

The tungsten pellet is the final metal after the full recycling process. The pellet is shown in Figure 12. The size and shape of the pellet depends on the die used in the pressing process. The sample in this research work was placed in a cold resin of radius 1.5 cm. There are different aspects that affects the metal properties such as the sintering temperature and time (which was discussed in the literature review, Chapter 2.9.2).



Figure 12 Tungsten pellet after pressing and sintering.

3.4 Methodology

3.4.1 Experimental Procedure

The sample used was heavy metal swarf, which was taken from machining waste. To prepare samples for elemental analysis and the oxidation process. The alloy was prepared first by washing the swarf in acetone in order to remove the oil that was used as the cooling

oil in the cutting machines. After washing, the swarf was dried at room temperature for 5 hours and then washed several times with distilled water in order to remove other possible deposits. The swarf was then dried again at room temperature for 5 hours.

The optical analysis requires the sample to be flat and finely polished. To prepare the swarf for polishing it was mounted in cold-setting resin and polished down starting with a sand paper of size 500 μm then gradually 200, 100, 50, and 10 sand paper, then a different type of cloth of size 6 μm used for polishing for 10 minutes. These procedures are necessary to obtain a very smooth surface for the accuracy of the optical examinations.



Figure 13 Swarf mounted and polished up to 6 microns

The pellet then etched by immersing the sample in "Nital" (the most common etchant for iron and steel, and contains 1-10 ml nitric acid and 90-99 ml methanol) for 30 seconds, to reveal one or two phase from the top surface. The metals dissolve in the etchant solution in time. To remove the minimum possible layer the sample immersed for a 30 seconds only. The sample was then washed and dried in order to observe the structure in the optical microscope, Figure 13. For XRD analysis, the sample was ground and sieved several times and a heavy metal powder of less than 150 μm was prepared for analysis.

3.4.2 Materials Characterisation

The samples were characterised using XRD and SEM after different treatments. The first characterisation was of the starting material, then after oxidation. A third characterisation was made after the reduction, and finally an analysis was carried out after pressing and sintering.

3.4.3 X-Ray Diffraction analysis

For x-ray diffraction analysis the heavy metal swarf was ground by hand in a pestle and mortar sufficiently fine to reach a size of about 40 μm . The quantity of powder sample used was approximately 0.4 grams and this packed into a holder and press firmly with a glass microscope glass to insure the corners are filled, another glass microscope slide draw over the recess to remove the excess sample. The holder placed in a position on the arm which moves around to cover the required angle (10° - 100°).

The x-ray diffraction analysis method used in this research work passed on known wave length x-ray which pass through the powder sample to identify the crystal structure according to Bragg's relationship

$$n\lambda = 2d \sin \theta$$

where n is a number, λ is the wavelength (meter), d is a line spacing between different plane of atom in the crystal lattice (meter), and θ is the diffracting x-ray angle.

3.4.4 Scanning Electron Microscopy (SEM)

For scanning electron microscope analysis, the prepared sample mentioned in 3.4.1 was placed on the holder and inserted inside the microscope chamber under the electron beam. The methods used in this research work was the energy dispersive analysis x-ray (EDAX) which measures the energy of the elements emitted from the sample when it is bombarded

by the electron beam according to the equation

$$E = h \nu$$

Where E is the energy (Joule), h is a Plank constant, and ν is the frequency (cycles/second)

3.4.5 Thermogravimetric Analysis (TGA)

Initially, isothermal TGA was used with small samples (20 mg) to study oxidation under a natural air environment. Four different experiments were carried out in order to determine the oxidation rate over the temperature range 20°C to 1100°C. Subsequently, different experiments were carried out at six different temperatures with fixed holding times. The conditions used in these experiments were 750°C, 800°C, 850°C, 900°C, 950°C and 1000°C for 3 hours.

3.4.6 Furnace

Oxidation of larger quantities (20 grams) of the tungsten alloy swarf was carried out using an electric "Carbolite" furnace to enable larger amounts of oxide powder to be produced. The heavy metal swarf powder was oxidised in a natural air at different temperatures and for times determined from the TGA data.

3.4.7 Oxidation Experiments

The oxidation experiments were carried out using two different instruments according to the required analysis. Initially isothermal TGA was used with small amount of sample (20 mg) to study oxidation in a natural air environment. The experiment was carried out in order to determine the oxidation rate over the temperature range from 20°C to 1100°C. Subsequently, different experiments were carried out at six different temperatures with fixed holding times. The conditions used in these experiments were 750°C, 800°C, 850°C, 900°C, 950°C, and 1000°C for 3 hours.



Figure 14 Ceramic boats.

Secondly, oxidation of larger quantities (20 grams) of the tungsten alloy swarf was carried out using an electric resistance "Carbolite" furnace to produce larger amounts of oxide samples. The heavy metal swarf powder was oxidised in air at the same temperatures and for the same times determined from the TGA data.

The sample was placed in the furnace in ceramic boats, Figure 14, since the ceramic has the ability to stay in a high temperature without changing or reacting with other elements.

3.4.8 Reduction Experiments

The reduction experiments were carried out using a "Vicstar Furnace" with a gas supply system. The furnace had an upper operating temperature of 1600°C and could accommodate large amounts (20grams) of powder. The reduction was studied at two different temperatures using the same amount of powder (300 mg).

The furnace was first flushed with argon for 10 minutes to remove the residual air from the

system. A hydrogen atmosphere was then established by allowing the hydrogen to purge to the system at a flow rate of approximately 2000 ml/min during all reduction process. According to dangerous use of hydrogen at high temperatures a previous publication by (Hornung and Karivan, 1999) was used to determine this rate. The furnace was heated to the required temperature at the rate of 300°C/hour.

After the reduction was completed, the furnace was flushed with argon again to remove any remaining hydrogen residuals, and the furnace temperature was lowered at the same rate that used for heating and the apparatus was allowed to cool. The product was removed for characterisation by x-ray diffraction and scanning electron microscopy and for subsequent processing to give a sintered product.

3.4.9 Pressing and Sintering

After the reduction experiment was completed, the reduced powder was tested using x-ray diffraction and scanning electron microscopy in order to ensure the full reduction of the powder sample. The reduced powder was placed into a 3.5 mm die and the die placed into a Draper press then pressed using a pressure of 20 Kg/cm². The press and the schematic drawing of the die are shown in Figure 15.

After this the compressed sample was then sintered in the same furnace used for reduction. The sintering was carried out in hydrogen gas in order to prevent the re-oxidation of the tungsten and at the same flow rate as that used for the reduction. The temperature was raised gradually at a rate of 300°C/hr to the sintering temperature. When the sintering process was completed the sample was removed to be analyzed in the scanning electron microscopy.



Figure 15 Draper press and 3.5 mm die

3.4.10 Microstructural Examination

After sintering, the specimen was metallographically polished to a 6 micron diamond finish. The polished specimen was then etched in "nital" for 30 second to reveal the layers in the sample. After etching the specimen was examined under the scanning electron microscope.

4 Chapter 4 Results and Discussion

4.1 Introduction

In this chapter the results from all the processes will be discussed in detail to show the chemical and physical reactions that occurred during the processes. The starting material is specified and a discussion of how it was cleaned and prepared for the analysis has been presented. Also, a microscopic analysis was conducted by SEM and XRD.

The second step was the oxidation process for the swarf. The oxidation was performed in two different steps at different temperatures. Reduction of the oxide powder results from the oxidation process was studied at different temperatures. Pressing for the reduced powder took place for different reduced powder. Finally, a selective oxide powder was reduced at certain temperature and the metal powder is pressed and sintered at certain temperature.

After the completion of the experiments, a microscopic comparison between the starting material and the final product was established using XRD and SEM.

4.2 Starting Material

The starting materials used in this research work were heavy metal alloy swarf Figure 16 which was mentioned in section 3.3. Different shapes of the spiral material has been selected to prepare for the analysis as shown in Figure 13. The larger size sample has been selected for the SEM analysis where the surface is polished and prepared for scanning. While the smaller size sample has been selected and sieved for the XRD analysis.

The characterization of the starting materials by Scanning Electron Microscopy (SEM) involved obtaining a micrograph that shows a two phases, a rounded white phase which represents the tungsten and a dark phase in between which represents the alloying elements (matrix).

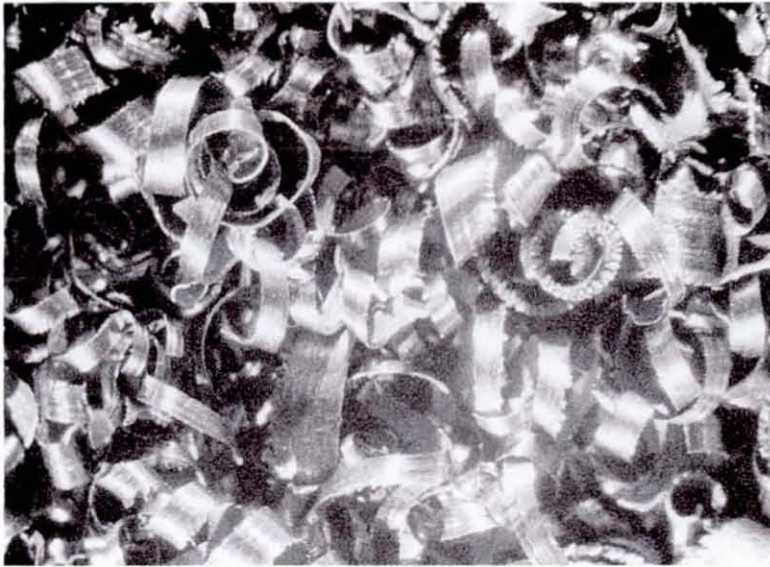


Figure 16 Tungsten alloy (swarf).

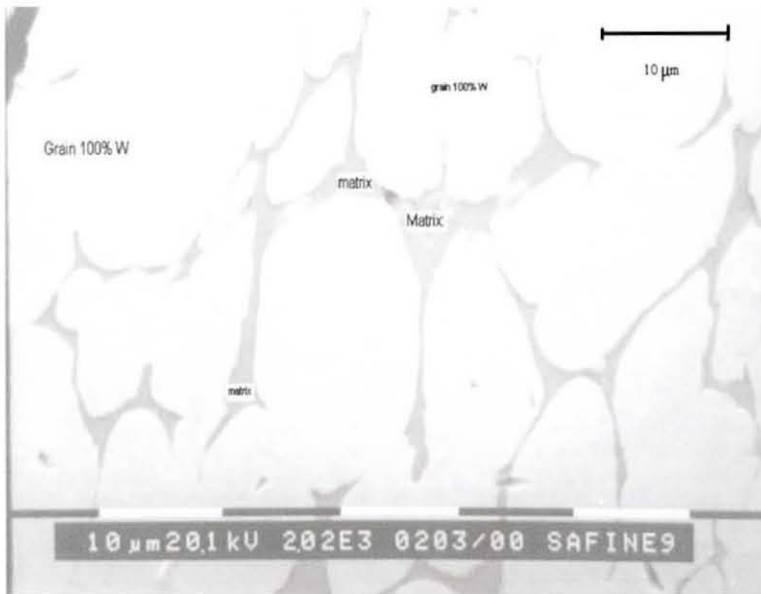


Figure 17 Heavy metal swarf material magnified $\times 200$.

From these phases it was concluded that the heavy metal swarf was a composite material with a grain size of 10 to 20 μm as shown in Figure 17.

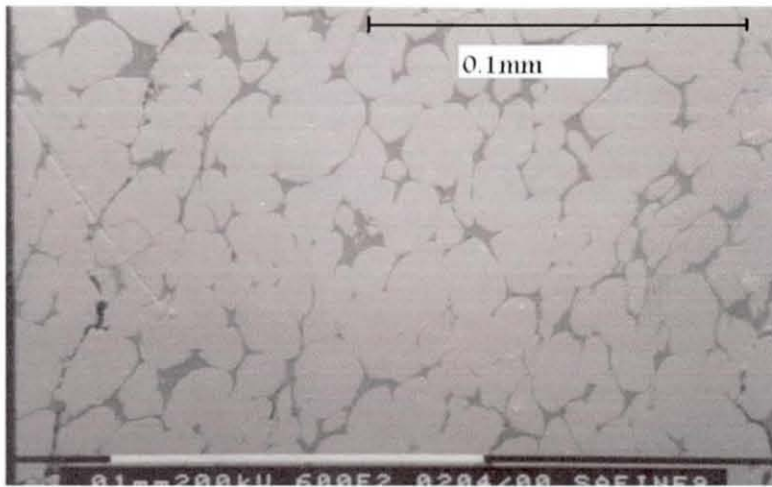


Figure 18 composite material contain 95.4% W

Figure 19 showed that the grains in part of the samples were elongated due to the mechanical work carried out by the cutting or shaping machines. The elongated grains look different from the original in Figure 18. These grains are less than 10 microns wide and 20 to 30 microns long, and more, the grains look to be connected to each other at the edge.

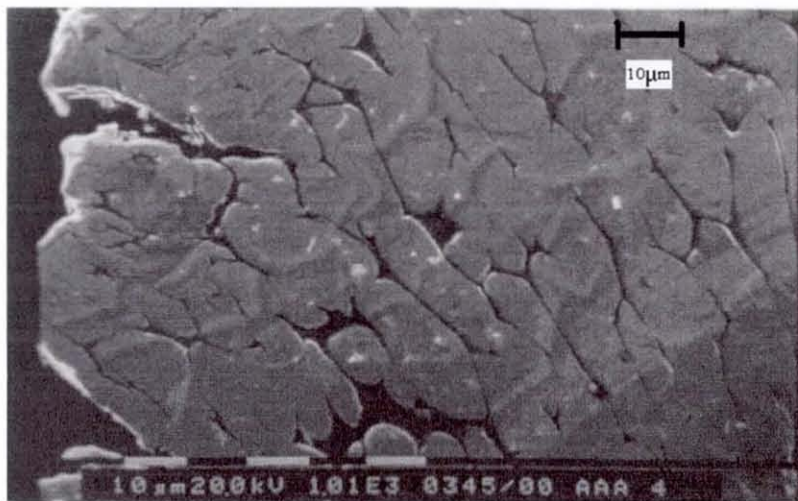
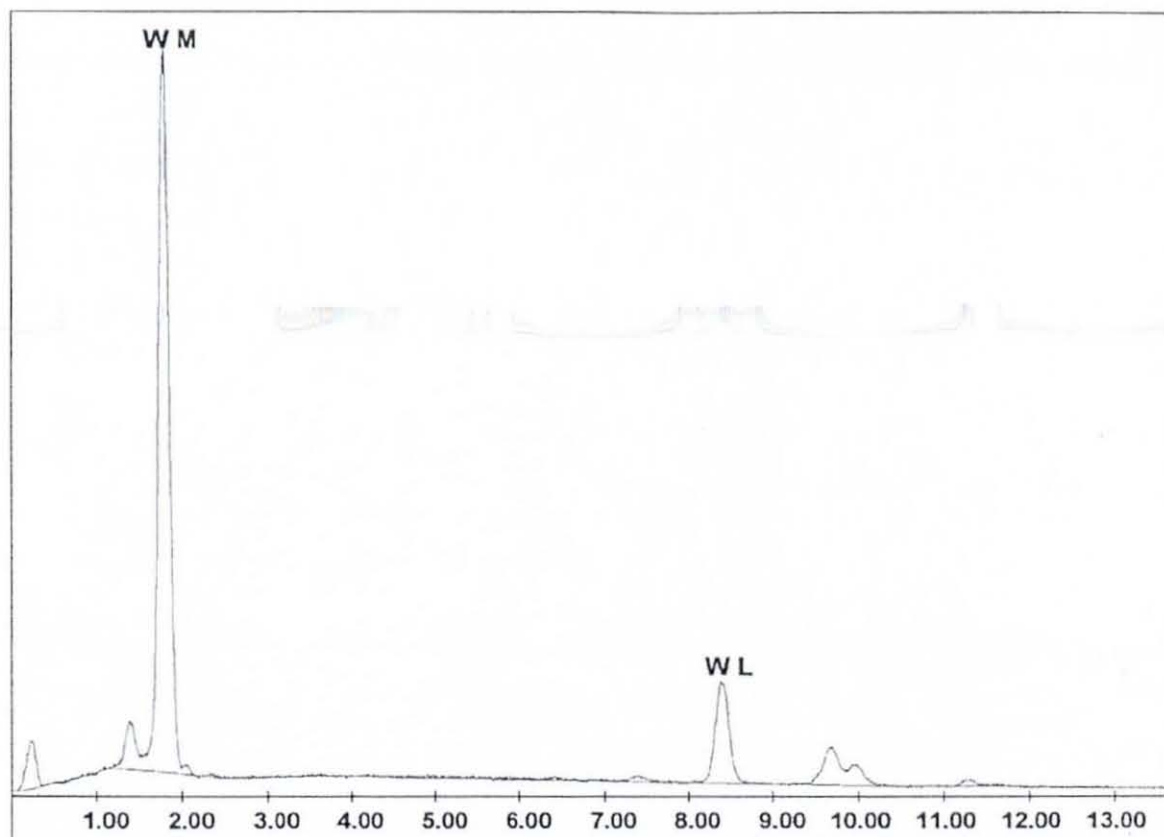


Figure 19 Elongated Grains ×1010.

The elemental analysis by the energy dispersive spectrometer (EDAX) showed that the grains in the composite (Swarf) consisted of 100% W, Figure 20, while the matrix contained approximately 36% Ni, 35% Fe, 15% W, 8% Cu, 3% Co, and 0.6% Mn, Figure 21. The mathematical calculation showed that the tungsten grains covered 95.4% of all the composite swarf as shown in Figure 18.

The X-ray diffraction analysis (Figure 22) showed a diffraction pattern containing peaks that were related to the tungsten grains and a collection of other peaks associated with the Fe-Ni-Cu matrix alloy.



EDAX ZAF Quantification (Standardless)
Element Normalized

Element	Wt %	At %	K-Ratio	Z	A	F
W L	100.00	100.00	1.0000	1.0000	1.0000	1.0000
Total	100.00	100.00				

Element	Net Inte.	Bkgd Inte.	Inte. Error	P/B
W M	3607.66	118.90	0.29	30.34
W L	696.44	72.46	0.69	9.61

Figure 20 EDS analysis of the grains in the swarf (starting material).

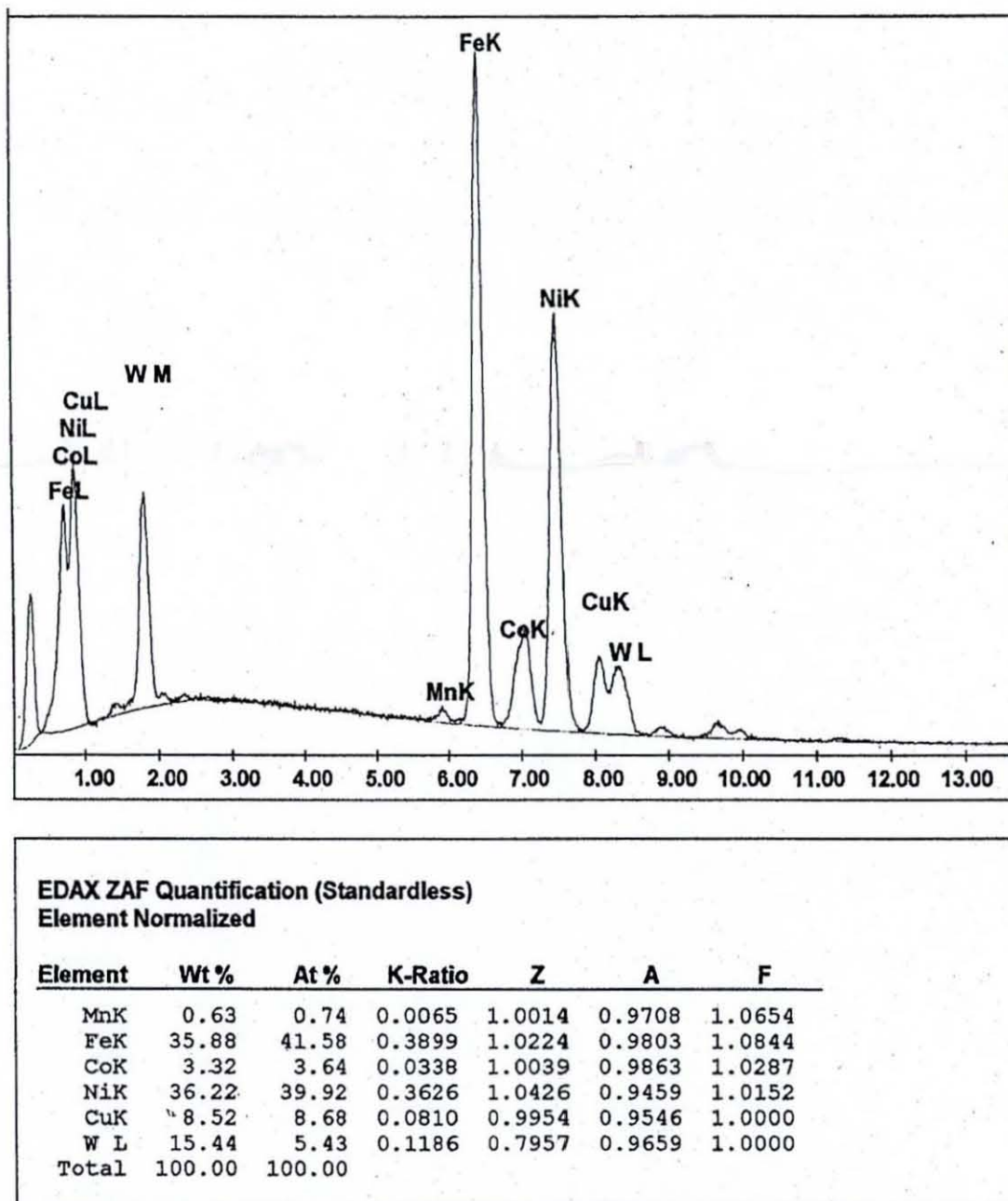


Figure 21 EDS Analysis of the matrix in the swarf (starting material).

Figures 20 and 21 shows ZAF quantitative chemical analysis for the microstructure of the tungsten swarf. This quantitative mathematical method measures the area under the curves (the analysis peaks curve) where they rises at the energy of each element as mentioned in section 3.4.4. as it can noticed in all elements in the Figure 21 where all the peaks rises in the K energy region except W which rises in L energy level.

The weight of the element in comparison to the compound percent (wt%) shows that Ni and Fe represent 72% of the alloying elements, while the others are traces. The atomic weight percent in comparison to all compound weight (At%) shows that the heaviest atomic weight is for the same elements, while At% for W is 5.43. The correction factors for the quantitative analysis (Z A F) shows analysis error of ± 1 .

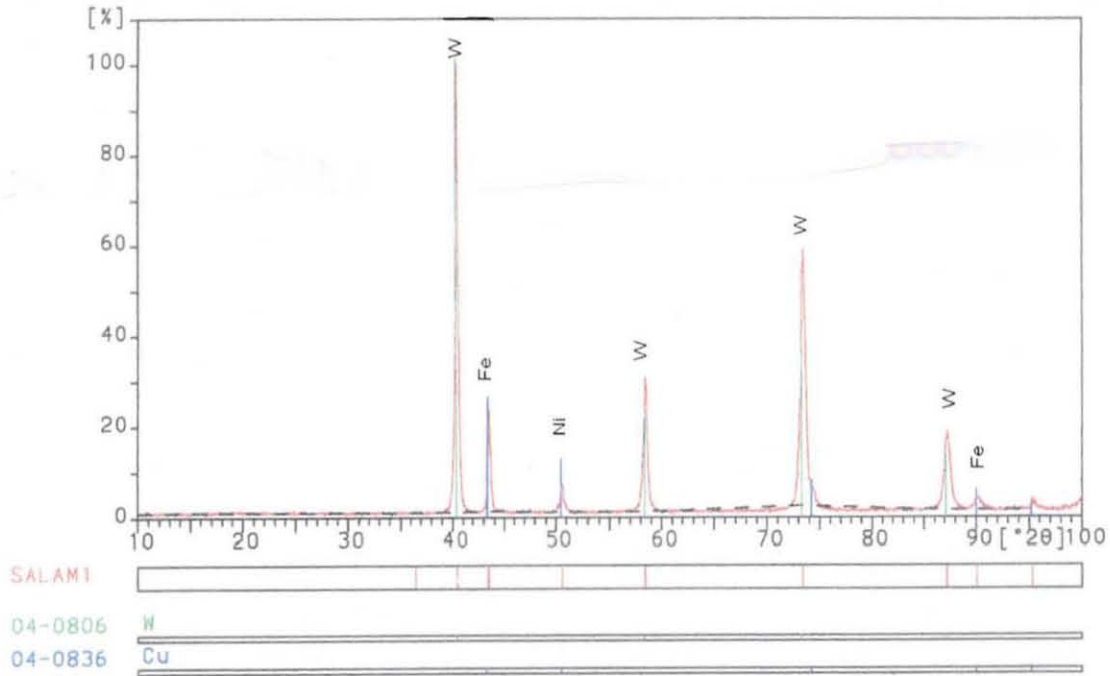


Figure 22 XRD analysis for the tungsten alloy swarf (starting material).

4.3 Oxidation Process

The oxidation experiments were carried out in two ways, first using an isothermal thermogravimeter (TGA), and next using a carbolite furnace and larger amount of tungsten.

4.3.1 TGA and Furnace

Scanning electron micrographs show that the swarf was a composite material with a grain size of 10 to 20 μm , as shown in Figure 17.

Figure 18 shows that the tungsten grains account 95.4% of the composite swarf as calculated by area measurement programming by MATLAB shown in the appendix B. Elemental analysis by EDAX in Figure 20 showed that the grains in the composite swarf consisted of 100% W, while the matrix contained approximately 36% Ni, 35% Fe, 15% W, 8% Cu, 3% Co, and 0.6% Mn (a typical EDS analysis is shown in (Figure 21). XRD analysis verified the EDAX analysis and showed a diffraction pattern containing peaks that could be related to the tungsten grains and a collection of other peaks associated with the Fe–Ni–Cu matrix alloy.

The TGA data showed the progress of the oxidation of 20 mg samples of the swarf, shown in Figures 23 and 24. The initial TGA run, Figure 23, was carried out to determine the temperature range over which the W-alloy oxidation took place. Subsequent TGA analyses determined the rate of oxidation at different temperatures within the range determined previously for the alloy oxidation. Figure 23 shows the trace obtained during first experiment, which was carried out over a temperature range of 20°C to 1100°C in 100 minutes.

It is observed that the oxidation process started at about 560°C (50 min after the start of the test). The oxidation was observed by measuring the increase in the mass of the sample during heating, in which the tungsten (W) reacts with oxygen to form tungsten oxide according to the following equation

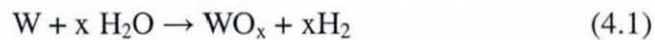


Figure 23 shows that rapid oxidation occurs around 700°C to 870°C after 65 min, and that the sample is fully oxidised at 960°C after 92 min. In order to determine the best oxidation rate, six isothermal experiments were carried out at 750°C, 800°C, 850°C, 900°C, 950°C and 1000°C. Five temperatures were chosen in the fast oxidation region (700–950°C) in addition to one in the fully oxidised region, in order to determine the best oxidation rate as a function of temperature.

99

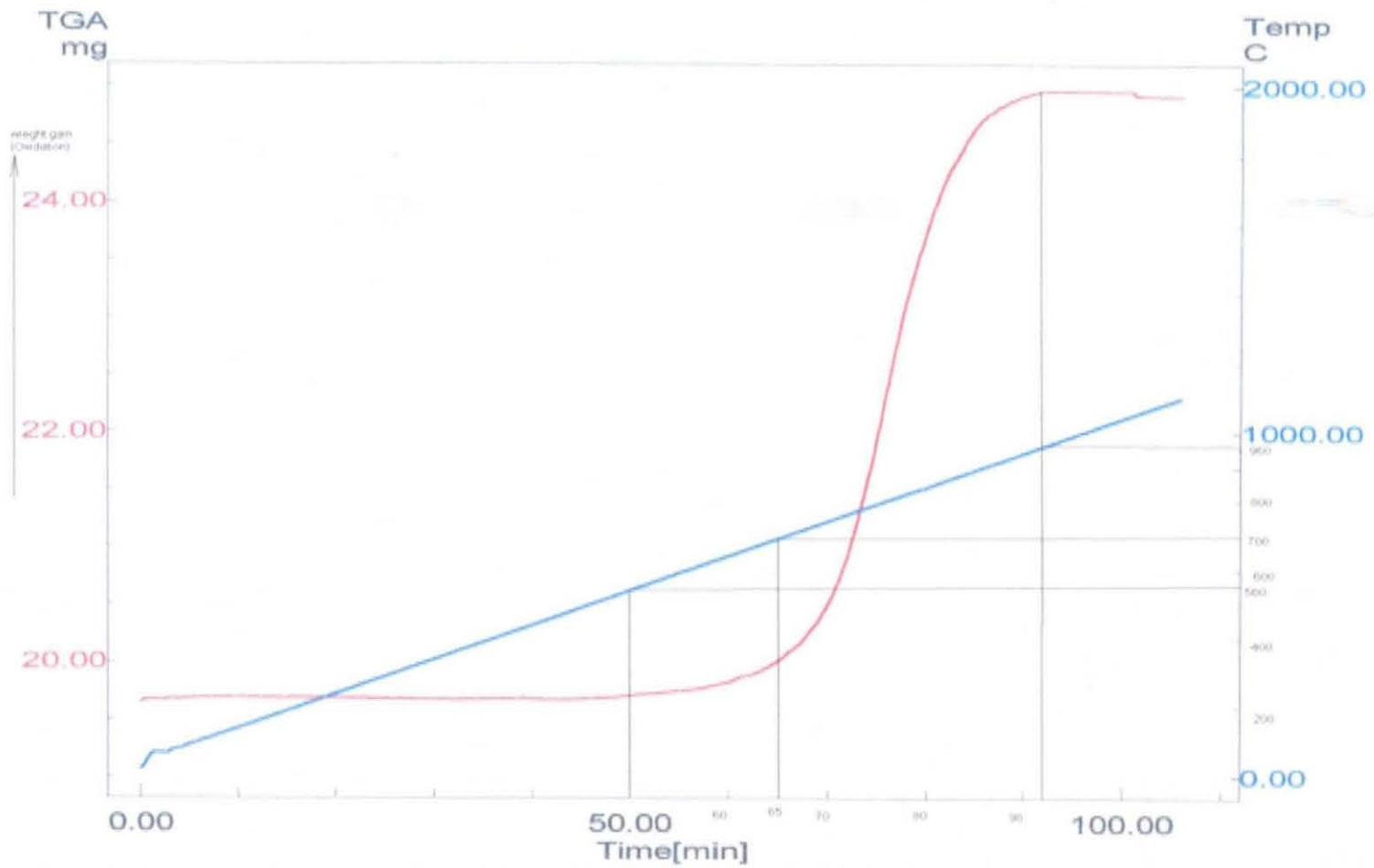


Figure 23 Oxidation of tungsten alloy in natural air.

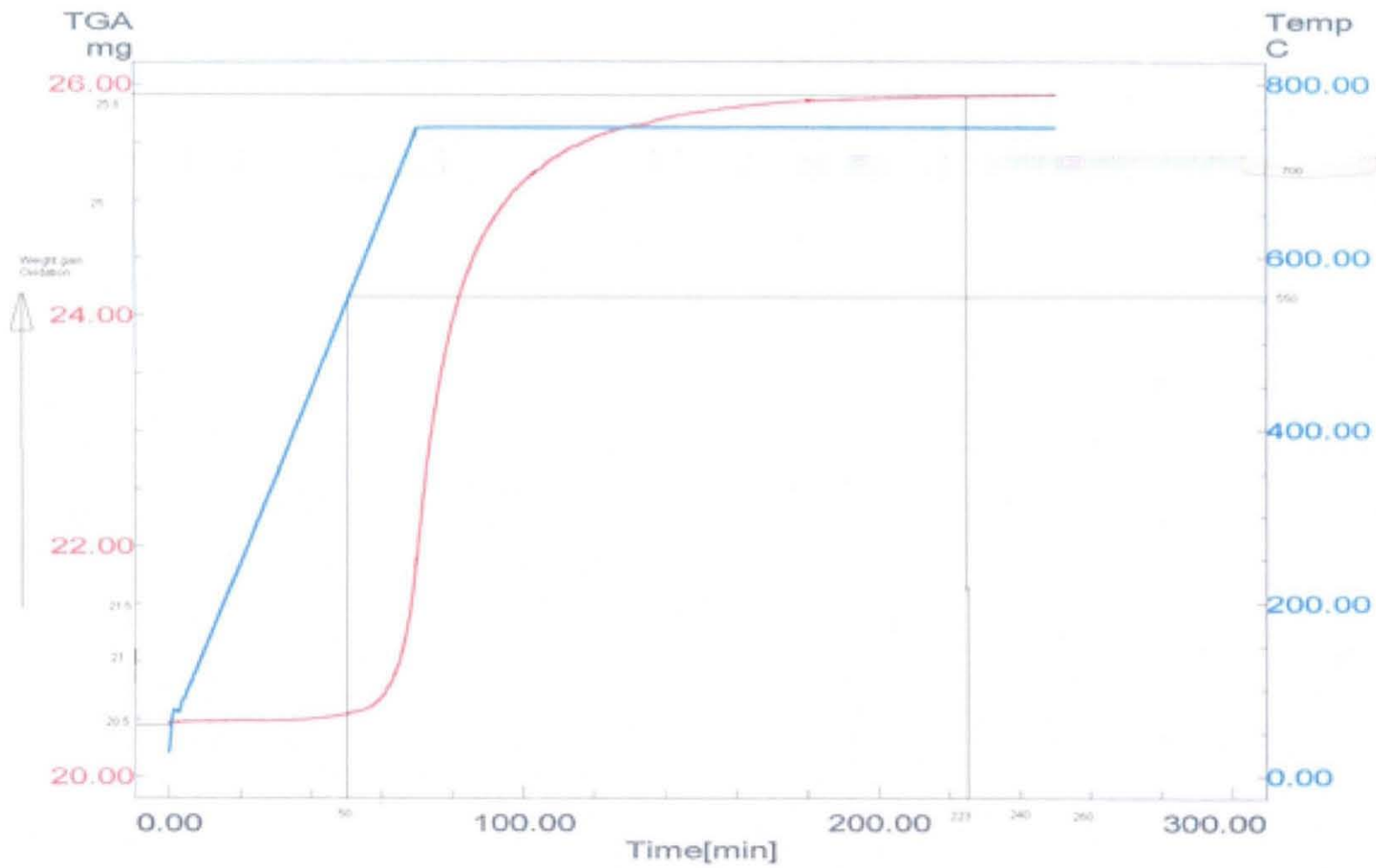


Figure 24 Oxidation of tungsten alloy at 750°C for 3 hrs.

Figure 24 shows the oxidation of the W-alloy at 750°C over a period of 3 hours during which the mass increased from 20.4 to 25.8 mg. The results show that oxidation started after 50 min at 550°C. After 220 min, the alloy was fully oxidised, exhibiting a mass difference of only 5.4 mg over 170 min.

At 800°C, the mass increased rapidly from 20.4 to 25.9 mg in 70 minutes, (Figure 25). The alloy was fully oxidised after 72 min with a maximum mass increase of 5.5 mg. In the experiment at 850°C it was found that the weight increased rapidly from 20.4 to 25.9 mg in slightly less than 70 min. The total mass change was 5.5 mg.

If the tungsten mass in the swarf is taken to be 95.4%, the oxidation of the tungsten component of the sample would have given a theoretical mass increase of only 4.8 mg. The Fe/Ni/Cu alloy matrix might have also oxidised to form the respective tungstates, accounting for an additional mass increase of 0.5 mg, giving a total mass increase of 5.3 mg. In these experiments it was observed that oxidation started at temperature of 550°C, with full oxidation occurring at various temperatures and times as shown in Table 1.

At 750°C, it was observed that the alloy took longer to fully oxidise and this agrees with Sikka and Rosa (1980) and Yuehui et al (2003), while at the higher temperatures the oxidation was faster. However, at higher temperatures the oxide was less friable and appeared to have a larger particle size, as shown in Figures 25 and 26. Hence, a greater quantity of powder (20 g) was oxidised at 900°C, 950°C, and 1000°C for 3 h in the furnace. Figure 33 shows the XRD spectrum of the oxidised specimen produced at 900°C.

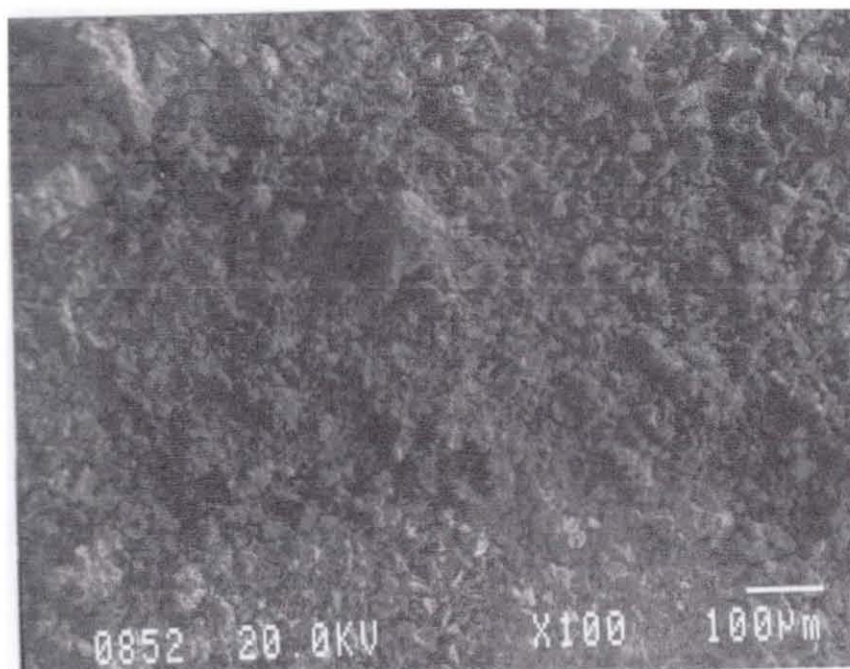


Figure 25 Oxide powder at 800°C.

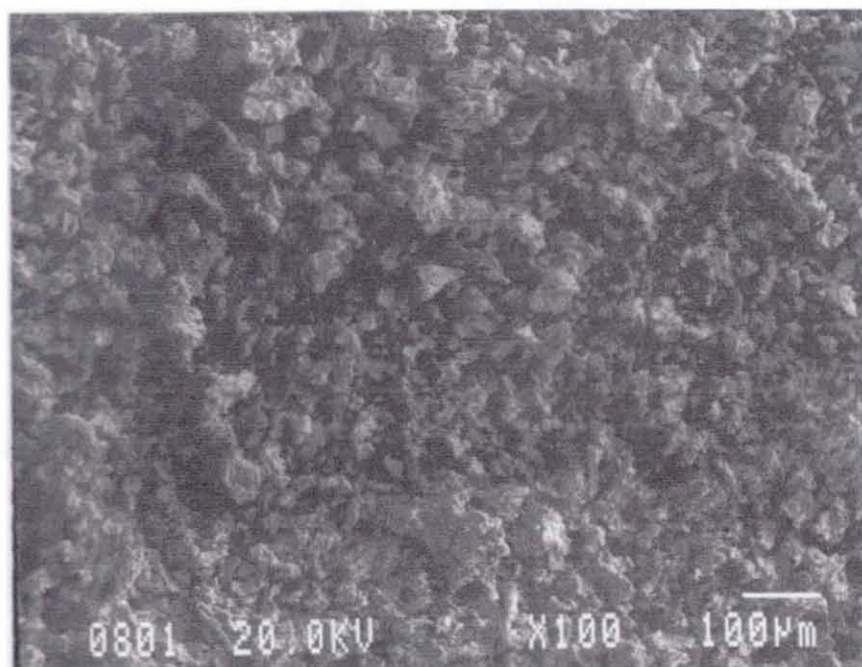


Figure 26 Oxide powder at 850°C.

Table 1 Time taken to fully oxidize sample of the tungsten swarf at different temperatures.

Temperature (°C)	Initial weight (mg)	Final weight (mg)	% of total mass (oxidation)	Time to fully oxidize for 20 mg sample (minutes)	Time to oxidize for 80 mg sample (minutes)
750	20.4	25.8	79.06	170	-
800	20.4	25.9	78.76	72	-
850	20.4	25.9	78.76	68	-
900	83	105	79.05	57	60
950	79	101	78.22	31	31
1000	76.5	97	79.35	29	29

For all quantities of swarf studied, a 3 hour oxidation period was selected to ensure that complete oxidation was achieved. The oxidation of these materials was verified by subsequent XRD analyses. At higher temperatures, 900°C, 950°C and 1000°C, 80 mg samples were evaluated by TGA, where the results are summarised in Figures 29, 30, and 31. The mass difference was 22 mg, 79% of the total mass, which is the same percentage mass of oxidised sample observed in the previous lower temperature experiments.

At 900°C, the sample started to oxidize after 24 minutes and was fully oxidized at 81 minutes. The oxidation time was $81 - 24 = 63$ minutes, and the weight increased from 79 mg to 101 mg, which is equal to $105 - 83 = 22$ mg as shown in Figure 29.

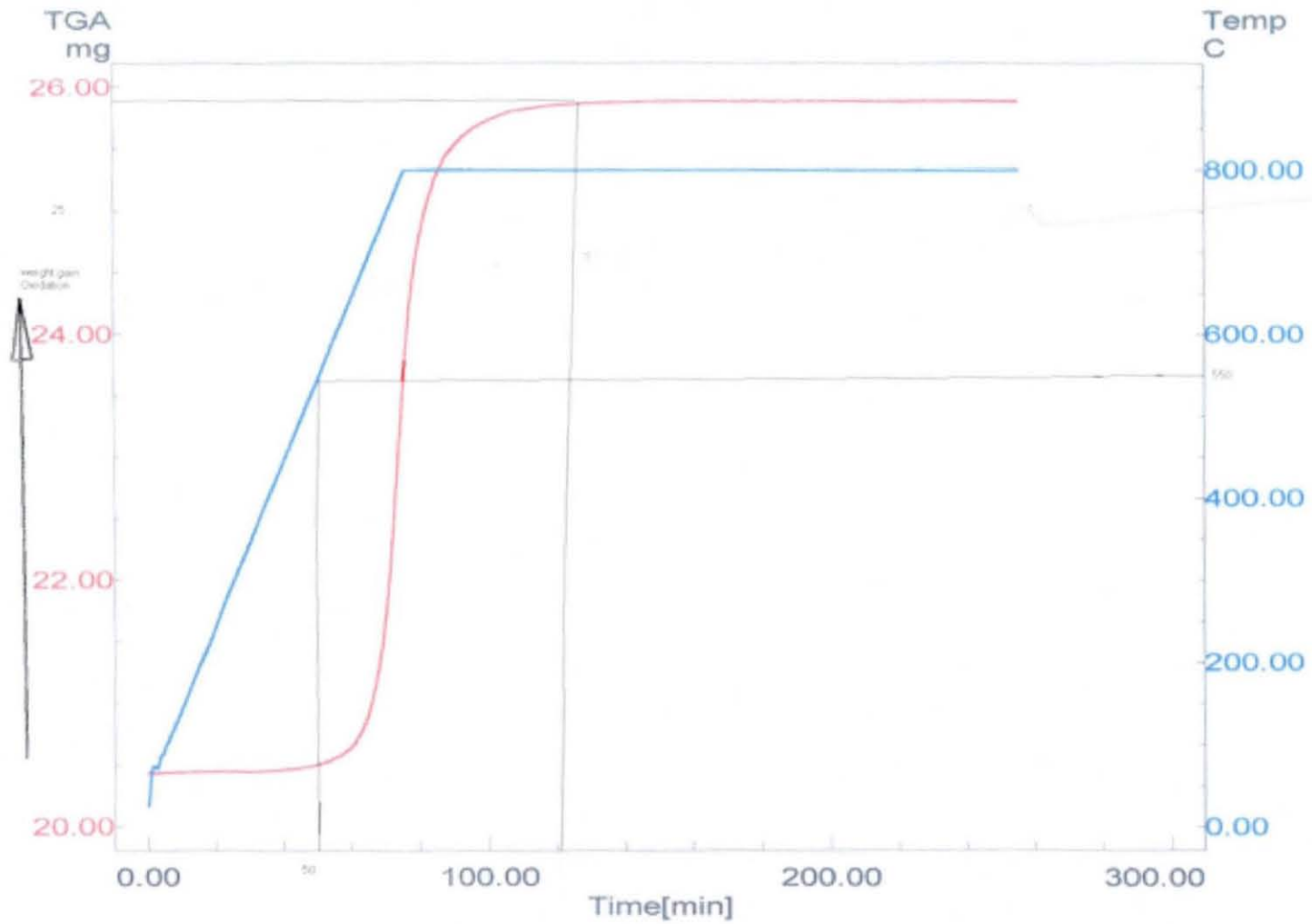


Figure 27 Oxidation of tungsten alloy at 800°C for 3 hrs.

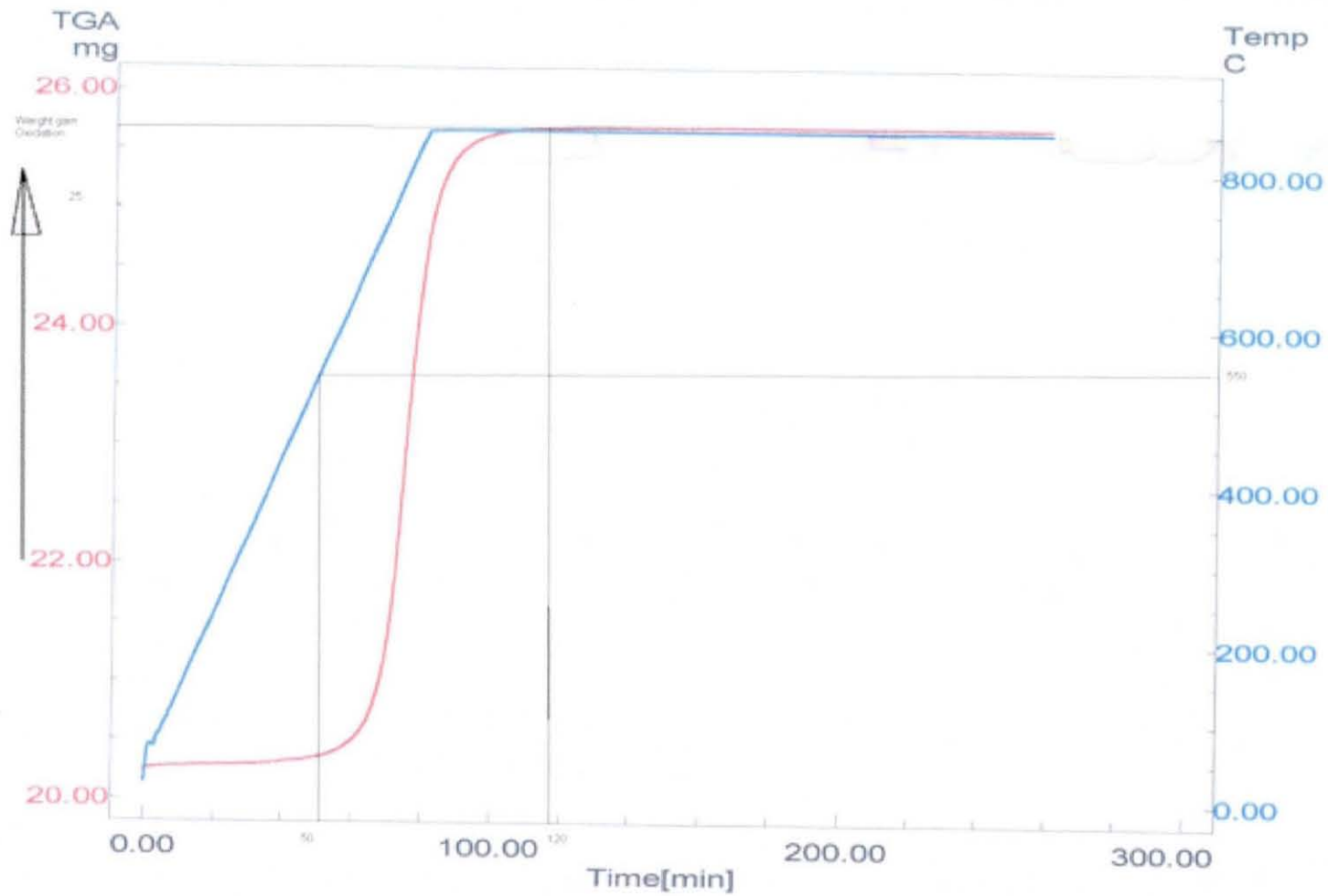


Figure 28 Oxidation of tungsten alloy at 850°C for 3 hrs.

At 950°C the oxidation starts at 23 minutes and it is fully oxidized at 54 minutes, hence the oxidation time is $54 - 23 = 31$ minutes. The start of the oxidation is known according to the weight increase, which was observed at the 23 minutes and reached to maximum 101 mg at 54 minutes. The total weight gain at this temperature is $101 - 79 = 22$ mg as shown in Figure 30.

At 1000°C it the oxidation starts at 23 minutes and it is fully oxidized at 52 minutes, where the oxidation time is $52 - 23 = 29$ minutes. The start of the oxidation observed at the 23 minutes and reached to maximum 97mg at 52 minutes. The total weight gain at this temperature is $97 - 76.5 = 22.5$ mg as shown in Figure 31 and Table 1.

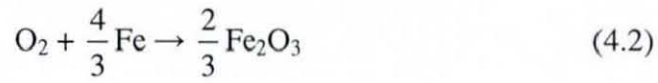
These experiments reveal that full oxidation of the tungsten alloy at high temperatures depends on both time and temperature, and the rate of oxidation (weight gain) is constant at all temperatures when sample is fully oxidized. At higher temperatures (900°C, 950°C and 1000°C) the microstructure of the particle sizes for the powder produced are larger, as presented in Figure 36, 37, and 38. At 1000°C, the oxidation is faster (see Table 1), and the particle size of the oxide powder is larger and has a better defined form Figure 38.

Figure 32 shows the energy dispersive analysis x-ray (EDAX) for the oxide powder achieved at 1000°C. The analysis showed peaks for tungsten (W), iron (Fe) and nickel (Ni). These elements are the main elements in the starting materials, which prove the existence of the alloying element in the powder.

The semi quantitative analysis carried out at these temperatures (900°C, 950°C, and 1000°C) by (EDAX ZAF) method shows the weight percent of all oxides in the powder. Tungsten trioxide represent about 93 wt%, iron oxide 3.5-3.8 wt%, and nickel oxide 3-3.2wt% as shown in Tables 2, 3, and 4.

The analysis shows almost similar quantity for the oxide powder at the three oxidation temperatures where the oxidation rate is the same and the oxidation time is 81 minutes at 900°C, 31 minutes at 950°C, and 29 minutes at 1000°C.

The oxidation processes for these elements with oxygen react according to the following equations



and



Where the tungsten reaction passes in different reactions during the oxidation mentioned in section 2.5 and initially the following reaction reacts with oxygen according to



Table 2 Quantitative analysis for the oxide powder at 900°C.

Element	Wt %	Mol %	K-Ratio	Z	A	F
Fe ₂ O ₃	3.54	7.72	0.0278	1.1385	0.9318	1.0594
NiO	2.98	13.9	0.0295	1.172	0.9569	1.1213
W ₂ O ₃	93.48	78.38	0.7555	0.9087	1.0054	1
Total	100	100				

Table 3 Quantitative analysis for the oxide powder at 950°C.

Element	Wt %	Mol %	K-Ratio	Z	A	F
Fe ₂ O ₃	3.65	7.89	0.0287	1.1376	0.9321	1.0595
NiO	3.19	14.73	0.0315	1.1709	0.9571	1.1208
W ₂ O ₃	93.16	77.37	0.7521	0.9078	1.0053	1
Total	100	100				

Table 4 Quantitative analysis for the oxide powder at 1000°C.

Element	Wt %	Mol %	K-Ratio	Z	A	F
Fe ₂ O ₃	3.79	8.23	0.0298	1.1376	0.9324	1.0594
NiO	3.05	14.14	0.0301	1.1709	0.9572	1.121
W ₂ O ₃	93.16	77.63	0.752	0.9078	1.0053	1
Total	100	100				

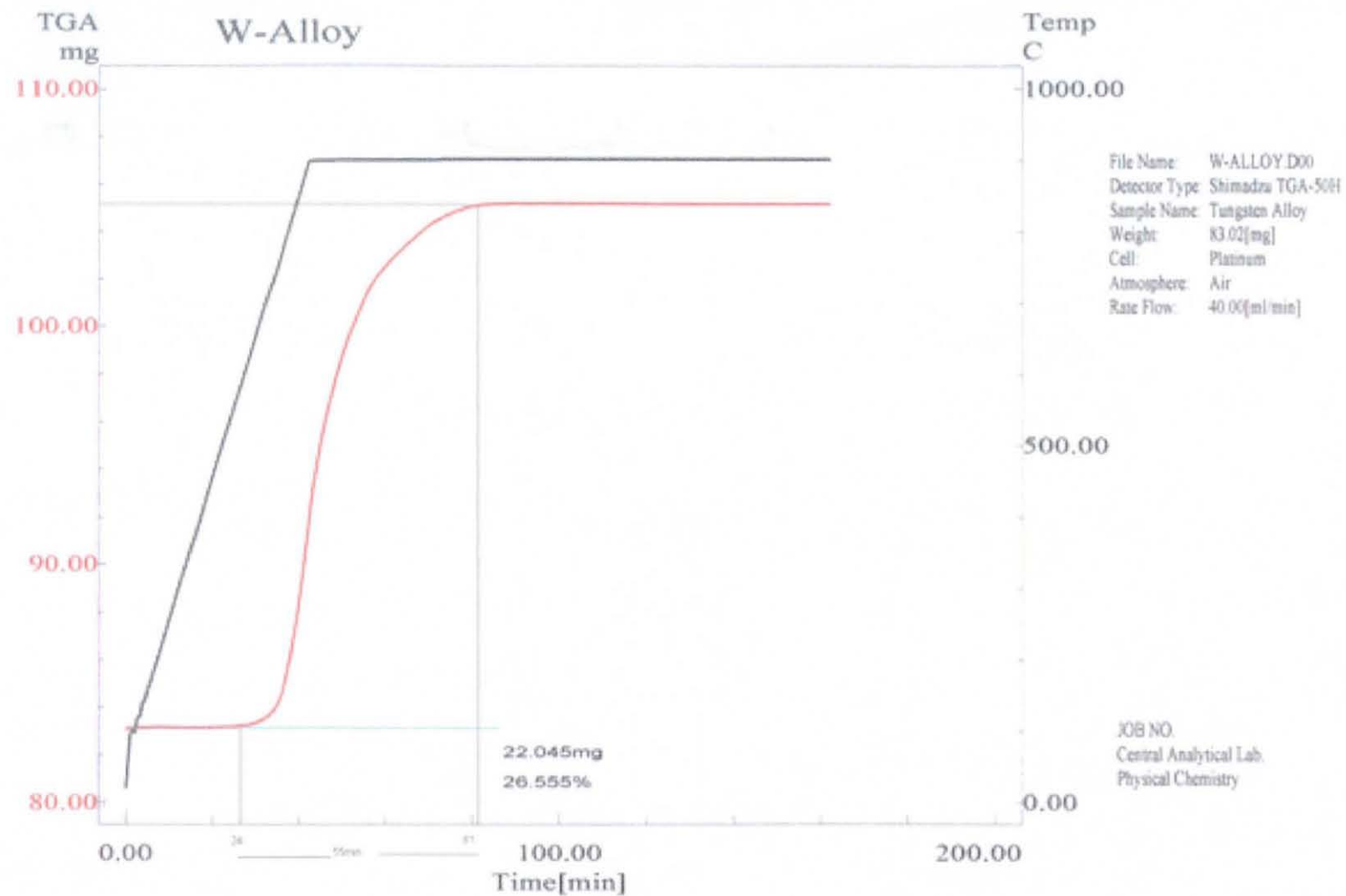


Figure 29 Oxidation of tungsten alloy at 900°C for 3 hrs.

77

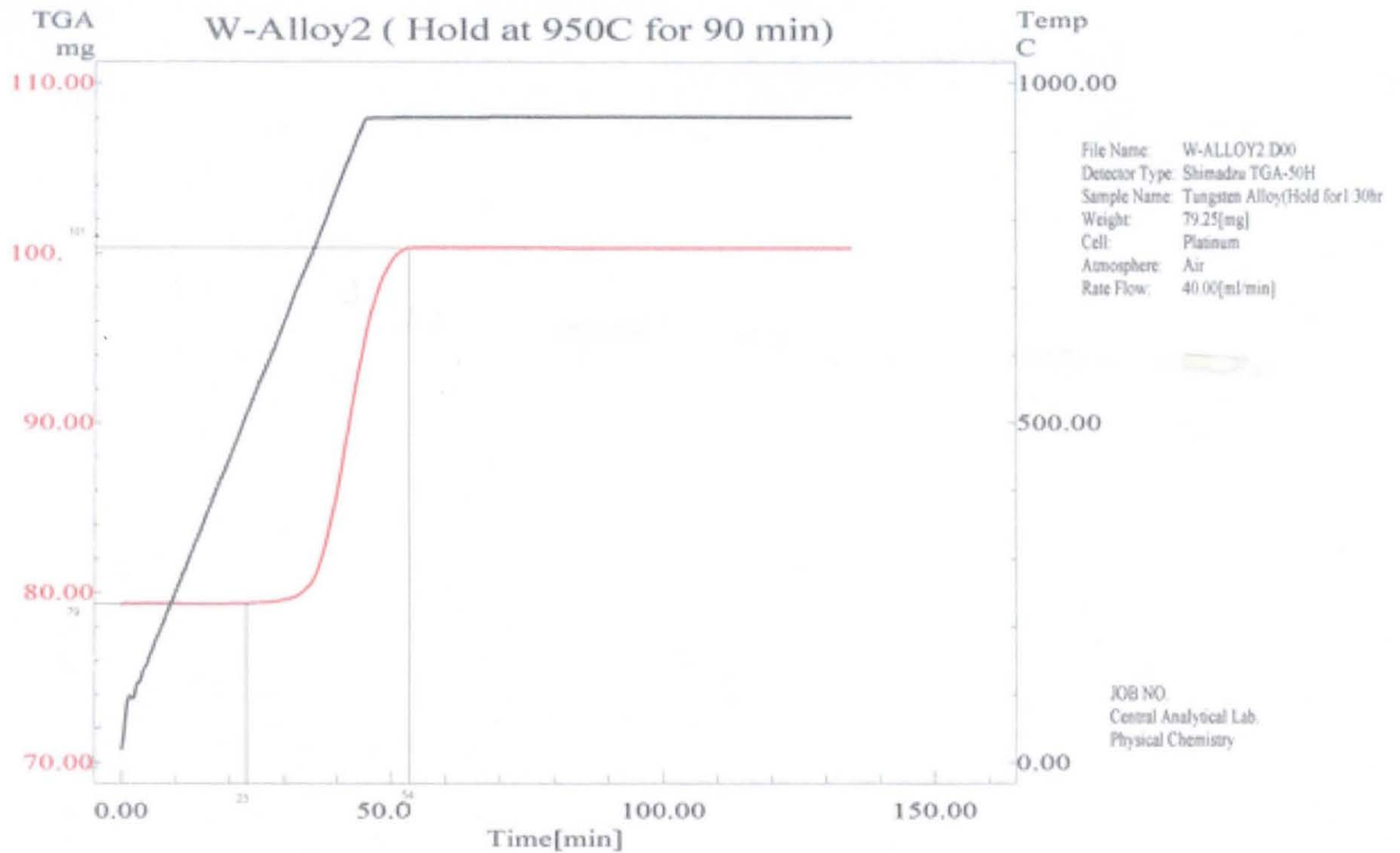


Figure 30 Oxidation of tungsten alloy at 950°C for 1.5 hrs.

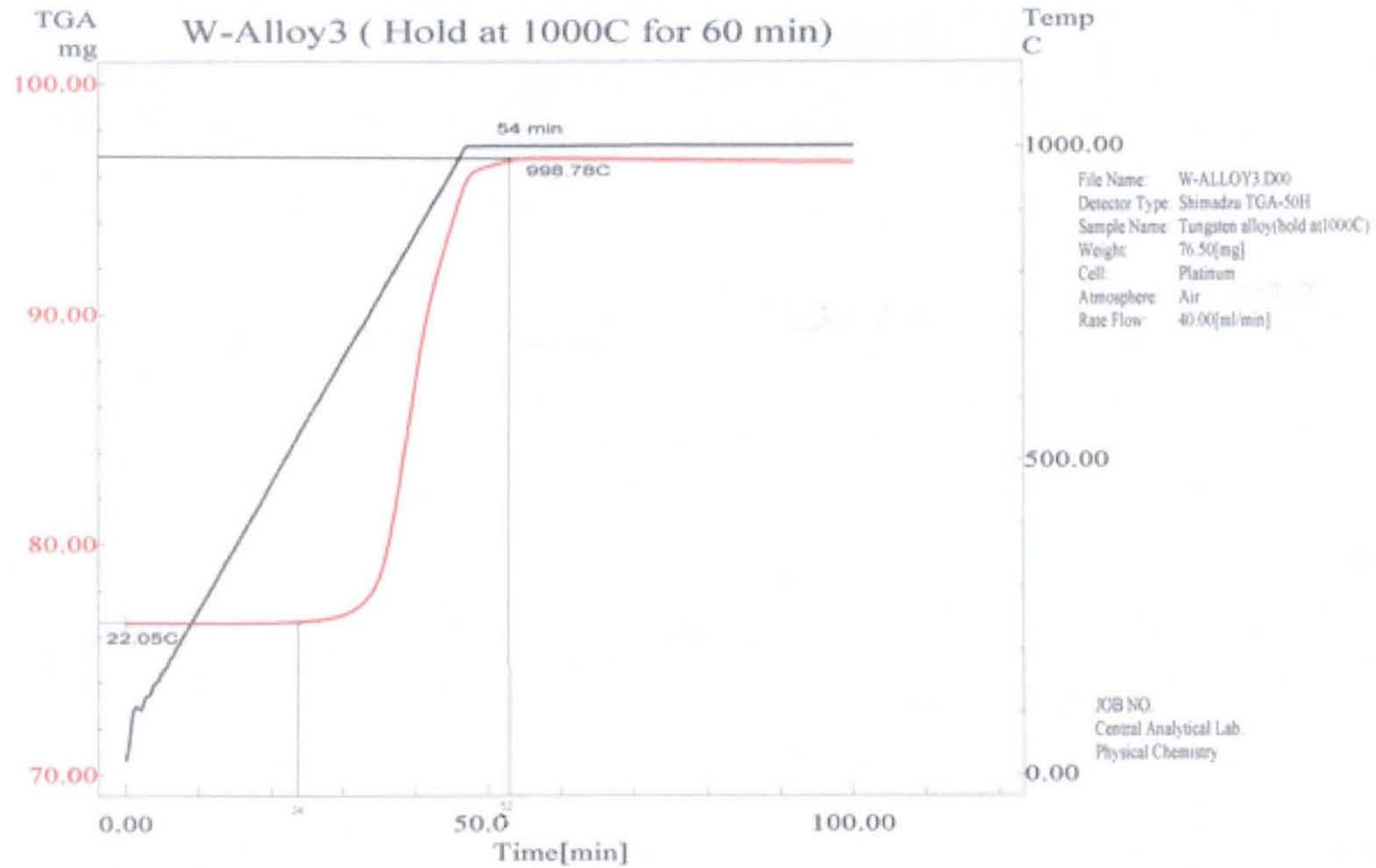


Figure 31 Oxidation of tungsten alloy at 1000°C for 1 hrs.

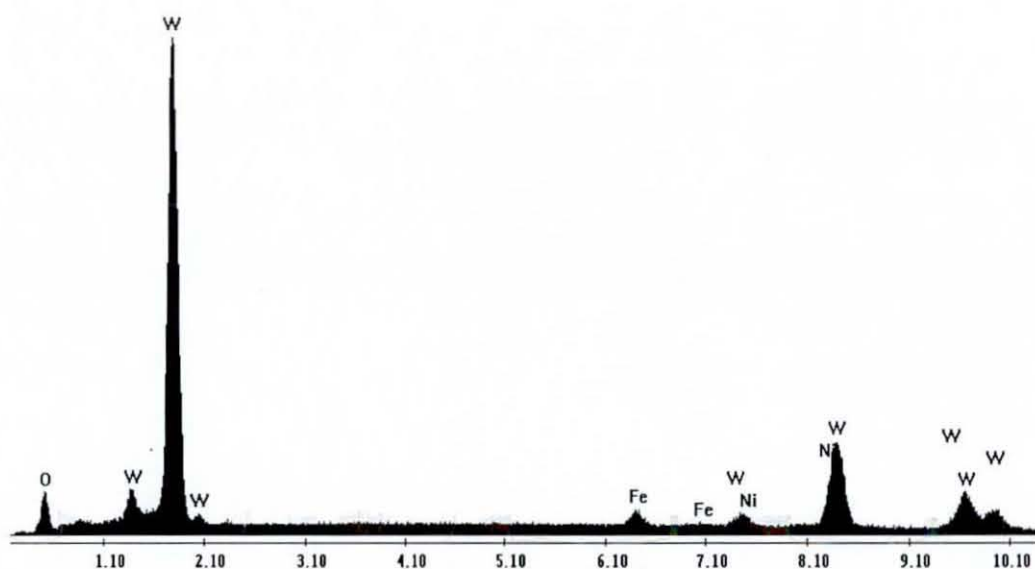


Figure 32 EDAX analysis for the W-oxide after oxidation at 1000°C.

4.3.2 X-ray diffraction

Figures 33, 34, and 35 show the X-ray diffraction (XRD) analysis for the oxide powder after oxidation at 900°C, 950°C, and 1000°C. The only peaks observed on this figure are associated with the oxide materials WO_3 , and Fe_2O_3 , and Fe_3O_4 which confirms full oxidation of the sample. It was observed that the samples yielded similar results at all temperatures (i.e., tungsten oxide and iron tungstate).

The tungsten content was 95.4% as calculated previously in the starting alloy and the matrix that comprised the remaining 4.6% contained 15% W and 85% other alloying elements. Thus, it is not surprising that evidence of some additional oxidised products was not observed, since the oxides were likely to be at levels lower than the detection limit of XRD. Also, there is evidence that NiO partially dissolves in W at 800-900°C (Yuehui et al, 2005, and Yih and Wang, 1979).

For all quantities of swarf, a 3 hour oxidation period was selected to ensure that complete oxidation occurred. The full oxidation of these material was proved by the XRD data presented in Figures 33, 34, and 35.

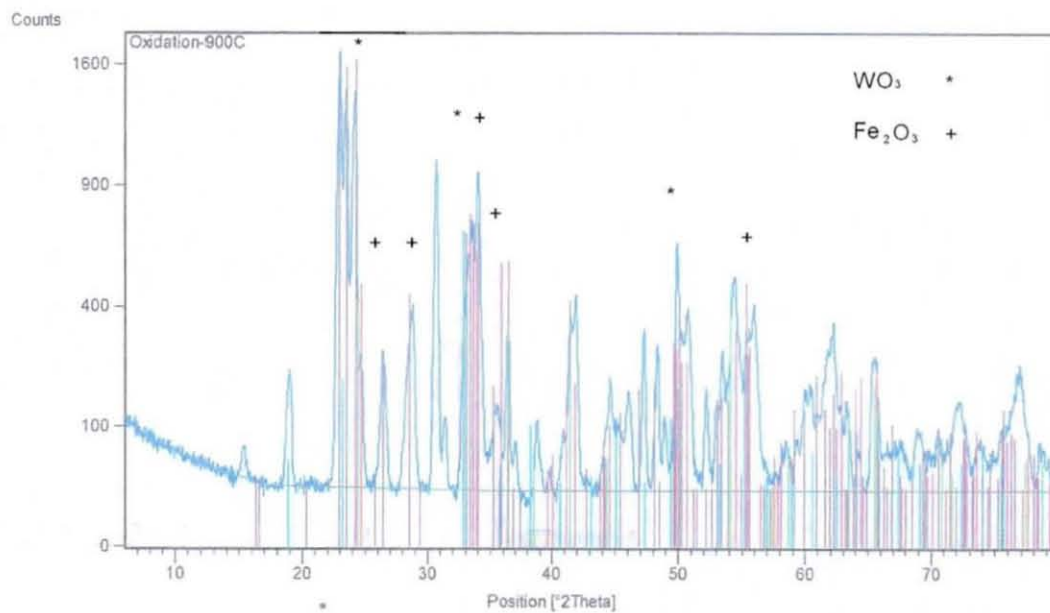


Figure 33 XRD analysis for the tungsten oxide at 900°C.

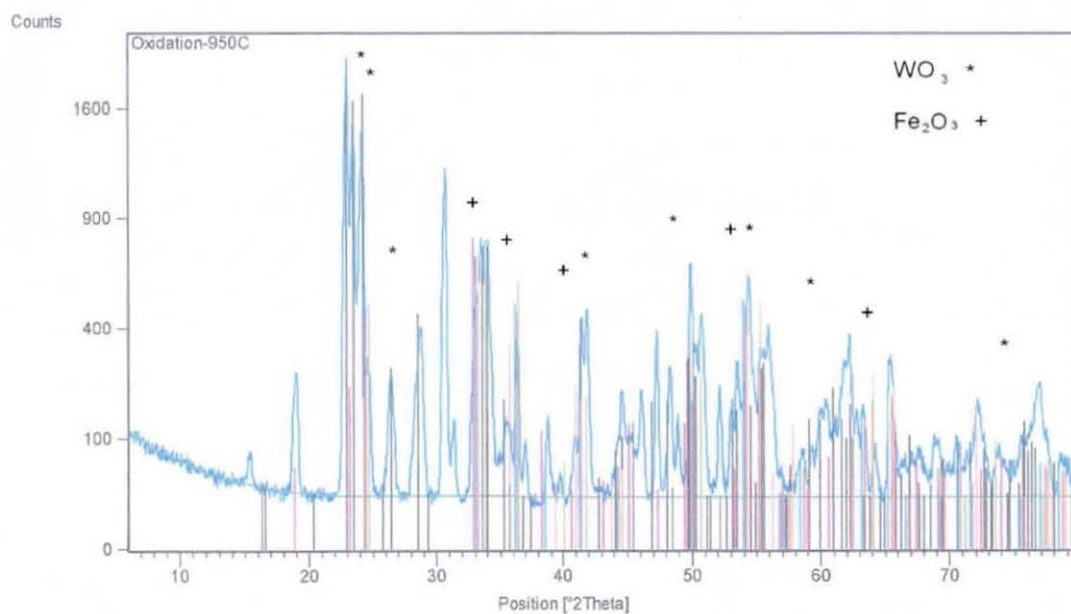


Figure 34 XRD for the oxide at 950°C.

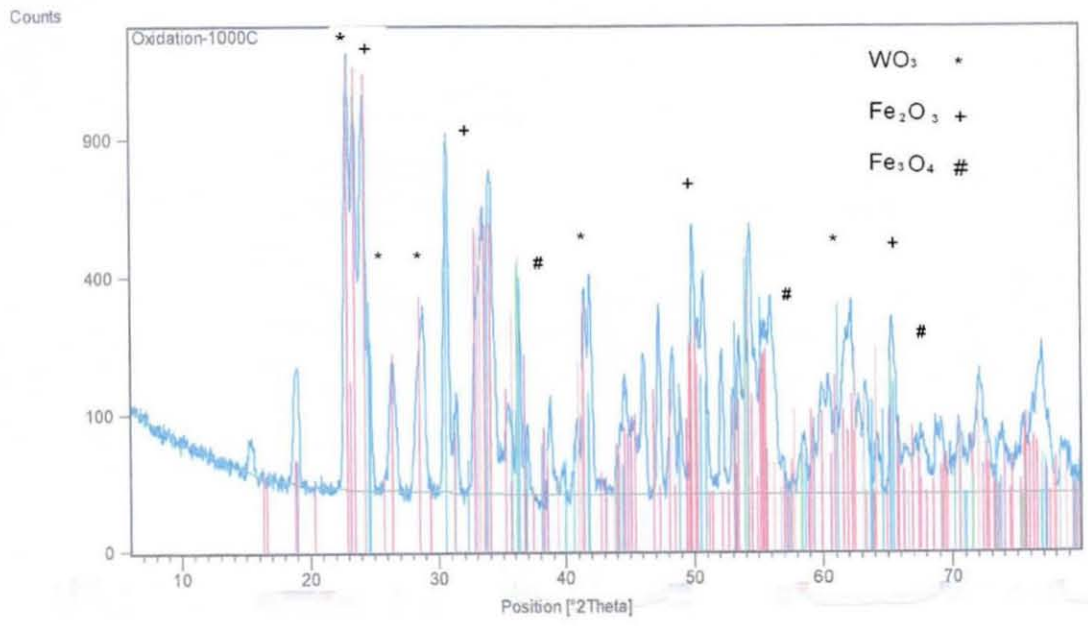


Figure 35 XRD analysis for the oxide at 1000°C

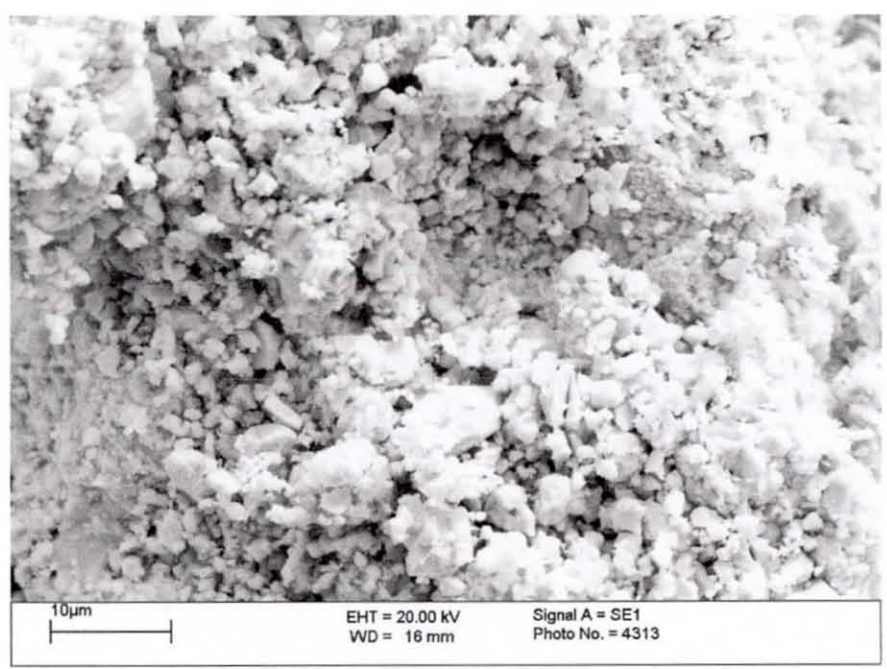


Figure 36 SEM image for the oxide after oxidation at 900°C.

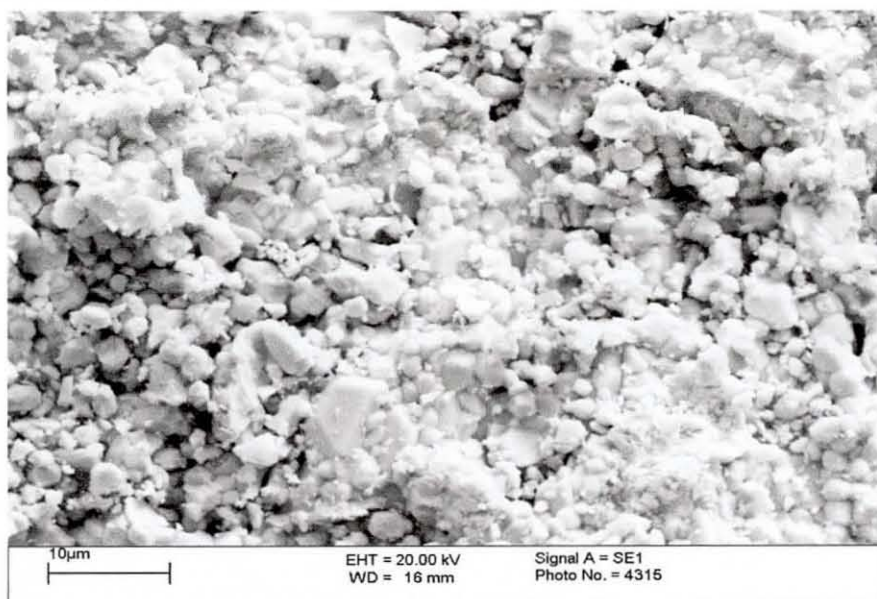


Figure 37 SEM image for the oxide after oxidation at 950°C.

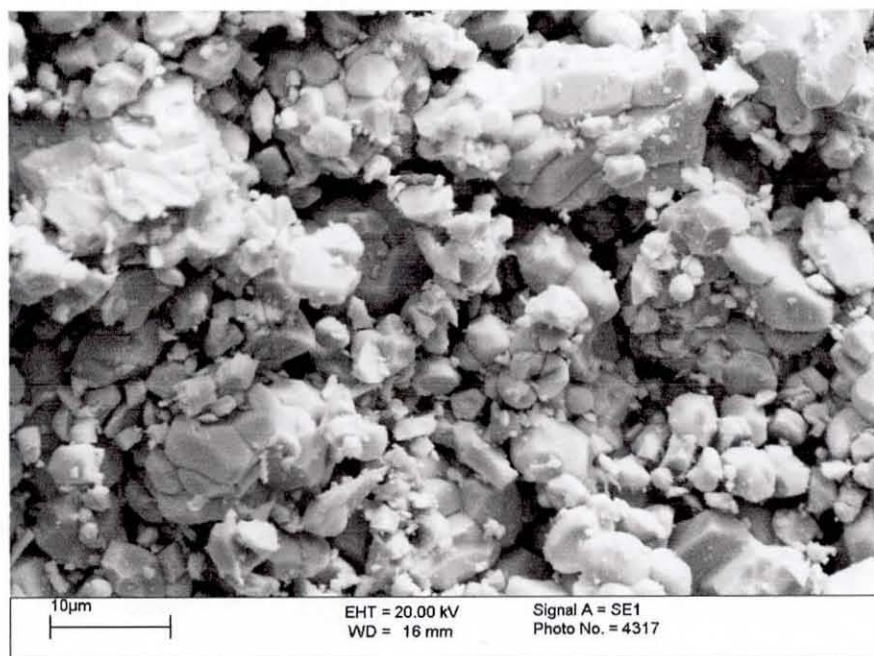


Figure 38 SEM image for the oxide after oxidation at 1000°C.

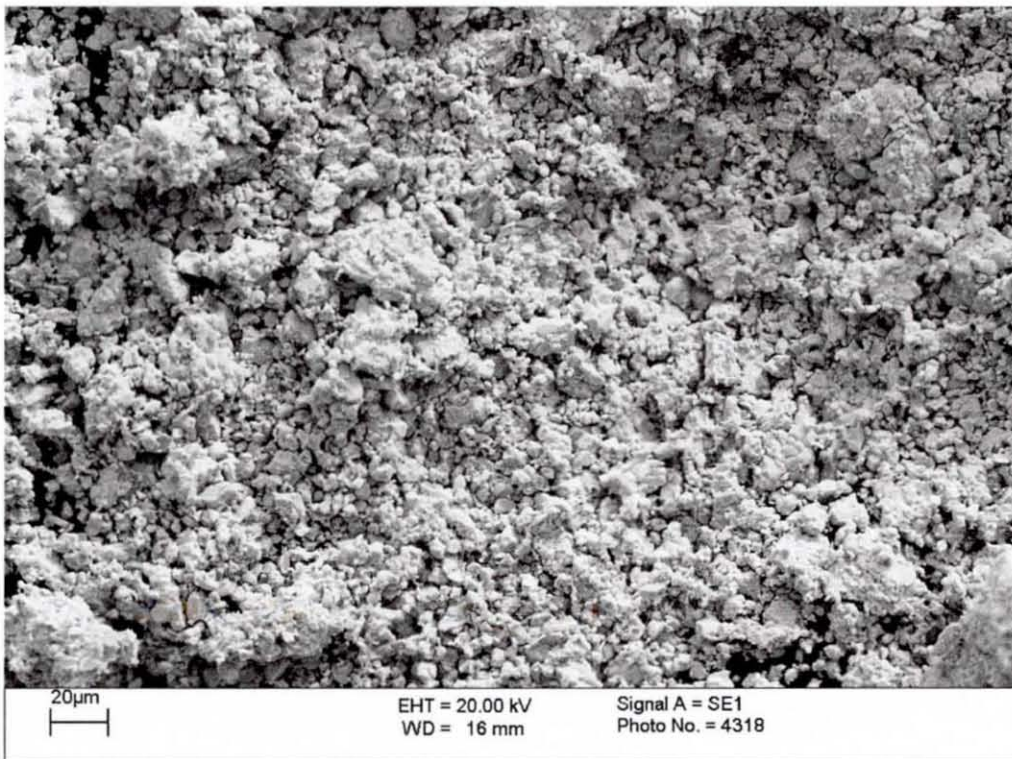


Figure 39 SEM image for the oxide powder at 1000°C.

4.3.3 Friability

In order to perform a fast check on the suitability of the oxide product for further processing, a simple finger friability test was carried out. The oxide obtained at higher temperatures was found to have more friability and larger particles as shown in Figures 25 and 26. However, in the first oxidation process the powder was sometimes found to be not fully oxidized. The friability test was carried out after the oxidation of the larger amounts of powder in the carbolite furnace.

4.4 Reduction Process

4.4.1 Furnace

Due to the danger of the hydrogen ignition in the TG instrument the reduction time study could not be done in this research work. The reduction study was carried out for all the oxide powder results from the oxidation process and the best results obtained

were for the oxides powders processed at temperatures 950°C where the results was discussed and further pressing and sintering is performed.

The furnace used in the reduction process was a Vecstar furnace with a gas supply system in order to reduce larger quantities of the oxide which could not be done in the TG instruments. Based on previously published works by Schubert (1989), Pierre et al (1962), Charlton (1954), and Hougen et al (1956), the temperature used for the reduction was 800°C.

Based on the morphological study and XRD analysis, it was decided to produce the oxide material at the higher temperatures (900-1000°C), but using a three hour period. On this basis, assuming that the three hour period was necessary because of mass transfer limitations, it was decided to use a three hour reduction period within this study.

4.4.2 X-ray Diffraction

X-ray diffraction analysis was necessary to prove that the reduction of the oxide was complete. In Figure 40 the powder is not fully reduced, in this spectrum, four types of peaks were found for WO_3 , WO_2 , $FeWO_4$, and W, which give a good agreement with the phase diagram presented by Pierre (1962). According to this phase diagram, the reaction sequence that takes place was:



The result in Figures 40 and 41 proved that the reduction process was in the final stages. It also showed that the rate-determining step in the reduction process was either $WO_3 \rightarrow WO_{2.72}$ or $WO_2 \rightarrow W$, because of the absence of $WO_{2.72}$ in the partially reduced product, i.e. as soon as $WO_{2.72}$ was produced it was further reduced to WO_2 . The appearance of $FeWO_4$ in the partially reduced product is interesting, when this phase could not be detected in the fully oxidized sample.

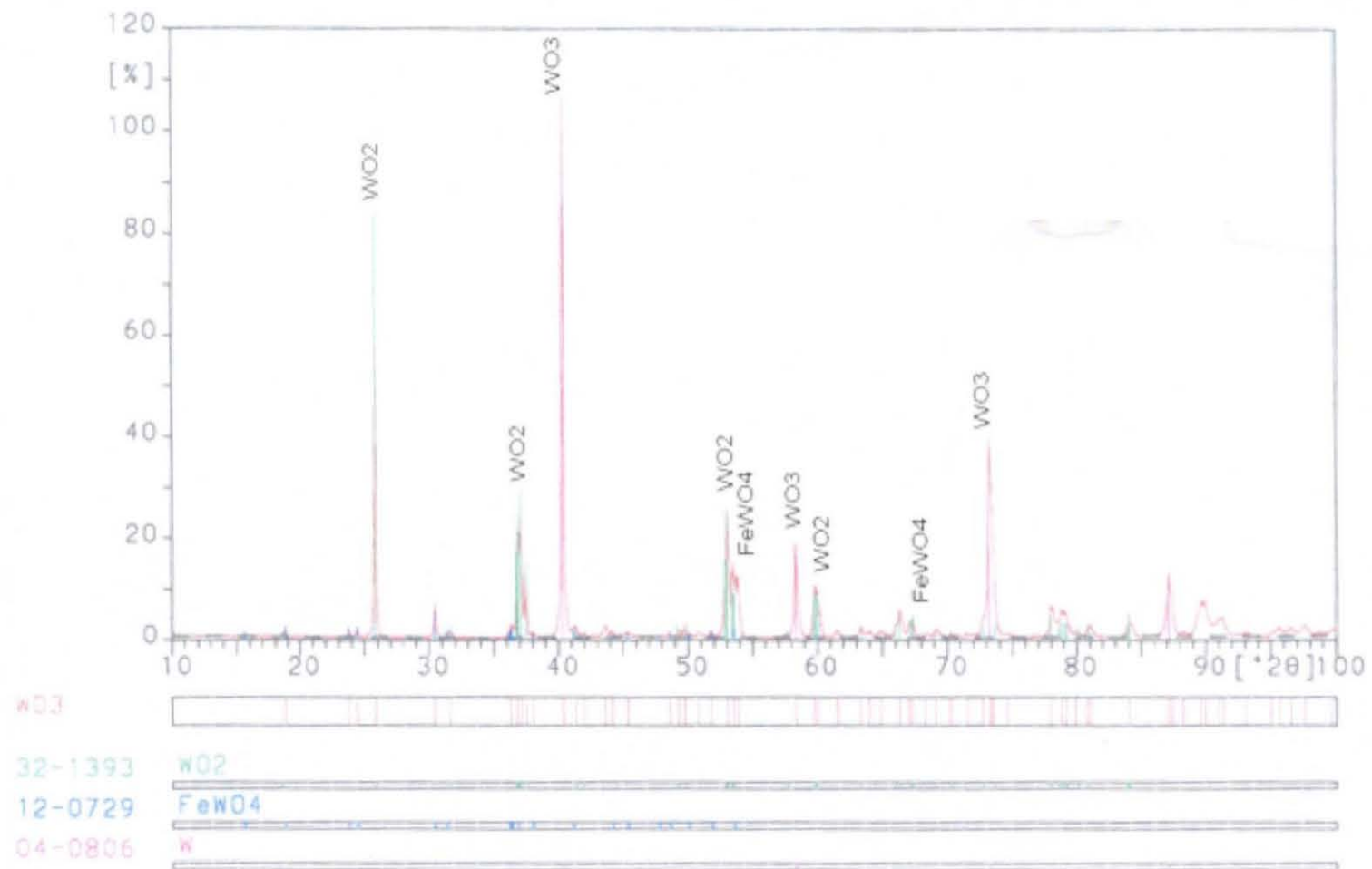


Figure 40 XRD for not fully reduced powder.

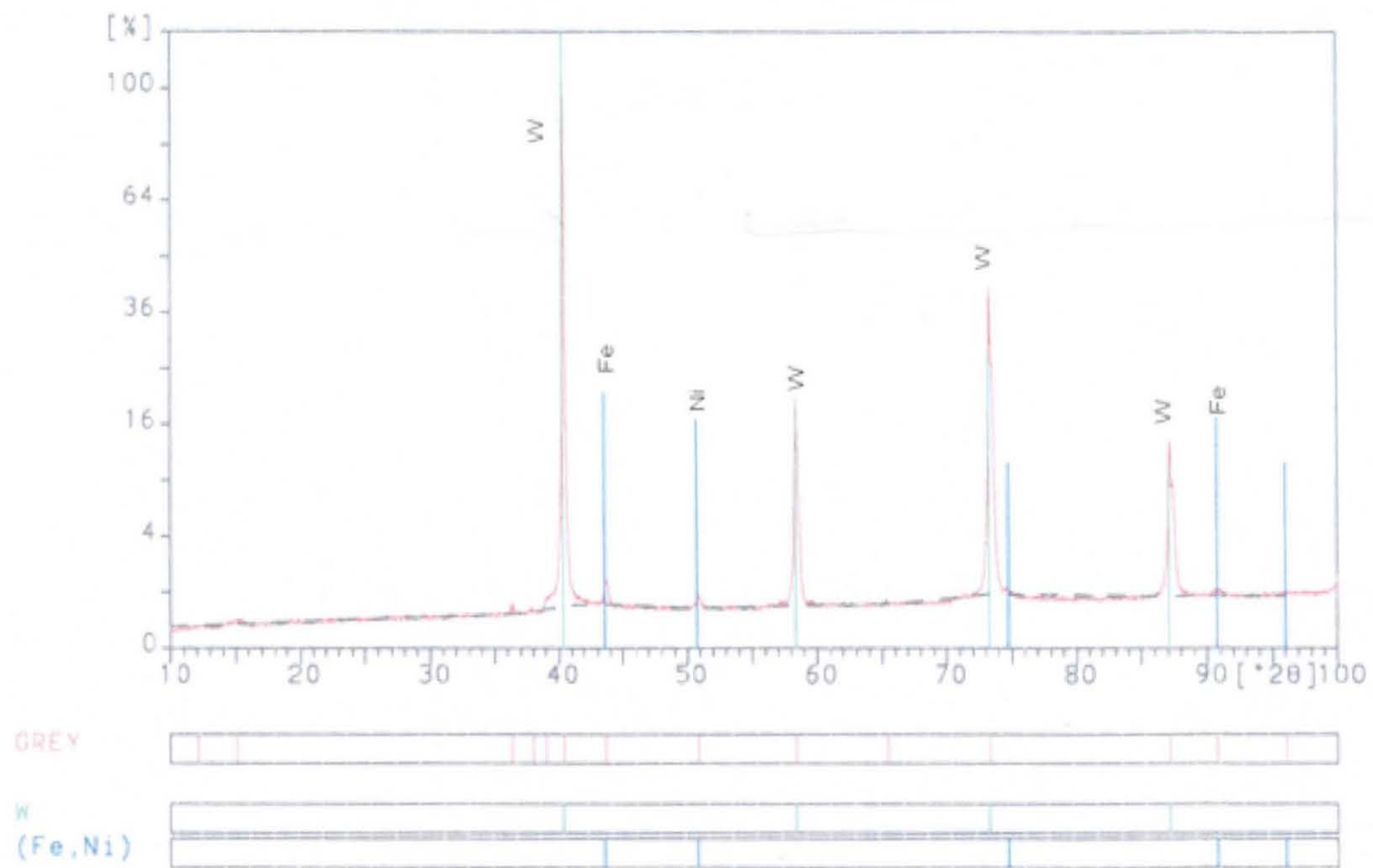


Figure 41 Fully reduced powder.

In order to complete the reduction, the process was carried out for three hours. The XRD data for a product obtained after three hours are shown in Figure 41. In this spectrum two types of peaks are present namely, W and a mix of Fe and Ni, and there was no evidence of any oxide in the material.

4.4.3 Scanning Electron Microscopy

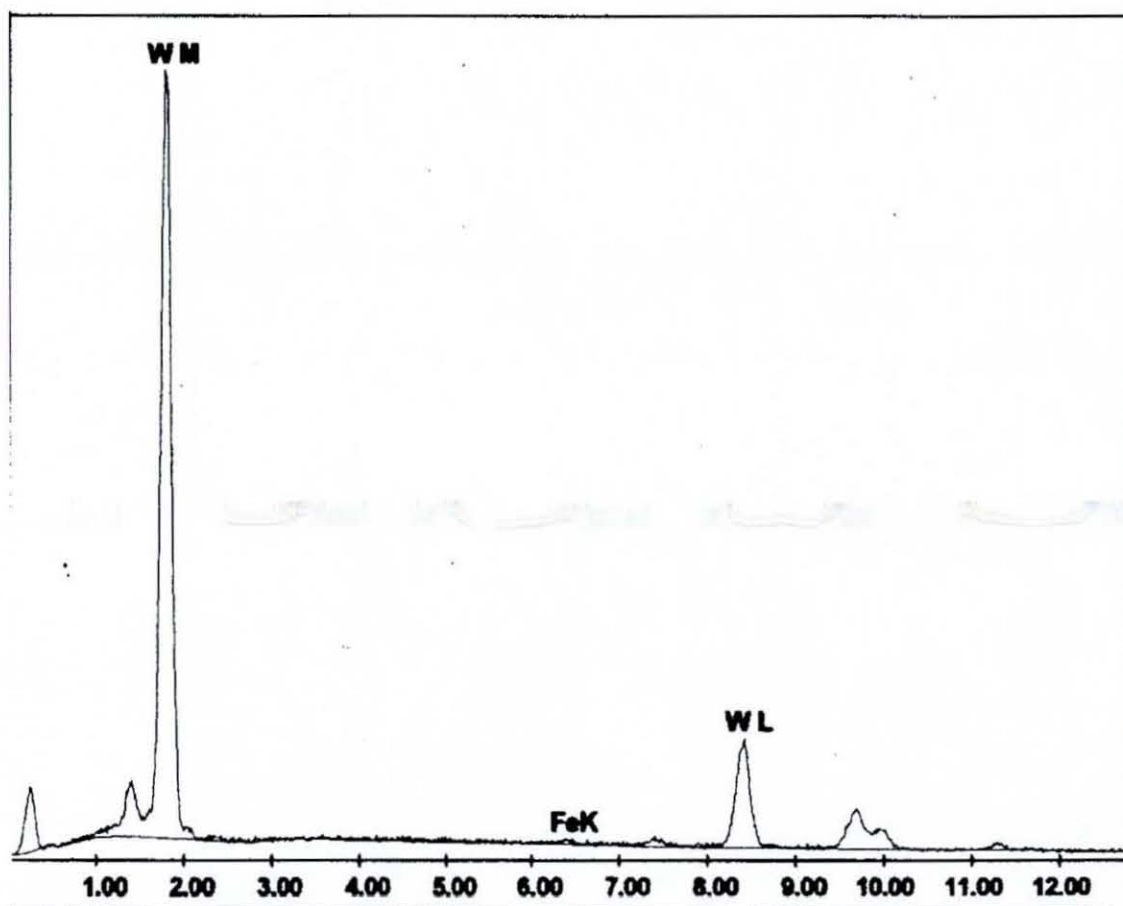
The EDS analysis data of the powder produced by reduction at 800°C in dry hydrogen atmosphere for three hours is shown in Figure 42. This spectrum showed a tungsten peak and a very small Fe peak. The quantitative analysis carried out in Figure 42 showed 0.77% of the Fe, which is just close to the claimed detection limit of the technique, and 99.23% tungsten. The Ni was not detected by EDAX due to the fact that Ni is partially soluble in tungsten (Lassner and Schubert, 1999) and its very small concentration.

4.4.4 Reduction Behaviour

Iron tungstate, FeWO_4 , shows intermediate reduction behaviour which eventually produces a mixture of tungsten and tungsten alloys. It is likely that any Fe_2O_3 formed in the fully oxidized product is reduced to FeO in the initial stages of reduction. It would appear that the FeO can react with residual WO_3 to produce the tungstate FeWO_4 at a stage in the reduction.



The quantitative analysis in Figure 42 shows that the iron Fe content is 0.77% which is less than the starting material. This is may be because the Fe is partially soluble in W as well as W is soluble in Fe during the reduction process which agrees with Geller et al (1977). Also the absence of the Ni in this analysis may add the quantity of Ni content to the W because of the solubility and the analysis calculation method which was mentioned previously.



**EDAX ZAF Quantification (Standardless)
Element Normalized**

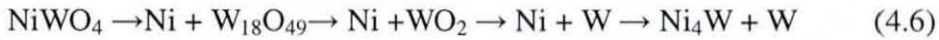
Element	Wt %	At %	K-Ratio	Z	A	F
FeK	0.77	2.50	0.0091	1.2382	0.8988	1.0578
W L	99.23	97.50	0.9894	0.9974	0.9997	1.0000
Total	100.00	100.00				

Element	Net Inte.	Bkqd Inte.	Inte. Error	P/B
W M	493.25	13.24	0.42	37.25
FeK	3.83	11.07	9.19	0.35
W L	93.41	8.06	0.98	11.59

Figure 42 EDS analysis for the reduced powder.

Also the nickel tungstate NiWO_4 level has been decreased to below that which is detectable, but evidence of the presence of Ni is there in XRD diagram, Figure 41. The reduction behaviour of the nickel tungstate can be predicted to start with a

mixture of nickel and $\text{WO}_{2.72}$ and this leads to the formation of WO_2 and ultimately tungsten metal which then react with nickel to form an alloy based on the formula Ni_4W , according to Basu and Sale (1978).



4.5 Pressing and Sintering

After the reduction of the oxide was completed and the XRD analysis showed the full reduction of the material Figure 41, the powder was prepared for pressing and sintering.

The reduced powder was pressed under a pressure of 20 Kg/cm^2 using a 3.5 mm single-action die. Based on a previously published paper (Albiston and Sale, 1986), a sintering temperature of 1150°C was used for all the compacted materials. The sample was placed in the furnace for three hours at a temperature 1150°C under a dry hydrogen atmosphere to prevent re-oxidation of the material.

Figures 43, 44, and 45 shows the compacted and sintered material obtained from the fully reduced powders. The micrograph shows that a microstructure with a very small grains (3- $5\mu\text{m}$), however some of the grains of the tungsten have taken the same shape and size (10-20 μm) as the undeformed grains in the starting material Figure 17. These are likely enlarged during the sintering process, where the prolonged sintering under dry hydrogen leads to swelling of the parts and significant embitterment (German and Churn, 1984).



Figure 43 Micrograph for the compacted pellet ×1000.

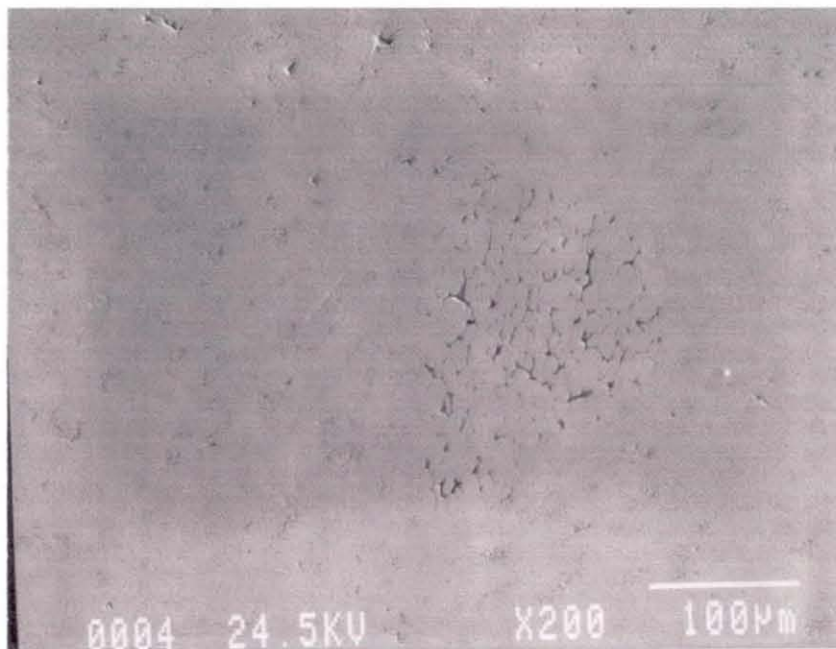


Figure 44 Micrograph for the compacted pellet ×400

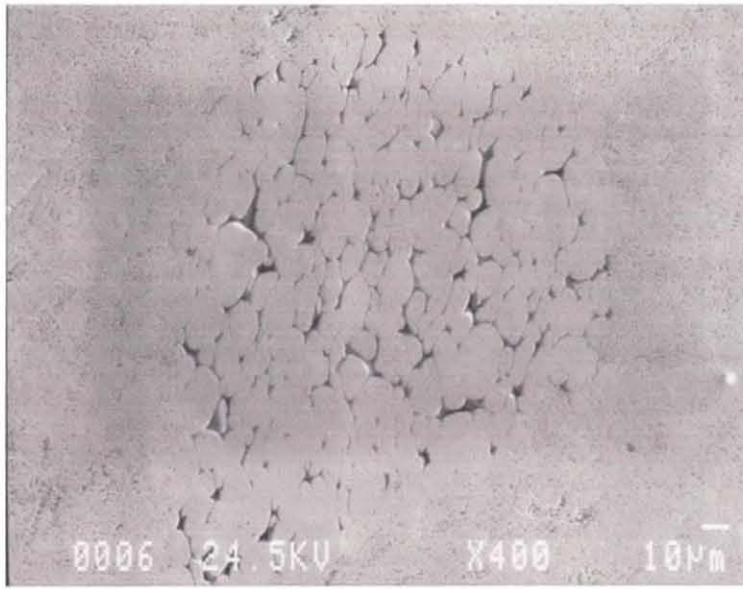


Figure 45 Enlarged grains in some region ×400.

A further pressing and sintering is performed on the not fully reduced powder. The aim of this process was to test if it could be fully reduced during the sintering process since the sintering process is carried out in dry hydrogen atmosphere. The micrographs and XRD analysis revealed that the sample is not fully reduced and the correct microstructure had not been obtained.

The EDS analysis for the final pellet showed only a tungsten peak Figure 46. Whereas the EDS analysis of powder obtained from the reduced process showed in Figure 42 the main elements W, Fe and a very small peak related Ni. It is noticed that in the final pellet there was no evidence of Fe and Ni this is because at the sintering process the Fe and Ni partially melt to form the matrix in the heavy alloy material since the melting points for Fe and Ni is close to the sintering temperatures.

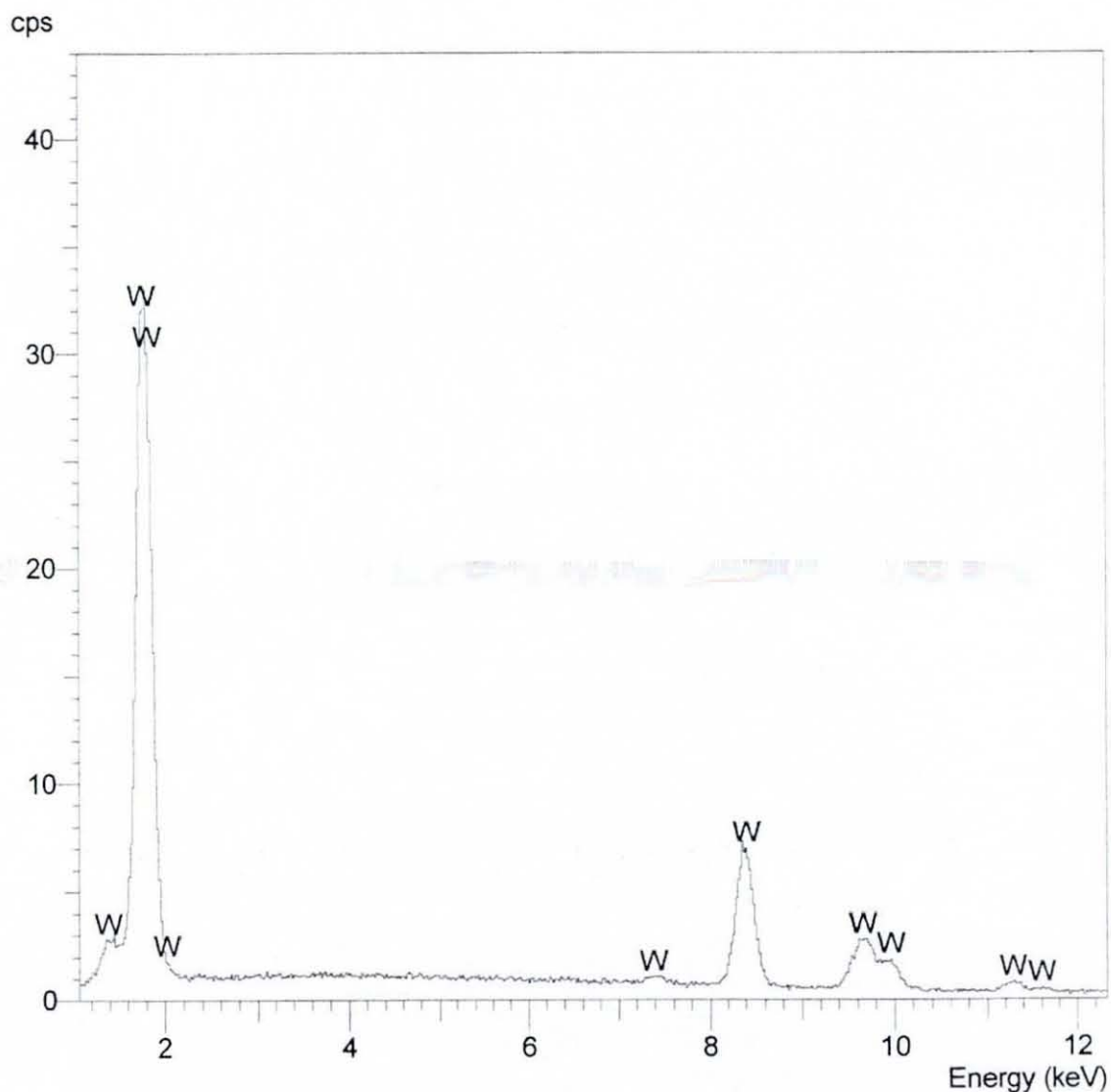


Figure 46 EDS analysis for the final reduced pellet.

4.6 Failure analysis

4.6.1 Oxidation

In the first experiment at temperature 750°C, the oxidation process was initially not completed because sample was placed in a way where the thickness is more than (2 mm) since the increase in the sample thickness will increase the diffusion resistance (Lassner and Schubert, 1999). The oxide powder was not fully oxidized where some of the tungsten swarf was still partially in a metal form as shown in Figure (47 and 48).

Furthermore, the reduction experiments carried out for the oxide at lower temperatures (750°C, 800°C and 850°C) shows a coarse powder as shown in Figures 25, and 26 . Figure 40 shows the XRD analysis for the not fully reduced powder.

Although, nitrogen is not a reducing agent, a reduction experiment was conducted by the TGA in nitrogen atmosphere since the nitrogen is a very safe substance to use under high temperatures. The results are presented in the appendix were not convincing and does not give a uniform reduction manner.

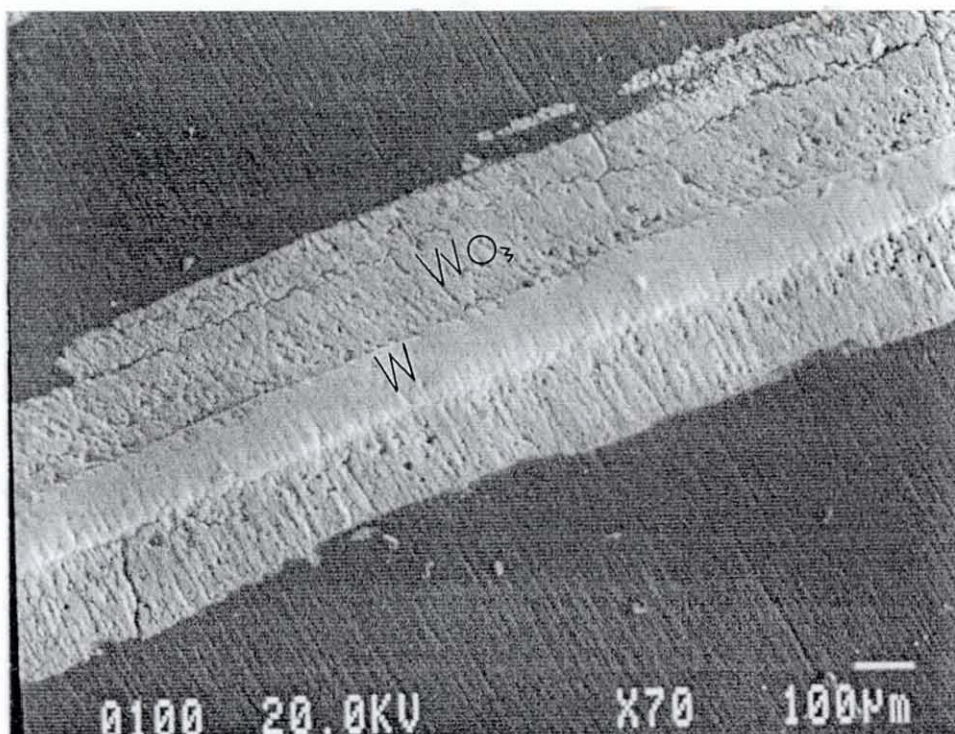


Figure 47 not fully oxidized tungsten alloy.

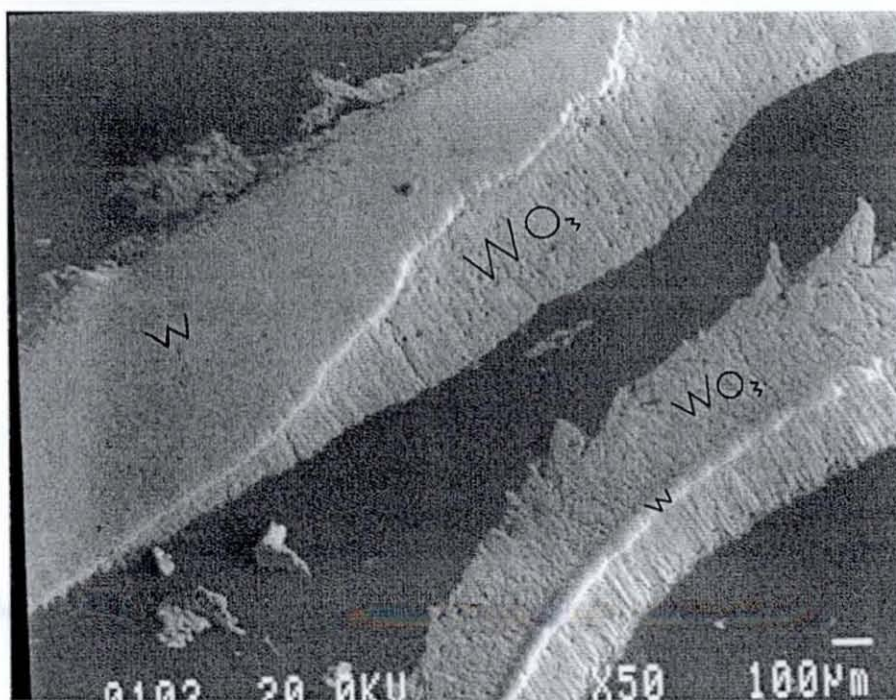


Figure 48 not fully oxidized tungsten alloy.

5 Chapter **5** Mathematical correlation and Modeling

5.1 Introduction

High temperature oxidation of tungsten was run under different temperatures to cover the oxidation rate between temperatures 750 and 1000°C. The correlation was developed for the temperatures to find an equation for the relation between time and weight. Furthermore, a diffuse interface model (DIM) is introduced to describe the high temperature internal oxidation. The zone has dissolved oxygen and metal atoms diffuse and react resulting in the inward movement of zone. The high temperature oxidation data for tungsten have been analysed using a nonlinear optimization method to obtain the optimal values for different parameters.

5.2 Mathematical Correlation

A data set was compiled, covering the effect of oxidation rate with respect to temperature (750°C to 1000°C) and the time taken for full oxidation. Figures 24, 27, 28, and 29 illustrate that, for a range of temperatures, the oxidation rate follows a similar pattern but that, if a different quantity of swarf were used, the rate could become dependent on both time and temperature.

To calculate a fitting equation for the oxidation curves a data fit for all temperatures is shown Figures 49-54, where in all figures time is in minutes and weight in mg. for all the oxidation curves. Also, a calculation for unknown parameters (A, B, C factor, and \bar{t}) has been performed to complete all the parameters in the equation.

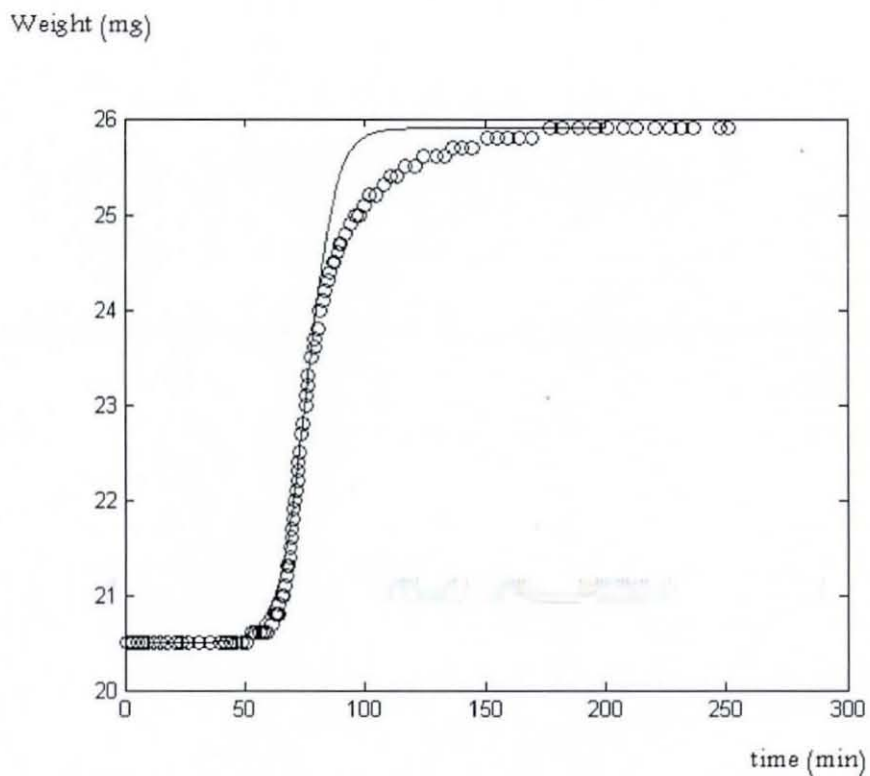


Figure 49 curve fit for oxidation at 750°C.

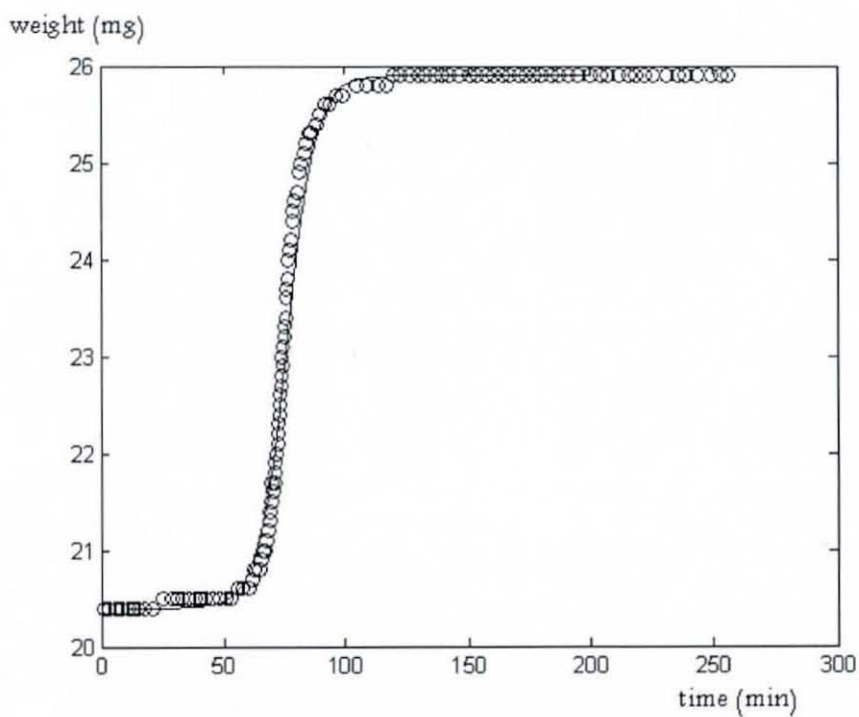


Figure 50 Curve fit for Oxidation at 800°C.

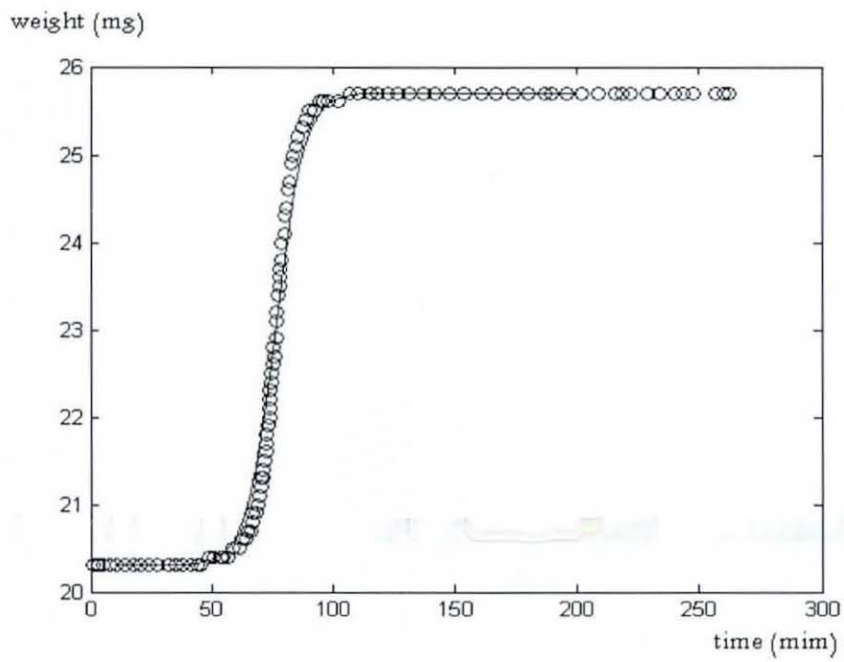


Figure 51 Curve fit for Oxidation at 850°C.

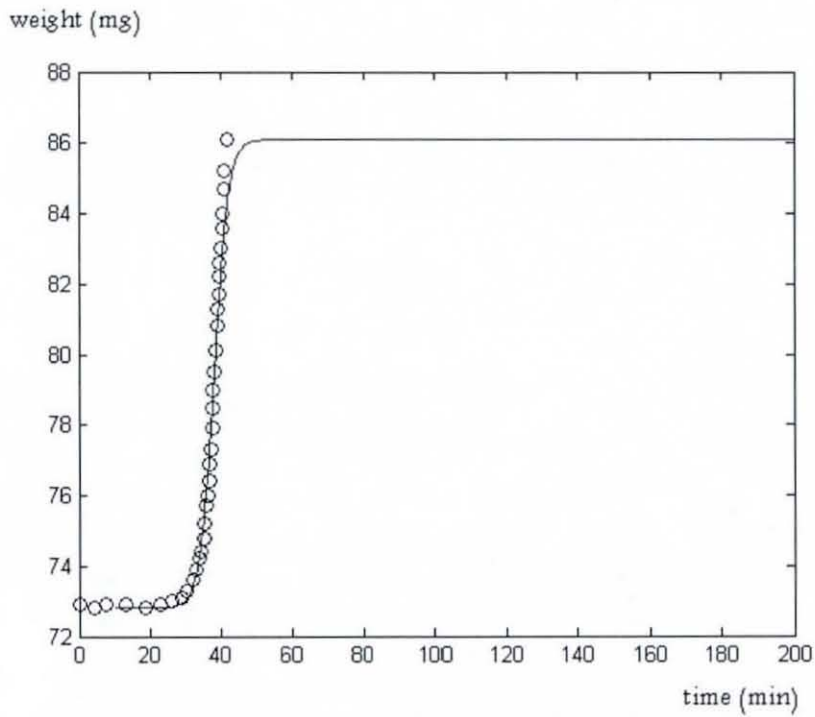


Figure 52 Curve fit for Oxidation at 900°C.

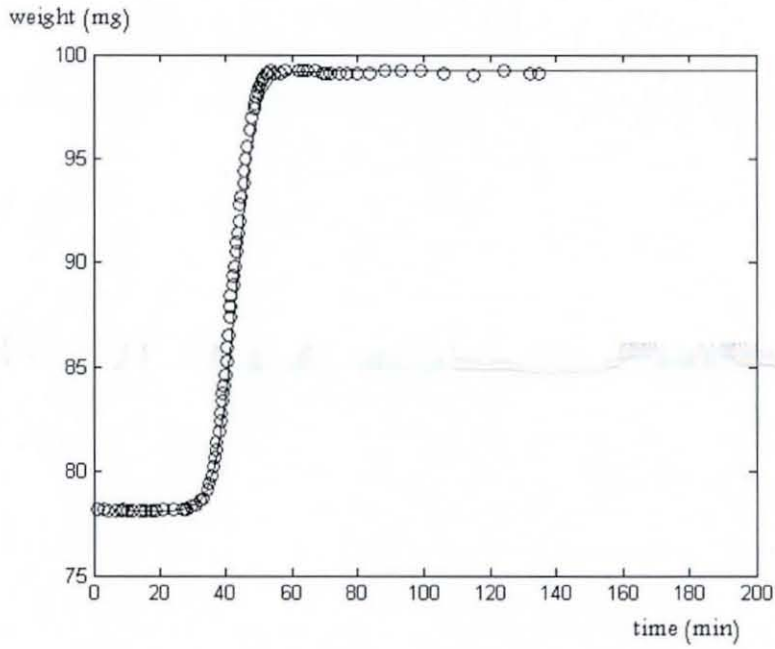


Figure 53 Curve fit for Oxidation at 950°C.

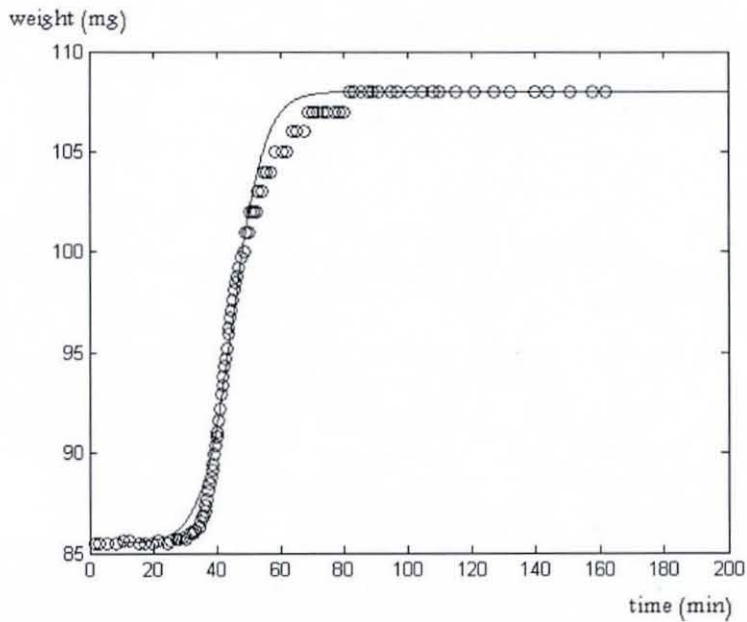


Figure 54 Curve fit for Oxidation at 1000°C.

The calculation for the un known parameters is been done by MAPLE programme, and is presented.

For As

$$y := AI - \frac{BI}{1 + e^{(CI(x-D1))}} + \frac{1}{200} e^{(13f - 1.7f^2 - 2.9f^3)}$$

$$f := \frac{x}{250} - 3$$

$$Y = AI - \frac{BI}{1 + e^{(CI(x-D1))}} + \frac{1}{200} e^{\left(\frac{13x}{250} - 39 - 1.7\left(\frac{x}{250} - 3\right)^2 - 2.9\left(\frac{x}{250} - 3\right)^3\right)}$$

$$AI := 85.4$$

$$BI := 60.4$$

$$CI := 0.15$$

$$D1 := 880$$

$$85.4 - \frac{60.4}{1 + 0.47111165802 \cdot 10^{-57} e^{(0.15x)}} + 0.1324456106 \cdot 10^9 e^{(-0.2204000000x)} e^{(0.0003904000000x^2)} e^{(-0.1856000000 \cdot 10^{-6} x^3)}$$

For Bs

$$y := AI - \frac{BI}{1 + e^{(CI(x-D1))}}$$

$$f := \frac{x}{250} - 3$$

$$Y = AI - \frac{BI}{1 + e^{(CI(x-D1))}}$$

$$AI := 22$$

$$BI := 17$$

$$CI := 0.065$$

$$D1 := 900$$

$$Y = 22 - \frac{17}{1 + 0.3924395858 \cdot 10^{-25} e^{(0.065 x)}}$$

For Cs

$$y := AI - \frac{BI}{1 + e^{(CI(x-D1))}} - \frac{1}{2000} e^{(11.1f - 4.4f^2)}$$

$$f := \frac{x}{250} - 3$$

$$Y = AI - \frac{BI}{1 + e^{(CI(x-D1))}} - \frac{1}{2000} e^{\left(0.04440000000x - 33.3 - 4.4\left(\frac{x}{250} - 3\right)^2\right)}$$

$$AI := 0.585$$

$$BI := 0.415$$

$$CI := 0.2$$

$$D1 := 880$$

$$0.585 - \frac{0.415}{1 + 0.3665820411 \cdot 10^{-76} e^{(0.2x)}}$$

$$- 0.1093710228 \cdot 10^{-34} e^{(0.1500000000x)} e^{(-0.00007040000000x^2)}$$

For Ds = t⁻

$$y := AI - \frac{BI}{1 + e^{(-CI(x-D1))}} + \frac{1}{200} e^{(10.5f - 3f^4)}$$

$$f := \frac{x}{250} - 3$$

$$Y = AI - \frac{BI}{1 + e^{(-CI(x-D1))}} + \frac{1}{200} e^{\left(0.04200000000x - 31.5 - 3\left(\frac{x}{250} - 3\right)^4\right)}$$

$$AI := 76$$

$$BI := 40.5$$

$$CI := 0.2$$

$$D1 := 880$$

$$76 - \frac{40.5}{1 + 0.2727902319 \cdot 10^{77} e^{(-0.2 \cdot x)}} + 0.3055868923 \cdot 10^{-121} e^{(1.338000000 \cdot x)} e^{\left(-\frac{3 \cdot x^4}{3906250000}\right)} e^{\left(\frac{9 \cdot x^3}{3906250}\right)} e^{\left(-\frac{81 \cdot x^2}{31250}\right)}$$

For each temperature, a number of points were recorded from the measured oxidation curve. The shape of the curves is well represented by the following equation:

$$W = A - \frac{B}{1 - \exp C \times (t - \bar{t})}$$

where W is the mass of the alloy (gram), t is the heating time (minutes), A is the maximum mass of alloy produced at full oxidation (gram), C is a factor related to the rate of mass change in the sample at 50% tungsten to tungsten oxide conversion, and \bar{t} is the oxidation time (minute) that corresponds to 50% conversion. B , given by A minus the initial mass of tungsten, is equal to $0.26 M_i$, where M_i is the initial mass found by

$$B = A - M_i \quad ; \text{ where } \frac{M_i}{A} = \frac{79}{100} \text{ as shown in Table 1}$$

$$A = \frac{M_i}{0.79} = 1.26 M_i$$

$$B = A - M_i = 1.26 M_i - M_i = 0.26 M_i$$

The experimental values obtained for A , B , C , and \bar{t} are shown in Table 5. An increase in the alloy mass is observed during the oxidation process, which is expressed by

$$\frac{A \times B}{A}$$

These data show that the mass percent is between 78.73% at 950°C and 84.55% at 900°C, Furthermore, the oxidation time at 900°C is a minimum of 38 minutes Figure 56, which gives the maximum C factor of 0.5 as presented in Figure 45.

$$\text{From the first equation } W = 1.26M_i - \frac{0.26M_i}{1 - \exp C \times (t - \bar{t})}$$

$$W = M_i \times \frac{1.26(1 - \exp(C \times (t - \bar{t})) - 0.26)}{1 - \exp C \times (t - \bar{t})}$$

$$W = M_i \times \frac{1.26\{(1 - \exp C(t - \bar{t})) - 1\} + 1}{1 - \exp C(t - \bar{t})}$$

$$W = M_i \times \frac{\{(1 - \exp C(t - \bar{t})) - 1\} + 0.79}{1 - \exp C(t - \bar{t})}$$

$$W = M_i \times \frac{0.79 - \exp C(t - \bar{t})}{1 - \exp C(t - \bar{t})}$$

$$W = M_i \times \frac{1 - 0.26 \exp C(t - \bar{t})}{1 - \exp C(t - \bar{t})}$$

$$\text{And finally } W = M_i \left(\frac{1 - 0.2 \exp(t - \bar{t})}{1 - \exp(-c(t - \bar{t}))} \right)$$

Using MAPLE program methods, the previous mathematical equation was obtained for the weight vs. temperature relationship, according to Table 5.

Table 5 Values of the equation parameters obtained at each temperature

Temperature °C												
	750°C		800 °C		850 °C		900 °C		950 °C		1000 °C	
	calc.	Exp.	calc.	Exp.	calc.	Exp.	calc.	Exp.	calc.	Exp.	calc.	Exp.
A	25.9	25.8	25.9	25.9	25.7	25.7	86.1	105.2	99.2	100.2	108	97
B	5.4	5.4	5.5	5.5	5.4	5.4	13.3	22	21.1	21	22.5	20.5
C	0.2	0.25	0.2	0.25	0.2	0.3	0.5	0.25	0.3	0.38	0.2	0.2
\bar{t}	76	78	76	73	76	78	38	45	43	43	45	40

Using this equation, an oxidation curve and C-factor were obtained over a temperature range of 750°C to 1000°C, as shown in the following graphs Figure 55 and 56.

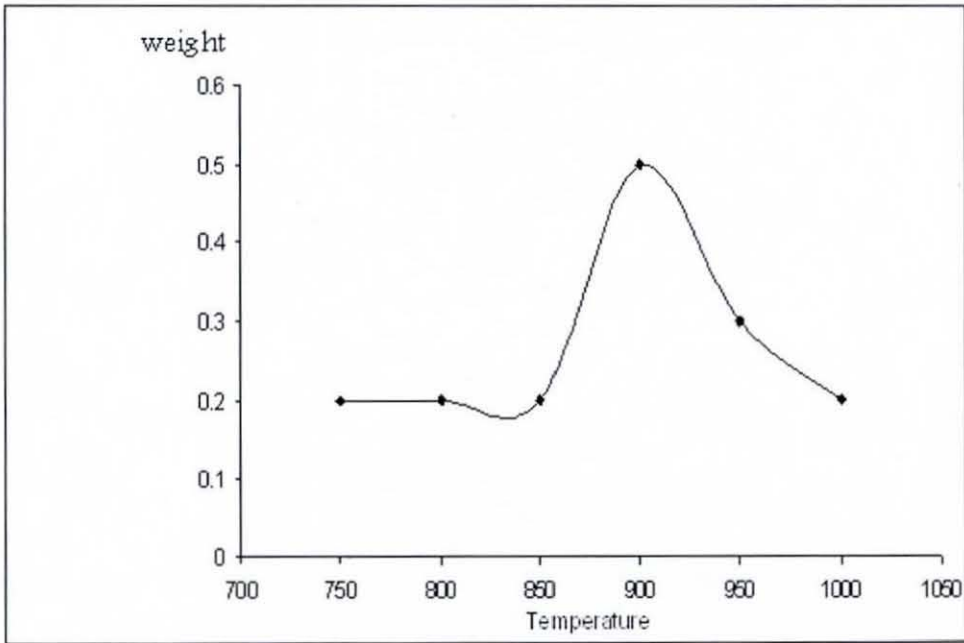


Figure 55 C-factor vs temperature.

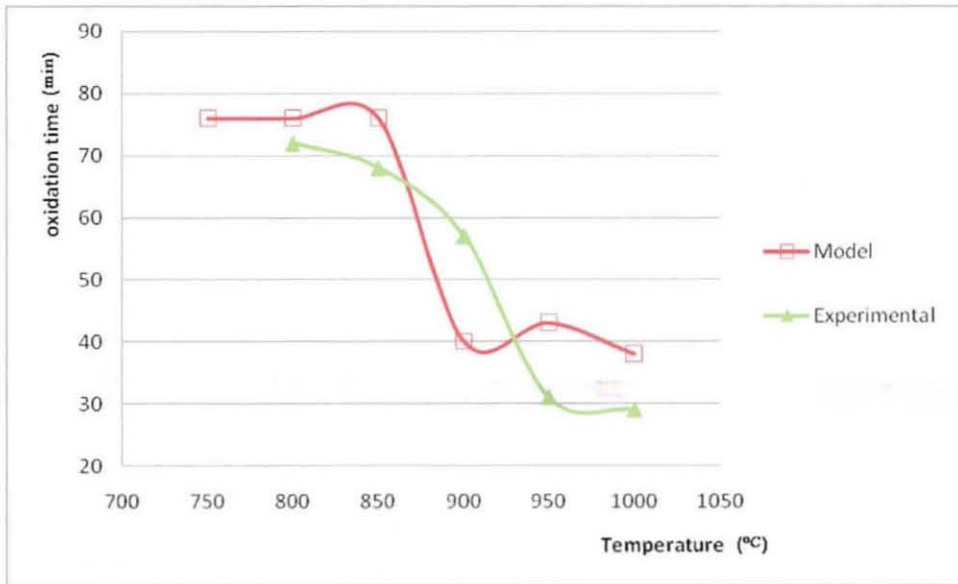


Figure 56 Oxidation time vs Temperature.

To find the oxidation time \bar{t} from these graphs, it is necessary to find the central point of the oxidation process, according to the following equation:

$$O_{\text{central}} = O_s + \frac{O_e - O_s}{2} ;$$

where O_s is start of Oxidation and O_e is the end of oxidation.

Finally, convert this point to axis where the oxidation time \bar{t} is located

For the C-factor, the following equation is used

$$C\text{-factor} = \frac{\frac{O_e - O_s}{O_e}}{\frac{t(\text{max}) - t(\text{min})}{t(\text{max})}}$$

It is important to use a curve for the unknowns in the previous equations. These unknowns are related to each factor with the temperature. Figures 57 to 60 show the relation between each factor with the oxidation temperatures. These figures show that at any temperature the unknown factors can be found easily from the curves, then the oxidation time can be calculated from the equation.

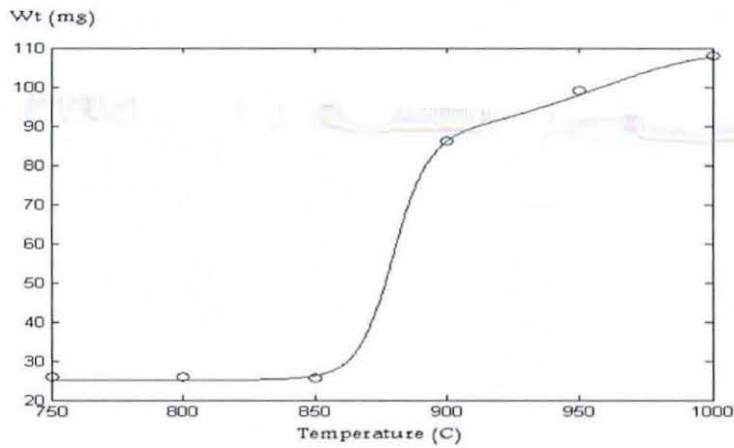


Figure 57 max. mass (mg) vs temperature (°C).

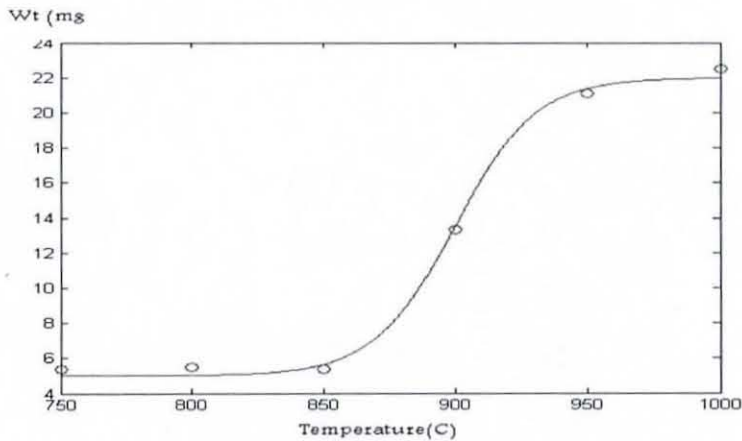


Figure 58 Mass (mg) vs temperature (°C).

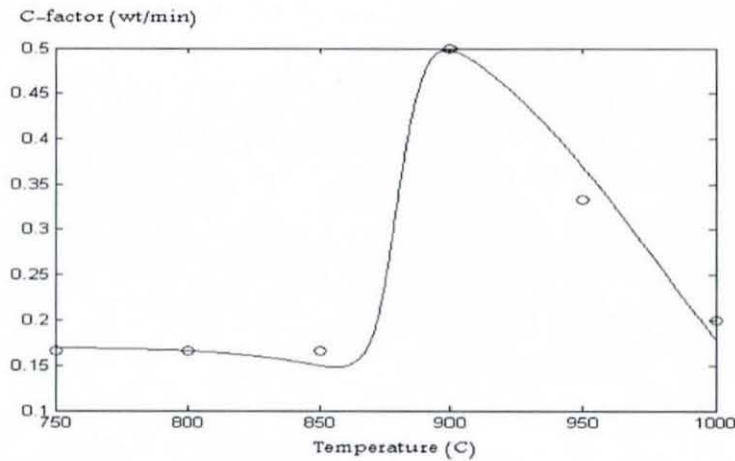


Figure 59 C factor (mg/min) vs temperature (°C).

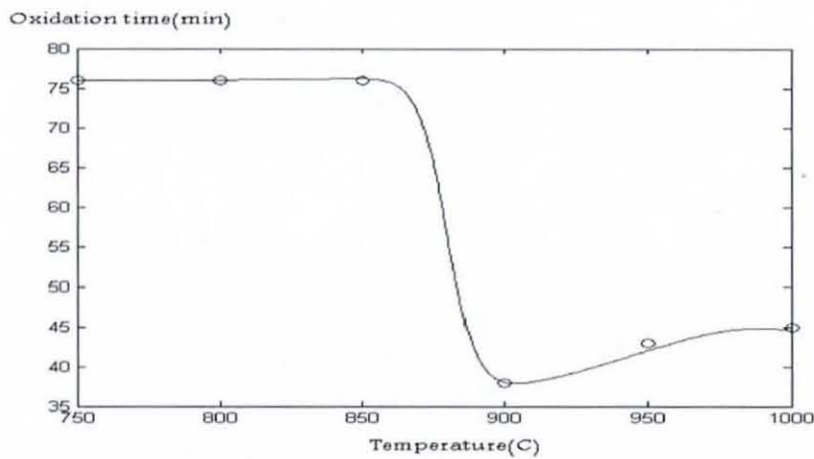


Figure 60 Oxidation time vs temperature (°C).

To demonstrate the full effect for temperature, time and weight, a three dimensional Figure 61 is presented. The x-axis presents the temperature, the y-axis presents the weight, and the z-axis represent the time. The blue area is for the lower temperature while the red is for higher temperatures. The red dotted lines represent the experimental temperatures.

It is noticed that at lower temperature the time was longer than in the higher temperatures. It was observed that after the oxidation is completed, the remaining curve is constant which means no more weight has been added to the sample. Values

for the equation parameters obtained at each temperature are presented in Table 5.

In this graph the tungsten alloy weight starts at 20 grams, time at zero, and temperature from 750°C. The time increases indirectly with weight and inversely with the temperature where at lower temperatures the full oxidation is close to 100 minutes as shown in the Figure 61 and it decreases to 50 minutes when it reaches the higher temperature where the slope of the oxidation curve increased. This three dimension graph is apply only for the given parameters where at lower temperatures the oxidation rate is totally different as mentioned previously in section 2.5.

Weight and time are related to the temperature and not to each other where the increment in the sample weight does not lead to increase in the oxidation time if the heat was distributed uniformly over the whole sample and the sample placed in a way which the height is 2 mm or less to insure the oxygen diffusion.

Finally, Figure 61 shows that the highest temperature was 1000°C, the maximum weight was 110 grams, and the maximum time was 300 minutes while it was 90 minutes at full oxidation at low temperatures.

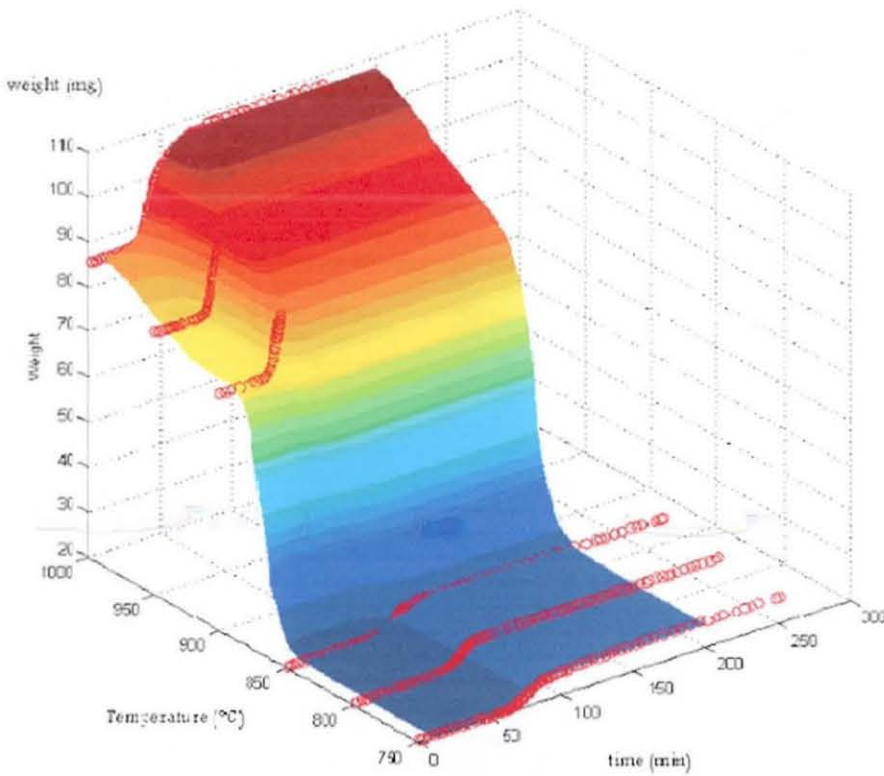


Figure 61 Three dimension curve fitting for the oxidation process.

5.3 Oxidation modeling

The high temperature corrosion rate of many common alloys can be described according to three kinetic laws described as linear, parabolic, or logarithmic. The rate of high temperature corrosion of alloys follows the parabolic rate law, which requires that the square of film thickness be proportional to time. If the rate diffusion of gases or metal ion through the corrosion product layer is controlling, the rate of film growth follows parabolic law, which can be written as:

$$w^2 = kt + \epsilon$$

1

Where W is the weight gain of the specimen, k is known as parabolic rate constant, t is the time, and c is constant.

The parabolic rate constant can be expressed as:

$$k = \text{constant } P^{1/2} e^{(-E/RT)} \quad 2$$

The present data are represented by equation 2 and shown in Figure 62 where the calculated value of energy of activation is 80.4 kJ/mole for tungsten corrosion in the temperature ranges 750 to 1000°C.

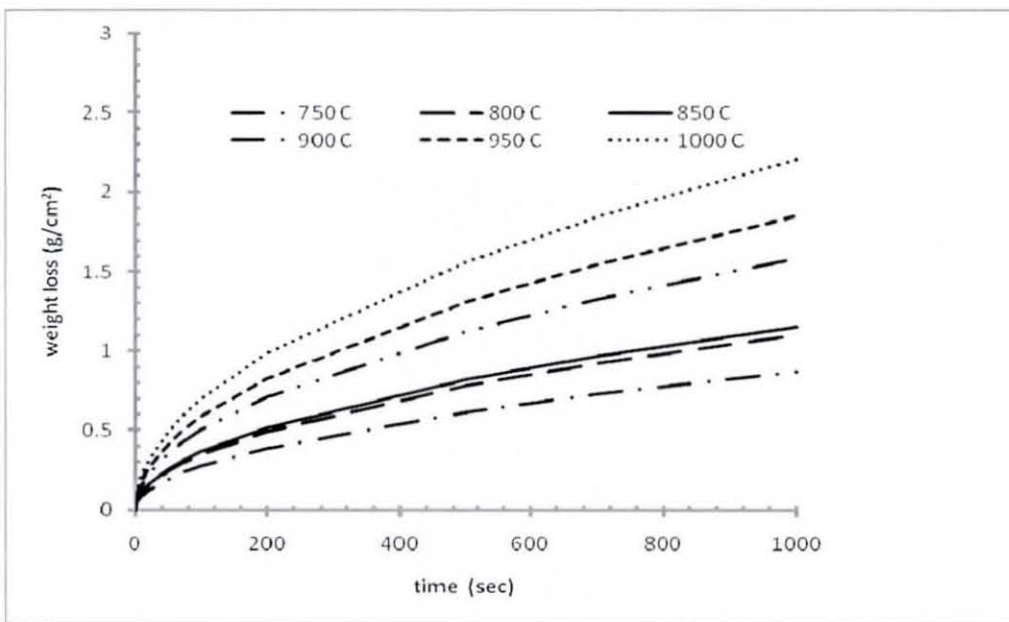


Figure 62 The experimental data for tungsten oxidation expressed as parabolic rate

The reaction (oxidation) between a metal or an alloy and a gas in the absence of water or aqueous phase is often called scaling, tarnishing, high temperature corrosion, or dry corrosion.

Khan et al., (1998) introduced a diffuse interface model (DIM) to describe the mechanism of high temperature oxidation for cobalt, iron, and nickel. The high temperature oxidation data for these metals was analyzed using a non linear optimization method to obtain the optimal values for different parameters used in DIM.

The reaction zone has dissolved oxygen and metal atoms diffuse into the zone and react resulting in the inward movement of the zone. The high temperature oxidation data for cobalt, iron and nickel, which were for metal deficit (p-type), were analyzed. The results of the model were successfully used to predict the experimentally determined parabolic rate constants for the oxidation of cobalt at high temperatures.

The (DIM) model is based on the rate constant of reaction (k), rate of diffusion of metal atoms in the oxide layer (D_M), and rate of diffusion of an oxidant in the corrosion product (D_p) and in the un-reacted core for the high temperature oxidation by oxygen at atmospheric pressure (D_c). The diffusion coefficients for product layer and un-reacted metal core for (cobalt, nickel and iron) were correlated to parabolic rate constants and were represented by the following equations.

$$D_p = 1.4 \times 10^{-8} k_g \quad 3$$

$$D_c = 6.9 \times 10^{-9} K_g \quad 4$$

In this research work the oxidation process rate for tungsten alloy is parabolic above 750°C for all temperatures for the alloying elements of mainly Ni and Fe that represent 4.6% of the alloy mass. The DIM model is applied for the oxidation of tungsten at all temperatures used in the experimental work.

The tungsten sample has spiral shape as shown in Figure 16 also it is along sheet of metal. The volume of the sample has a three dimensions, length, width, and thickness as shown in Figure 63.

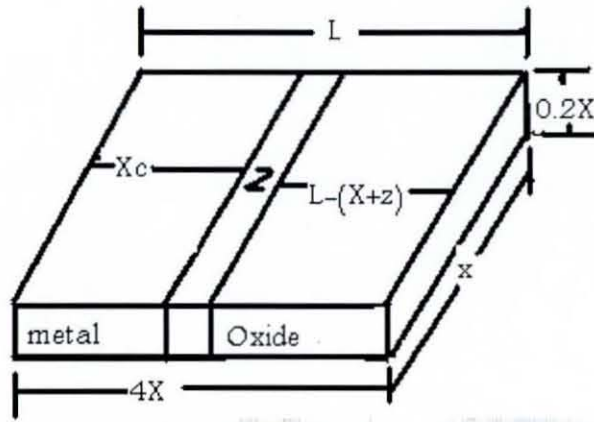


Figure 63 A schematic diagram for small piece of tungsten

The mass (w) of the sample in grams and the volume (V) in cubic centimeters, the equation for volume of the sample can be written as:

$$V = \frac{w}{\rho} \quad 5$$

where ρ is the density of tungsten in (grams/cm³), the dimension of the sample, width is equal to X , length equal to $4X$ and thickness equal to $0.2X$

$$\text{Volume of the sample} = 4X \times X \times 0.2X = 0.8X^3$$

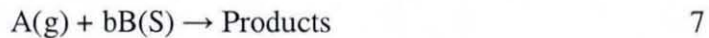
$$0.8X^3 = \frac{w}{\rho}$$

$$X = \sqrt[3]{\frac{w}{0.8\rho}} \quad 6$$

Khan et al, (1998) made a number of assumptions for the DIM application for the high temperature oxidation of metals. The assumptions are as follows: (i). The scale is

homogeneous diffusion barrier; (ii). only a single oxidation product forms; (iii). the flux of oxygen is unidirectional and independent of distance for a given scale thickness (quasi-steady state scale growth) and (iv). local equilibrium is maintained at the metal/scale and scale/gas interface and throughout the thickness of the scale. This is to insure that a parabolic oxidation growth is maintained.

For an irreversible gas/solid reaction:



p-type or positive semiconductors mechanism is due to either a deficit of metal or an excess of nonmetal (intrinsic semi-conduction). This phenomenon is represented by the formation of metal deficit p-type semiconductor, with the cation vacancies and electron holes by incorporation of oxygen into the metal lattice.



The rate of reaction (r) can be written as follows

$$r = \frac{dN_A}{dt} = -kC_i^m q^n \quad 9$$

Assuming that diffusivity of metal atom D_M , in the reaction zone, the rate of diffusion can be given as:

$$\frac{dN_A}{dt} = -D_M \frac{q_0}{z} \quad 10$$

Where N_A is the diffusivity of metal D_M in the reaction zone (Defect), C_i is the interfacial concentration of gas, q is the concentration radiant, and k is the reaction rate coefficient or rate constant.

Where the concentration gradient can be expressed as q_0/z in the reaction zone.

The concentration of metal ions can be represented in terms of oxidant gas concentration. The diffusivity in the reaction zone, D_z is regarded as a total resistance consisting of one half to be corrosion product and another half being un-reacted metal core (a simple harmonic mean of diffusivities of corrosion product, D_p and that of the un-reacted metal core, D_c)

$$D_z = \frac{2}{\frac{1}{D_p} + \frac{1}{D_c}}$$

In this investigation, the diffusivity in the reaction zone D_z was defined differently allowing for contribution of the corrosion product and the un-reacted metal core as a function of fraction of reaction zone reacted, f :

$$D_z = \frac{1}{\frac{f}{D_p} + \frac{1-f}{D_c}} \quad 11$$

The diffusion coefficient of metal ions, D_M can be expressed in terms of zone diffusivity, D_z or vice versa. Neglecting any accumulation of oxidant gases in the corrosion product layer, the rate of diffusion and the reaction can be equated as:

$$D_M = \frac{q_0}{z} = D_z \frac{C_i}{z} = k \frac{C_i q_0 z}{6} \quad 12$$

And, thus, the thickness of the reaction zone Figure (63), z is

$$z = \sqrt{\frac{6D_z}{kq_0}} \quad 13$$

and from reaction expressed as equation (7) the following equations can be derived

$$\frac{dN_B}{dt} = b \frac{dN_A}{dt} \quad 14$$

and, since,

$$\frac{dN_A}{dt} = \frac{q_o dx_c}{b dt} \quad 15$$

thus,

$$\frac{1}{b} \frac{dx_c}{dt} = \frac{k c_i z}{6} \quad 16$$

The concentration gradient of metal ions can be interpreted as a function of gaseous concentration. Assuming oxygen concentration in the gas bulk and diffuse through a gaseous film with resistance equivalent to gas-phase mass-transfer coefficient has been taken into consideration. Equating the gaseous rate of diffusion to rate of diffusion into the product layer to the rate of diffusion in the reaction zone, the following relationship can be obtained between the bulk concentration of gas C_o and the interfacial concentration C_i as follows Figure 63:

$$k_M (C_o - C_s) = D_p \frac{C_s - C_i}{(L - X_C - z)} = D_z \frac{C_i}{z}$$

$$C_i = \frac{C_o}{\left(1 + \frac{D_z}{D_p} \frac{(L - X_C - z)}{z}\right) + \frac{D_z}{k_M z}} \quad 17$$

Substituting C_i in equation 16:

$$\frac{dX_C}{dt} = \frac{b}{6} \frac{k C_o z}{\left(1 + \frac{D_z}{D_p} \frac{(L - X_C - z)}{z}\right) + \frac{D_z}{k_M z}} \quad 18$$

This equation can be integrated to obtain the calculated time t_{calc} for the thickness of the corrosion product formed $L-X_c$:

$$t_{calc} = \frac{(L - (L - X_c))[2 + \beta(2\phi - (L + (L - X_c)))] + \gamma}{\alpha} \quad 19$$

where

$$\alpha = \frac{bkC_o z}{3} \quad 20$$

$$\beta = \frac{D_z}{D_p z} \quad 21$$

$$\phi = L - z \quad 22$$

$$\gamma = \frac{D_z}{k_M z} \quad 23$$

Solution Methodology

Microsoft Office 2007, solver function was used as a multi-variable search to find the optimum values of mass transfer diffusion constant (k_M), velocity constant of reaction (k), diffusivity of oxidant gas in the core (D_c), diffusivity of the oxidant gas in the corrosion product (D_p), and the fraction of the zone reacted (f). The optimization technique is based on minimizing the following objective function:

$$E = \sum_{i=1}^{n_T} (t_{calc}^i - t_{exp}^i)^2 \quad 24$$

where t_{exp}^i is the experimental time for the i th observations? The experimental time is obtained from the corrosion rate data given for the oxidation reactions in equation 8. Experimental fraction conversion (X) can be calculated from the corrosion rate data and from Figure 63, it can be seen that:

$$X_c = L(1 - X) + (1 - f)z \quad 25$$

Where f is the fraction of the zone already reacted.

and the gas constant

$$R = 8.314 \text{ kJ/mol}$$

And energy of activation for parabolic rate constant is $E = 9.68 \times 8.314 = 80.48 \text{ kJ/mol}$

Number	Experimental time (sec)	Predicted time (sec)	Weight loss (gram/cm)
1	10	10	0.01145
2	20	20	0.01620
3	30	30	0.1984
4	40	40	0.02291
5	50	50	0.02561
6	60	60	0.02805
7	70	70	0.03030
8	80	80	0.03239
9	90	90	0.03436

Table 1: An example of the computer output used to predict the kinetic parameters for tungsten oxidation at 1000°C by air.

Applying DIM to the corrosion data with different temperatures, various parameters have been evaluated by using Microsoft office 2007 built in function “Solver” in Excel. The most important parameters are product diffusivity D_p , core diffusivity D_c , rate constant k and gas film mass transfer coefficient k_m . The rate constant k and gas film mass transfer coefficient k_m have high values and are almost constant for all temperatures while D_p and D_c are related by Arrhenius equation with temperature. Figure 65 shows the dependency of D_p and D_c on temperature.

Figure 66 is a plot of the experimentally obtained parabolic rate constant versus the diffusion coefficients in the reaction zone predicted by the diffuse interface model (DIM). It is clear that the core and product layer diffusion coefficients (cm^2/s) are related to parabolic rate constant k_g ($\text{gm}^2/\text{cm}^2\text{-sec}$) according to following equations.

$$D_p = 24.6 \text{ kg}$$

$$D_c = 20.91 \text{ kg}$$

27

This equation is valid for tungsten at temperatures 750-1000°C. Thus the diffuse interface model was able to predict a universal relationship between experimentally determined parabolic rate constant to model predict diffusion coefficients of oxygen in the product layer and in the reaction zone. The effect of temperature is simply related to the value of k_g since the experimental values of k_g are determined by plotting weight gain square against time for different temperatures.

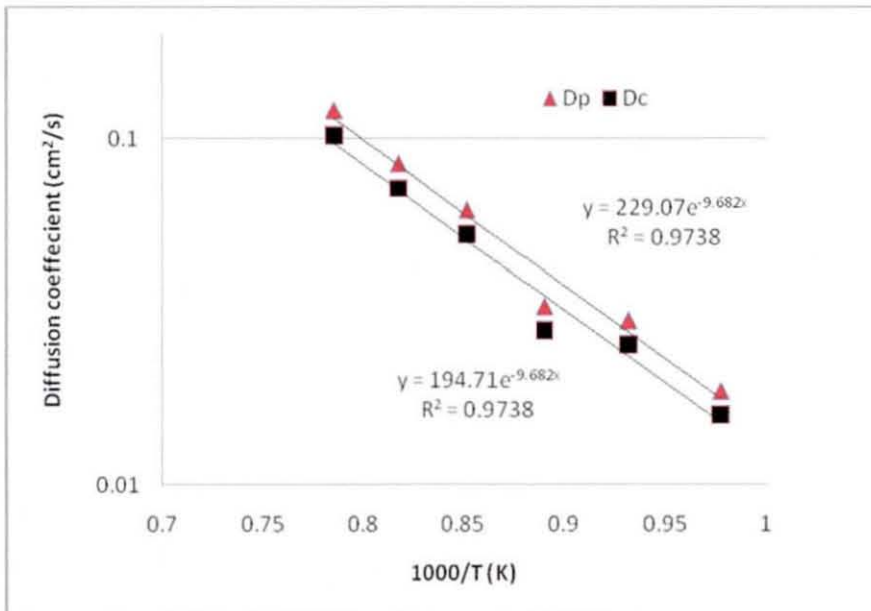


Figure 65 An Arrhenius type plot for diffusion coefficients for oxygen for tungsten corrosion.

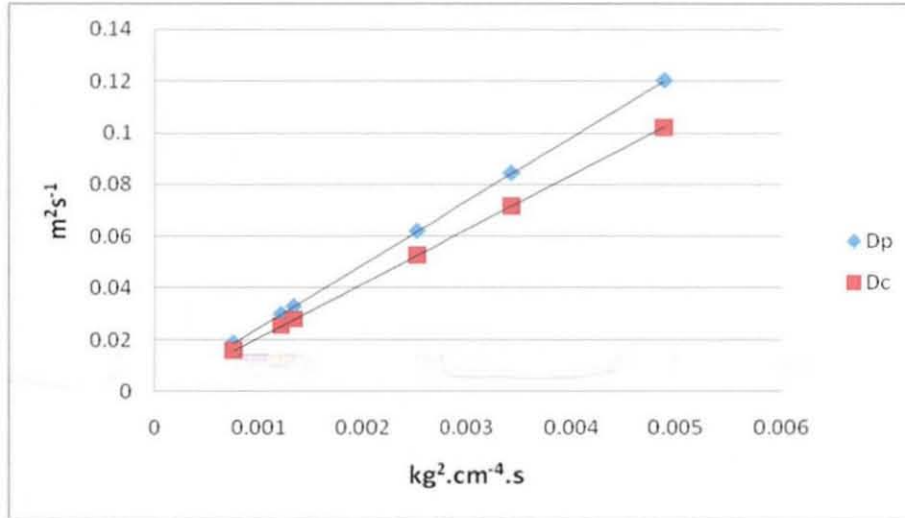


Figure 66 Diffusion coefficient in the core and product layer versus the parabolic rate constant for tungsten

Experimental data for high temperature oxidation of tungsten have been presented by parabolic rate expression. The parabolic rate constants were related to temperature by Arrhenius equation resulting into energy of activation equal to 80.4 kJ/mol. DIM was applied successfully for all temperatures evaluating velocity constant k , diffusion coefficients of product WO_3 , core W, and gas film diffusion coefficient k_M . The value of rate constant k and gas film resistance have very large values that are not dependent on temperature. Diffusion coefficients of product and core are function of temperature and are related by Arrhenius expression resulting into same energy of activation. These diffusion coefficients are also related to the parabolic rate constant and one can predict value core diffusivity or product diffusivity from parabolic rate constant value

6 Chapter **6** Conclusion and Recommendations for
future work

6.1 Conclusions

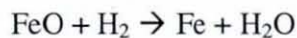
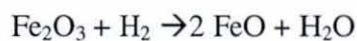
Recycling of tungsten alloy swarf involves processing used materials into new products in order to prevent waste of potentially useful materials, reduce the consumption of fresh raw materials, and reduce energy usage. This research work contains three main parts, oxidation, reduction, and pressing and sintering. The conclusion in the first part is an important aspect for the second and the third part of the research.

- The tungsten particles in the "as received" swarf were found to be elongated in heavily deformed regions affected by the cutting or shaping machines.
- The particle sizes at the low temperature oxidation are coarser than the particle at the high temperatures. At 800°C and 850°C the particle size is slightly less than 100 µm while at 900°C and above the particle size is finer (3-10 µm) while at 950°C and 1000°C the particle crystal shape is better and have a complete crystal shape.
- The oxidation process at high temperatures (900°C to 1000°C) has less oxidation time and particle properties. The best oxidation process was at 950°C where the oxidation process took 31 minutes to oxidize and the best particle crystal shape and size.
- The oxidation process is a weight, temperature and time relation, where time relate indirectly to weight and in reverse to the temperature. A combination from experimental and mathematical data shows that the best oxidation powder to be used for further reduction process is the powder obtained from oxidation at 950°C where the powder is in good crystal shape and the oxidation time is low.
- The formation of WO_3 starts at 750°C and above, and it takes a parabolic curve and becomes substantial at the saturation point.

- The reduction process in dry hydrogen is found to be the best reduction method where other reducing agents are not effective according to high contamination when reduced by carbon, also the reduction with nitrogen is not effective since it is not a reducing agent but it could be used for the sintering process as neutral media to prevent re-oxidation of the material.
- The sample placement of the oxide powder in the reduction process should be placed horizontally and the thickness should be less than 2 mm to allow the hydrogen gas to diffuse freely in the powder oxide. On this basis the coarse powder takes longer time in the reduction process than the finer particle powder.
- The reduction sequence can be summarized



and



- The particle size in the final pellet was very fine (1-3 μm) which is different than the starting material where the particles was about 10 μm , this is because the starting material was exposed to a heavily deforming and cutting processes, according to this fact the over sintering time produce some region in the sample have the same size and shape.

The diffusion interface model under the Wagner model assumptions can be applied successfully to investigate kinetic parameter during high temperature oxidation.

The diffuse coefficient of metal ion in metal oxide is related to the values of diffusivity of zone and interface oxidant gas concentration. The predicted values of D_p and D_c are unique and are function of temperature only and are independent of velocity constant for reaction

and fraction of the zone converted.

The generalized diffuse interface model predicts diffusion coefficients, pre-exponential factor, and activation energies for diffusion which are generally in agreement with those reported in the literature.

The predicted value of velocity constant of reaction obtained are highly dependent on the fraction of the zone reacted and the reaction zone thickness. This follows from the assumption made that the concentration profile of oxygen in the reaction zone is linear.

6.2 Recommendations for future work

This preliminary study has shown that the oxidation-reduction processing of heavy-metal tungsten swarf is potentially a technically-viable process. However, further work is required to characterise fully the effects of experimental variables in order that the robustness of the reprocessing sequence can be assessed fully. In particular, the following experiments need to be performed.

- The oxidation process carried out in the first step for a small amount of heavy metal swarf is suggested to be analysed using trace metal chemical analysis to find the oxidation effect on the trace elements in the alloy Fe, Ni, and others.
- In the reduction process the reduction time is an important aspect, where the reduction study required a thermogravimetric analyser with a system allow the hydrogen gas to purge.
- Adding additives to the sintering product could enhance the final material in different manners. It can be added on the compressed pellet or it can be mixed with the powder prior to compacting. This study has been discussed before but it can be a good add to further research work to produce better mechanical properties for the alloy.

- Mathematical corrosion model has to be refined to take into consideration the variability of velocity constant and external gas film mass transfer coefficient as a function of temperature.
- DIM has a gross assumption that concentration profiles in product and reaction zone are linear. It is suggested that DIM should be applied with exponential or powder functional concentration profiles in product layer and reaction zone.

References

- Aitken, E., Brassfield, H., Conn, P., Duderstadt, E. & Fryxell, R. 1967, "Permiability of Tungsten to Hydrogen from 1300 to 2600°C. and to Oxygen from 2000 to 2300°C", *AIME Met Soc Trans*, 239 (10), 1565-1574.
- Albiston, J.N. & Sale, F.R. 1986, "Thermogravimetric Studies of the Hydrogen Reduction of Nickel Tungstate", *Thermochim.Acta*, 103 (1), 175-180.
- Arevalo, E.F., Stichnothe, H., Thoeming, J. & Calmano, W. 2002, "Evaluation of a leaching process coupled with regeneration/recycling of the extractant for treatment of heavy metal contaminated solids", *Environmental Technology*, 23 (5), 571-581.
- Bailar, J.C., Emeleus, H.J., Nyholm, R. & Trotman-Dickenson, A.F. 1973, *Comprehensive inorganic chemistry*, Pergamon Press, Oxford.
- Barbier, C., 1971, "The Economics of tungsten", *Metal Bulletin Books Ltd.*, London.
- Basu, A.K. & Sale, F.R. 1979, "The controlled reduction of copper tungstate in H₂ O/H₂ mixtures", *Journal of Materials Science*, 14 (1), 91-99.
- Basu, A.K. & Sale, F.R. 1978, "Copper-tungsten composite powders by the hydrogen reduction of copper tungstate", *Journal of Materials Science*, 13 (12), 2703-2711.
- Basu, A.K. & Sale, F.R. 1977, "Reduction of 'Blue' WO₂ Dry H", *Trans. Inst. Min. Metall.*, Sept. 1977, 86 C (86), 134-139.
- Bewlay, B.P. and Briant, C.L., 1995. The formation and the role of potassium bubbles in NS-doped tungsten. *International journal of refractory metals & hard materials*, 13 (1-3), 137-159.

- Bose, A., Jerman, G. & German, R.M. 1989, "Rhenium Alloying of Tungsten Heavy Alloys", *Powder Metall. Int.*, 21 (3), 9-13.
- Braconi, P. and Dufour, L.C., 1976. Investigation of Cobalt (II)-Tungsten (VI)-Oxide Reduction in Hydrogen: Part I. *Metallurgical and Materials Transactions B*, 7(3), 321-327.
- Butterworth, G.J., Forty, C.B.A., Turner, A.D. & Junkison, A.J., 1998, "Recycling of copper used in fusion power plants", *Fusion Engineering and Design*, 38 (4), 441-458.
- Cai, W.D., Li, Y., Dowding, R.J., Mohamed, F.A. & Lavernia, E.J. 1995, "A Review of Tungsten-Based Alloys As Kinetic Energy Penetrator Materials", *Reviews in Particulate Materials*, (3), 71-132.
- Charlton, M.G. 1954, "Hydrogen Reduction of Tungsten Oxides", *Nature*, 174, (4432), 703.
- Cheney, R.F., 1984, Sintering of refractory metals. *ASM Metals Handbook*, 7 (3), 389-393.
- Cheney, R.F., Seydel, E.R. and Kapoor, D., 1990. Rapidly Solidified Tungsten Alloy Powders. *Advances in Powder Metallurgy*, 1, 81-93.
- Cotton, F.A. & Wilkinson, G. 1988, *Advances In Organic Chemistry*, 5th edn, Wiley.
- Danninger, H. & Lux, B. 1997, "Tungsten heavy alloys with low binder content", *14 th International Plansee Seminar'97.*, Tirol; Austria, 315.
- Donten, M., Cesiulis, H. & Stojek, Z. 2000, "Electrodeposition and properties of Ni-W, Fe-W and Fe-Ni-W amorphous alloys. A comparative study", *Electrochimica Acta*, 45 (20), 3389-3396.

- Dowding, R.J., Hogwood, M.C., Wong, L. & Woodward, R.L. 1994, "Tungsten Alloy Properties Relevant to Kinetic Energy Penetrator Performance", *Proceedings of the second international conference on tungsten and refractory metals*, McLean, VA, USA. China, 3.
- Ebreo, A. & Vining, J. 2001, "How similar are recycling and waste reduction? Future Orientation and Reasons for Reducing Waste as Predictors of Self-Reported Behavior", *Environment and Behavior*, 33 (3), 424-448.
- Ekbom, L., Holmberg, L. & Persson, A. 1992, "A Tungsten Heavy Alloy Projectile With Spiculating Core", *Tungsten & Tungsten Alloys. 1992*, 551-558.
- Enesca, A., Enache, C., Duta, A. & Schoonman, J. 2006, "High crystalline tungsten trioxide thin layer obtained by SPD technique", *Journal of the European Ceramic Society*, 26 (4-5), 571-576.
- French, G.J. & Sale, F.R. 1985, "The hydrogen reduction of cobalt-tungsten mixed oxides", *Journal of Materials Science*, 20 (4), 1291-1300.
- Gellar, R., 1977. Circularly symmetric normal and subnormal operators. *Journal d'Analyse Mathématique*, 32 (1), 93-117.
- German, R.M. 1997, "Novel powder metallurgy techniques for refractory metals and hard materials", *14th International Plansee Seminar'97.*, Tirol; Austria, 194.
- German, R.M. 1992, "Critical Developments in Tungsten Heavy Alloys", *Tungsten & Tungsten Alloys, 1992*, 3-13.
- German, R.M. 1985, "Microstructure Limitations of High Tungsten Content Heavy Alloys", *11 th International Plansee Seminar85*, Reutte; Austria (1), 143-161.
- German, R.M. & Chum, K.S. 1984, "Sintering Atmosphere Effects on the Ductility of W-Ni-Fe Heavy Metals", *Metallurgical and Materials Transactions A*, 15 (4), 747-754.

- Goryachkovskii, Y., Kostikov, V. & Solodkin, G. 1976, "Interaction of W With Water Vapour at High Temperatures", *Zhurnal Fizicheskoi Khimii*, 50 (8), 1959-1962.
- Greenfield, M.S. "Reduction, reuse and recycle of wastes over the lifecycle of steel", 1993, *Annual Conference of Metallurgists-Metallurgical Society of the Canadian Institute of Mining and Metallurgy*, Pergamon Press, (32), 287.
- Haase, V., Manes, L., Schultz, B., Schumacher, G., Vollath, D., Keim, R. and Keller, C., 1979. *Gmelin Handbook of Inorganic Chemistry*.
- Halliday, T.D., 1979. MSc Thesis, Victoria University of Manchester
- Hamad, A., Varma, V., El-Halwag, M. & Krishnagopakan, G., 1995 "Systematic integration of source reduction and recycle/reuse for the cost-effective compliance with the cluster rules", *AIChE Annual Meeting*, Miami.
- Hamamura, T. 1959, "The Kinetic Study of Surface-chemical Reactions at Extremely Low Pressures. IV. The Thermal Reaction between Water Vapor and a Tungsten Filament. Part IV", *Bulletin of the Chemical Society of Japan*, (32), 1180-1204.
- Hansen, M. & Anderko, K. 1958, "Constitution of Binary Alloys", *Mc Graw-Hill*, New York, 256.
- Haubner, R., Schubert, W., Hellmer, H., Lassner, E. & Lux, B. 1985, "The Reduction to Tungsten", *11 th International Plansee Seminar85, Reutte; Austria* (2), 161-179.
- Haubner, R., Schubert, W., Hellmer, H., Lassner, E. & Lux, B. 1983, "Mechanism of Technical Reduction of Tungsten. II.--Hydrogen Reduction of Tungsten Blue Oxide to Tungsten Powder", *Int.J.Refract.Hard Met.*, 2 (4), 156-163.
- Haubner, R., Schubert, W., Hellmer, H., Lassner, E. & Lux, B. 1983, "Thermodynamic and Kinetic Considerations on Technical Hydrogen Reduction of Tungsten Blue Oxide to Tungsten Powder", *Advances in Hard Metal Production*, 2 (1), 108-115.

- Haubner, R., Schubert, W., Lassner, E., Schreiner, M. & Lux, B. 1983, "Mechanism of Technical Reduction of Tungsten. I.--Literature Review", *Int.J.Refract.Hard Met.*, 2, (3), 108-115.
- Hellmer, H., Schubert, W.D. & Lassner, E. 1985, "Kinetik der Wolframoxi Dreduktion [A]", *Proceedings of the 11th Plansee-Seminar, Austria*, 43.
- Hogwood, M.C. & Bentley, A.R. 1994, "The development of high strength and toughness fibrous microstructures in tungsten–nickel–iron alloys for kinetic energy penetrator applications", *Proceedings of Tungsten Refractory Metal*, Princeton Metal Powder Industry, 37.
- Hopson, R.K. 2000, "Source reduction", *Environmental Protection*, 11 (1), 38-39.
- Hornung, M. & Karivan, V. 1999, "Solid sampling electrothermal atomic absorption spectrometry for analysis of high-purity tungsten trioxide and high-purity tungsten blue oxide", *Spectrochimica Acta*, B54, 1177-1191.
- Hougen, J.O., Reeves, R.R. & Mannella, G.G. 1956, "Reduction of Tungsten Oxides with Hydrogen", *Industrial & Engineering Chemistry*, 48 (2), 318-320.
- Jing-lian, F., Tao, L., Hui-chao, C. & Deng-long, W. 2008, "Preparation of fine grain tungsten heavy alloy with high properties by mechanical alloying and yttrium oxide addition", *Journal of Materials Processing Technology*, 208 (1-3), 463-469.
- Jiqiao, L., Baiyun, H. & Zhiqiang, Z. 2001, "Determination of physical characterization of tungsten oxides", *International Journal of Refractory Metals and Hard Materials*, 19 (2), 79-84.
- Khan, A.R., Alhajji, J.N. & Reda, M.R. 1998, "Generalized diffuse interface model for determination of kinetic parameters in high-temperature internal corrosion reactions (Gas/Solid Systems)", *International Journal of Chemical Kinetic*, 30, 903-912

- Kirk, R. & Othmer, D. 1983, *Encyclopedia of Chemical Technology*, 23.
- Koch-Bienemann, 1989, E. *Gmelin handbook of inorganic chemistry, Tungsten: supplement*, Springer-Verlag, Heidelberg A3 (54).
- Koch-Bienemann, E., Berg, L., Czack, G. and Wagner, J., 1989. *Gmelin Handbook of Inorganic Chemistry*, Springer-Verlag, Heidelberg A3 (54).
- Lassner, E. & Schubert, W.D. 1999, "Tungsten Properties, Chemistry, Technology of the Element, Alloys, and Chemical Compounds", (*Kluwer Academic, New York, 1999*).
- Lee, C.H. 1964, "Oxygen Diffusion in Tungsten", *Nature*, 203 (4950), 1163.
- Lenel, F. 1980, "Powder metallurgy principal and application", *Princeton NJ: Metal Powder Industries Federation*, 337-48.
- Li, K.C. & Wang, C.Y. 1955, "Tungsten: Its History, Geology, Ore-Dressing, Metallurgy, Chemistry", *Analysis, Applications, and Economics, 3rd ed.*(*Reinhold Publishing Corporation*, New York.
- Magness, L.S. & Kapoor, D. 1994, "Flow-softening tungsten composites for kinetic energy penetrator applications", In: A Bose and R Dowding, Editors, *Proceedings of the 2nd International Conference on Tungsten and Refractory Metals*, 11-20.
- Masek, K., Nemsak, S., & Matolin, V. "Structural Study of Epitaxial Tungsten Oxide Nanolusters", *Vacuum*, 80 (2005), 58-63.
- Mullendore, J.A. & Pink, E. 1989, "In the Metallurgy of Doped/Non-Sag Tungsten", eds E Pink & L Bartha. *Elsevier*, New York, 71.
- Ong Jr, J.N. & Fassell Jr, W.M. 1962, "Kinetics of Oxidation of Columbium and other Refractory Metals", *Corrosion*, 18, 382-389.

- Organization for Economic Co-operation and Development. 2008, OECD Environmental Outlook to 2030, Denver, USA.
- Parsons, D.S. 1965, "The Reduction of Tungsten Oxides by Hydrogen", *Electrochem Tech*, 3 (9), 280-283.
- Penrice, T.W. 1984, "Metals Handbook, Vol. 7", *Metals Park*, Ohio, 688-691.
- Pierre, G.R.S., Ebihara, W., Pool, M. & Speiser, R. 1962, "Tungsten-Oxygen System", *Trans. Metall. Soc. AIME*, 224, 259-64.
- Pink, E. & Eck, R. 1996, "Refractory metals and their alloys", *Materials Science and Technology: a Comprehensive Treatment*, 8, 589-642.
- Rieck, G. 1967, *Tungsten and its Compounds*, Pergamon Press, Oxford.
- Ristow, N.E., Whittington-Jones, K., Corbett, C., Rose, P. & Hansford, G.S. 2002, "Modelling of a recycling sludge bed reactor using AQUASIM", *Water S. A.*, 28, (1), 111-120.
- Rosenbrock, H.H., 1960, "An Automatic Method for finding the greatest or Least Value of a Function", *Computer Journal*, 3, 175-184.
- Sale, F.R. & Albiston, J.N. 1988, "Production and Sintering of Ag-W Composites Containing Nickel", *Modern Developments in Powder Metallurgy*, 19, 75-89.
- Sberveglieri, G. 1995, "Recent developments in semiconducting thin-film gas sensors", *Sensors and Actuators B: Chemical*, 23,(2-3), 103-109.
- Sberveglieri, G., Depero, L., Groppelli, S. & Nelli, P. 1995, "WO₃ sputtered thin films for NO_x monitoring", *Sensors and Actuators B: Chemical*, 26,(1-3), 89-92.
- Schmidbaur, H., 1987. *Gmelin Handbook of Inorganic Chemistry*, Springer, Berlin .

- Schubert, W.D. 1991, "Production and characterization of hydrogen-reduced submicron tungsten powders--Part II: Controlled decomposition of APT and hydrogen reduction of oxides", *International Journal of Refractory Metals and Hard Materials*, 10 (4), 178-191.
- Schubert, W. 1989, "Kinetics of the Hydrogen Reduction of Tungsten Oxides", *12 th International Plansee Seminar'89: High Temperature and Wear Resistant Materials in a World of Changing Technology*, 4, 41-78.
- Sikka, V. & Rosa, C. 1980, "The Oxidation Kinetics of Tungsten and the Determination of Oxygen Diffusion Coefficient in Tungsten Trioxide", *Corros Sci.*, 20 (11), 1201-1219.
- Sriyudthsak, M. & Supothina, S. 2006, "Humidity-insensitive and low oxygen dependence tungsten oxide gas sensors", *Sensors & Actuators: B.Chemical*, 113 (1), 265-271.
- Stephen, H.W., Yih & Chun, W.T. 1979, "Tungsten-Source, Metallurgy, Properties and Application", Plenum Press, New York and London.
- Swinkels, F.B. & Ashby, M.F. 1981, "A Second Report on Sintering Diagrams", *Acta Metall.*, 29 (2), 259-281.
- Tabak, H.H., Scharp, R., Burckle, J., Kawahara, F.K. & Govind, R. 2003, "Advances in biotreatment of acid mine drainage and biorecovery of metals: 1. Metal precipitation for recovery and recycle", *Biodegradation*, 14 (6), 423-436.
- Tan, R. & Khoo, H.H. 2005, "Zinc Casting and Recycling", *International Journal of Life Cycle Assessment*, 10 (3), 211-218.
- Vogt, G.M., Liu, H.W., Kennedy, K.J., Vogt, H.S. & Holbein, B.E. 2002, "Super blue box recycling (SUBBOR) enhanced two-stage anaerobic digestion process for

- recycling municipal solid waste: laboratory pilot studies", *Bioresource technology*, 85(3), 291-299.
- Walkden, P. & Sale, F.R. 1982, "silver-tungsten Contacts by the hydrogen reduction of silver tungstate", *28th Holm conference on electrical contacts*, Chicago, 101-107.
- Walter, J.L. & Lou, K.A. 1989, "Structures and chemistry of tungsten powder from doped and undoped tungsten blue oxide", *Journal of Materials Science*, 24, (10), 3577-3587.
- Warren, A., Nylund, A. & Olefjord, I. 1996, "Oxidation of Tungsten and Tungsten Carbide in Dry and Humid Atmospheres", *International Journal of Refractory Metals and Hard Materials*, 14 (5), 345-353.
- Weber, L. and Egli, U., 1977. Phase relations in the system NiO-WO sub 3. *Journal of Materials Science*, 12(10), 1981-1987.
- Wittenauer, J.P., Nieh, T.G. & Wadsworth, J. 1992, "Tungsten and its alloys", *Advanced Materials & Processes*, 142 (3), 28-37.
- Yamazoe, N. & Miura, N. 1992, "New Approaches in the Design of Gas Sensors", *Gas Sensors: Principles, Operation, and Developments*, Kluwer Academic, Netherlands, 1-42.
- Yih, S.W.H. & Wang, C.T. 1979, *Tungsten Sources, Metallurgy, Properties, and Applications*, Plenum Press, New York and London.
- Yuehui, H., Libao, C., Baiyun, H. & Liaw, P. 2003, "Recycling of heavy metal alloy turnings to powder by oxidation–reduction process", *International Journal of Refractory Metals and Hard Materials*, 21 (5-6), 227-231

Appendix A

Publications

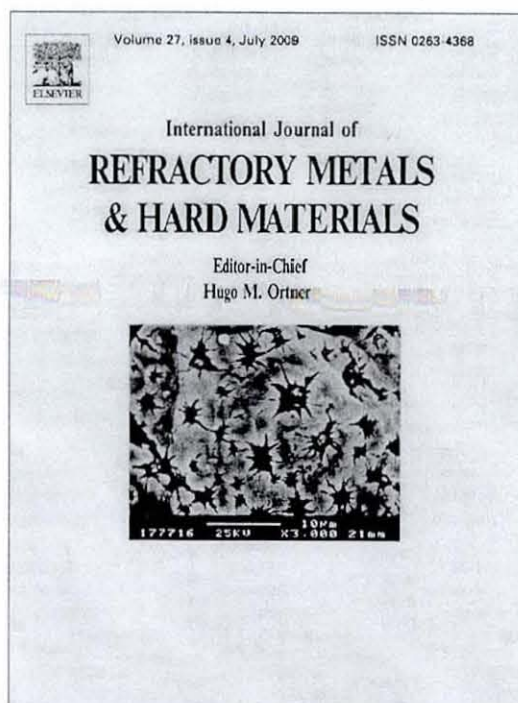
A. Alhazza, Oxidation of tungsten alloy at high temperatures in air. *Saudi innovation conference*

A. Alhazza, Reduction, Pressing and sintering for tungsten alloy swarf. *Saudi innovation conference*.

A. Alhazza, Oxidation and reduction of tungsten alloy swarf. *International Journal of refractory metal and hard materials*

A. Alhazza, Recycling of tungsten alloy swarf. *Proceedings of World Academy of Science, Engineering and Technology (WASET) Volume 35 November 2008 ISSN 2070-3740*

Provided for non-commercial research and education use.
Not for reproduction, distribution or commercial use.



This article appeared in a journal published by Elsevier. The attached copy is furnished to the author for internal non-commercial research and education use, including for instruction at the authors institution and sharing with colleagues.

Other uses, including reproduction and distribution, or selling or licensing copies, or posting to personal, institutional or third party websites are prohibited.

In most cases authors are permitted to post their version of the article (e.g. in Word or Tex form) to their personal website or institutional repository. Authors requiring further information regarding Elsevier's archiving and manuscript policies are encouraged to visit:

<http://www.elsevier.com/copyright>



Contents lists available at ScienceDirect

Int. Journal of Refractory Metals & Hard Materials

journal homepage: www.elsevier.com/locate/IJRMHM

Oxidation and reduction of tungsten alloy swarf

A.A. Alhazza*

Department of Chemical Engineering, Loughborough University, Loughborough, LE11 3TU, UK

ARTICLE INFO

Article history:
Received 18 August 2008
Accepted 13 November 2008

Keywords:
Oxidation
Heavy metal
Reduction
Swarf
Tungsten

ABSTRACT

Oxidation of a heavy metal alloy (swarf) followed by reduction in dry hydrogen atmosphere was studied. The swarf was oxidised at 750 °C to 1000 °C and then reduced at 800 °C. Analysis of the resulting powder was studied using thermogravimetry, X-ray diffraction, and scanning electron microscopy. The average particle size of the reduced powder was 1–3 μm. The chemical composition of the reduced powder was the same as the primary heavy alloy swarf.

© 2008 Elsevier Ltd. All rights reserved.

1. Introduction

Transition metals show outstanding properties, and tungsten oxide is an important material for applications, such as electrical devices, catalysis and chemical sensors [1–4]. The wide range of electrical conductivity is one characteristic property of tungsten oxides, from that of semiconductors (WO_3) to that of conductors (WO_2). The range of tungsten oxides includes stoichiometric oxides, WO_3 , $WO_{2.9}$, $WO_{2.7}$, and WO_2 , in addition to non-stoichiometric structures. The non-stoichiometric systems consist of ordered or partially ordered defect structures of the oxygen-rich oxide, in which the central W atom is octahedrally surrounded by six oxygen atoms [9–11]. In WO_3 , neighbouring octahedra are in contact only at the corners, which increases oxygen deficiency, progressively forming common edges and surfaces.

The aim of this work is to produce a homogeneous powder from "heavy metal swarf" for recycling or reuse. The process route envisaged was a controlled oxidation reaction to breakdown the swarf followed by temperature-controlled reduction with dry hydrogen to remove the oxide and form a heavy metal powder. The microstructure of the swarf was characterised using optical metallography, scanning electron microscopy (SEM) and X-ray diffraction (XRD). Characterisation was followed by a controlled oxidation reaction to mechanically breakdown the oxide. In this step, thermogravimetry (TGA) was used to determine the optimal oxidation temperature and to give an indication of the process kinetics. A reduction process was then performed in a Carbolite furnace (Vecstar Furnace) under dry hydrogen atmosphere. XRD and SEM

were used to chemically analyse and determine the morphology of the powder.

2. Experimental procedure

2.1. Sample preparation

This work was carried out using heavy metal (tungsten) swarf obtained from cutting machine waste. Samples were prepared by washing the swarf in acetone in order to remove any residues of the oil used as cooling fluid in the cutting machines. After washing with acetone, the swarf was dried at room temperature for 5 h. It was then washed several times with distilled water to remove any other deposits, and dried at room temperature for another 5 h.

The swarf was mounted in cold-setting resin and polished to 6 μm for 10 min and then etched by immersing the sample in "Nital" for 30 s (Nital is an acid that removes the lighter elements from the surface of the polished samples to uncover two or more layers on the surface, revealing the underlying microstructures). The samples were then washed and dried for observation with an optical microscope.

For XRD analysis, samples were ground and sieved, resulting in a heavy metal powder of less than 150 μm.

2.2. Materials characterisation

The samples were characterised using XRD and SEM. Characterisation was performed on the materials present before and after each step of the homogenising process, including the starting

* Tel.: +44 (0) 7501769751; fax: +44 (0) 9654989059.
E-mail addresses: cgaaa@lboro.ac.uk, alhazza2@yahoo.com



Fig. 1. Micrograph of the tungsten swarf material, showing tungsten grains embedded in a matrix material.

material and the materials resulting from the oxidation and reduction processes.

2.3. Oxidation experiments

Oxidation experiments were carried out using two types of instruments for the required analysis. Initially, isothermal TGA was used with 20 mg of sample to study oxidation in a natural air environment. The experiment was carried out to determine the oxidation rate over the temperature range from 20 °C to 1100 °C. Subsequently, experiments were carried out at six different temperatures with fixed holding times. The conditions used in these experiments were 750 °C, 800 °C, 850 °C, 900 °C, 950 °C, and 1000 °C, each with a holding time of 3 h.

Oxidation of larger quantities (20 g) of the tungsten alloy swarf was carried out using an electric resistance Carbolite furnace to produce larger amounts of oxide samples. The heavy metal swarf powder was oxidised in air at the same temperatures and for the same times determined from the TGA data. The samples were positioned within the furnace in inert ceramic boats to avoid unwanted side reactions.

2.4. Reduction experiments

The reduction experiments were carried out at 800 °C for 3 h in a dry hydrogen atmosphere using a "Vecstar Furnace" with a gas supply system. The oxide powder, with a 2 mm layer height, was reduced in a constant hydrogen flow of approximately 2000 ml/min. The reduced powder was analysed by XRD and SEM.

3. Results and discussion

3.1. Oxidation

Scanning electron micrographs show that the swarf was a composite material with a grain size of 10 to 20 μm, as shown in Fig. 1. Fig. 1 shows that the tungsten grains account for more than 95% of the composite swarf in view. Elemental analysis by EDS showed that the grains in the composite swarf consisted of 100% W, while the matrix contained approximately 36% Ni, 35% Fe, 15% W, 8% Cu, 3% Co, and 0.6% Mn (a typical EDS analysis is shown in Fig. 2). XRD analysis verified the EDS analysis and showed a diffraction pattern containing peaks that could be related to the tungsten grains and a collection of other peaks associated with the Fe–Ni–Cu matrix alloy.

The TGA data showed the progress of the oxidation of 20 mg samples of the swarf, shown in Figs. 3 and 4. The initial TGA run, Fig. 3, was carried out to determine the temperature range over which the W-alloy oxidation took place. Subsequent TGA analyses determined the rate of oxidation at different temperatures within the range determined previously for the alloy oxidation. Fig. 3 shows the trace obtained during first experiment, which was carried out over a temperature range of 20 °C to 1100 °C in 100 min. It is observed that the oxidation process started at about 560 °C (50 min after the start of the test). The oxidation was observed by measuring the increase in the mass of the sample during heating, in which the W reacts with oxygen to form tungsten oxide. Fig. 3 shows that rapid oxidation occurs around 700 °C to 870 °C after 65 min, and that the sample is fully oxidised at 960 °C after 92 min. In order to determine the best oxidation rate, six isothermal experiments were carried out at 750 °C, 800 °C, 850 °C, 900 °C, 950 °C and 1000 °C. Five temperatures were chosen in the

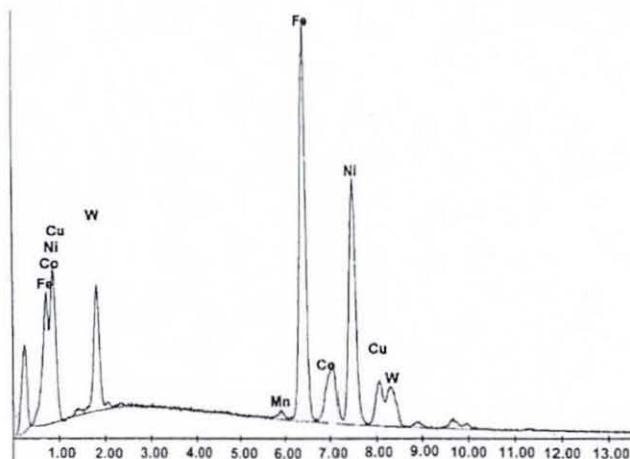


Fig. 2. EDS analysis of the matrix material in the swarf (the starting material).

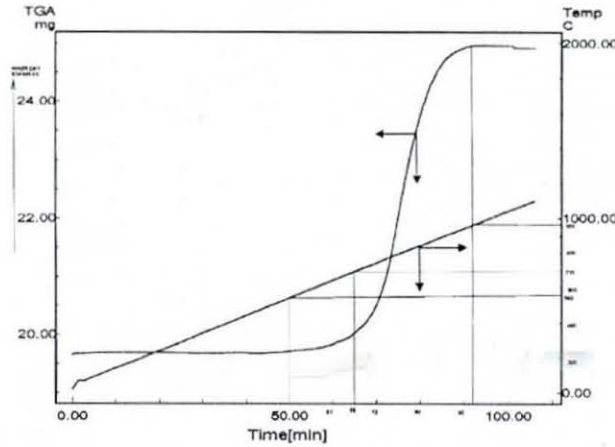


Fig. 3. Oxidation of the tungsten alloy swarf in air, from 20 °C to 1100 °C.

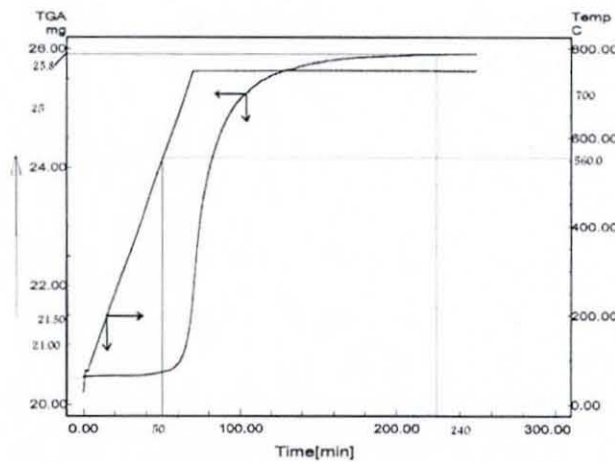


Fig. 4. Oxidation of the tungsten alloy swarf in air at 750 °C for 3 h.

fast oxidation region (700–950 °C) in addition to one in the fully oxidised region, in order to determine the best oxidation rate as a function of temperature.

Fig. 4 shows the oxidation of the W-alloy at 750 °C over a period of 3 h during which the mass increased from 20.4 to 25.8 mg. The results show that oxidation started after 50 min at 550 °C. After 220 min, the alloy was fully oxidised, exhibiting a mass difference of only 5.4 mg over 170 min.

At 800 °C, the mass increased rapidly from 20.4 to 25.9 mg in 70 min. The alloy was fully oxidised after 72 min with a maximum mass increase of 5.5 mg. In the experiment at 850 °C it was found that the weight increased rapidly from 20.4 to 25.9 mg in slightly less than 70 min. The total mass change was 5.5 mg.

If the tungsten mass in the swarf is taken to be 95%, the oxidation of the tungsten component of the sample would have given a

theoretical mass increase of only 4.8 mg. The Fe/Ni/Cu alloy matrix might have also oxidised to form the respective tungstates, accounting for an additional mass increase of 0.5 mg, giving a total mass increase of 5.3 mg. In these experiments it was observed that oxidation started at temperature of 550 °C, with full oxidation occurring at various temperatures and times as shown in Table 1.

At 750 °C, it was observed that the alloy took longer to fully oxidise [5,6], while, at the higher temperatures, the oxidation was faster. However, at higher temperatures, the oxide was less friable and appeared to have a larger particle size, as shown in Fig. 5. Hence, a greater quantity of powder (20 g) was oxidised at 800 °C, 900 °C, 950 °C, and 1000 °C for 3 h in the furnace.

Fig. 6 shows the XRD spectrum of the oxidised specimen produced at 900 °C. The only peaks observed on this figure are associated with the oxide materials WO_3 , Mn_2O_3 , and Fe_2O_3 , which

Table 1
Time taken to fully oxidise sample of tungsten swarf at different temperatures.

Temperature (°C)	Time to fully oxidise ~20 mg sample (min)	Time to oxidise ~80 mg sample (min)
750	170	–
800	72	–
850	68	–
900	–	60
950	–	31
1000	–	29

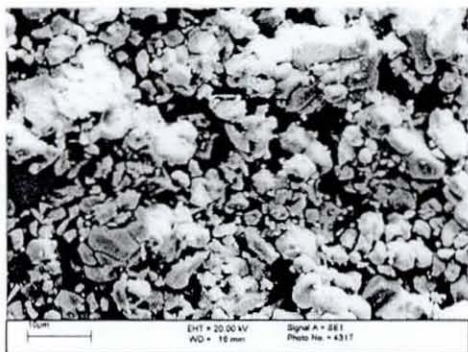


Fig. 5. SEM micrograph of the oxide after oxidation at 1000 °C.

confirms full oxidation of the sample. It was observed that the samples yielded similar results at all temperatures (i.e., tungsten oxide and the other metals tungstates). The tungsten content was more than 95% in the starting alloy and the matrix that comprised the remaining 5% contained 15% W and 85% other alloying elements. Thus, it is not surprising that evidence of some additional oxidised products was not observed, since the oxides were likely present at levels lower than the detection limit of XRD.

For all quantities of swarf studied, a 3-h oxidation period was selected to ensure that complete oxidation was achieved. The oxidation of these materials was verified by subsequent XRD analyses.

At the higher temperatures, 900 °C, 950 °C and 1000 °C, 80 mg samples were evaluated by TGA, where the results are summarised in Fig. 7. The mass difference was 22 mg, 79% of the total mass, which is the same percentage mass of oxidised sample observed in the previous lower temperature experiments. The oxidation time, however, was different. At 900 °C, the oxidation time was 60 min, while at 950 °C and 1000 °C it was 31 and 29 min, respectively. These experiments reveal that full oxidation of the W alloy at high temperatures depends on both time and temperature, and that the rate of oxidation (weight gain) is constant for complete oxidation. At higher temperatures (900 °C, 950 °C and 1000 °C) the particle sizes produced are larger. At 1000 °C, the oxidation is faster (see Table 1), resulting in larger oxide powder and particles with a better defined form (Fig. 5).

3.2. Reduction

The reduction experiment was carried out at 800 °C for 3 h in dry hydrogen atmosphere [12]. The XRD results for the product obtained after 3 h are shown in Fig. 8. In this spectrum two main peaks are observed, corresponding to W and a mix of Fe and Ni. There was no evidence of oxide in the material.

The EDS analysis data shows a tungsten peak (W) and a very small iron peak (Fe). The quantitative analysis shows 99.23% tungsten and 0.77% Fe, which is close to the detection limit for this technique. Ni was not detected by EDS, likely due to its very low concentration.

4. Mathematical model

A data set was compiled, covering the effect of oxidation rate with respect to temperature (750 °C to 1000 °C) and the time taken for full oxidation. Figs. 3 and 4 illustrate that, for a range of temperatures, the oxidation rate follows a similar pattern but that, if a different quantity of swarf were used, the rate could become dependent on both time and temperature.

For each temperature, a number of points were recorded from the measured oxidation curve. The shape of the curves is well represented by the following equation:

$$W = A - \frac{B}{1 - \exp C \cdot (t - t_0)}$$

where W is the mass of the alloy (g), t is the heating time (min), A is the maximum mass of alloy produced at full oxidation (g), C is a

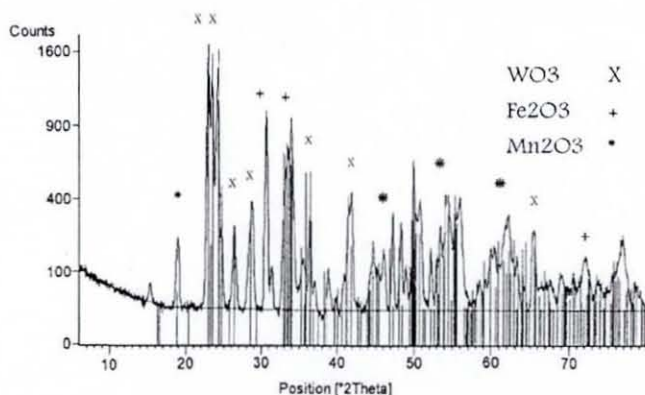


Fig. 6. XRD analysis of the tungsten alloy oxide.

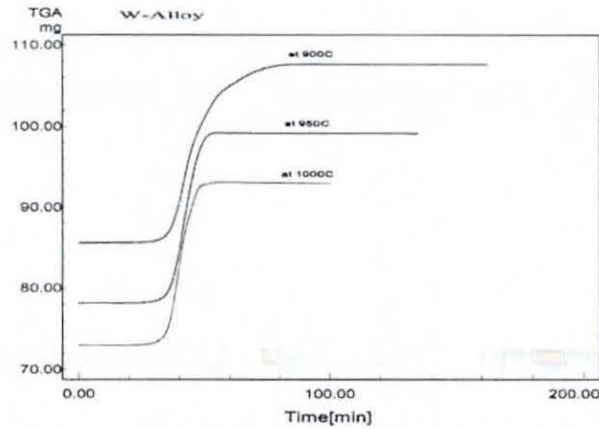


Fig. 7. Progress of the oxidation of 20 mg samples at 900 °C, 950 °C and 1000 °C.

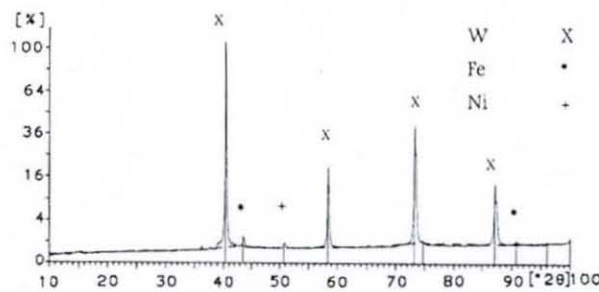


Fig. 8. XRD for the final, fully reduced powder.

factor related to the rate of mass change in the sample at 50% tungsten to tungsten oxide conversion, and \bar{t} is the oxidation time (min) that corresponds to 50% conversion. B, given by A minus the initial mass of tungsten, is equal to $0.26 M_i$.

The experimental values obtained for A, B, C, and \bar{t} are shown in Table 2. An increase in the alloy mass during is observed during the oxidation process, which is expressed by $(A-B)/A$. These data show that the mass percent is between 78.73% at 950 °C and 84.55% at 900 °C. Furthermore, the oxidation time at 900 °C is a minimum of 38 min, which gives the maximum C-factor of 0.5.

$$W = 1.2M_i - \frac{0.2M_i}{1 - \exp(C \cdot (t - \bar{t}))} = M_i \left(\frac{1 - 0.2 \exp(t - \bar{t})}{1 - \exp(-c(t - \bar{t}))} \right)$$

Using suitable statistical methods, a mathematical equation was obtained for the weight vs. temperature relationship, according to Table 2.

Using this equation, an oxidation curve was obtained over a temperature range of 750 °C to 1000 °C, as shown in the following graphs.

Table 2
Values of the equation parameters obtained at each temperature.

	750		800		850		900		950		1000	
	Calc.	Exp.	Calc.	Exp.	Calc.	Exp.	Calc.	Exp.	Calc.	Exp.	Calc.	Exp.
A	25.9	25.8	25.9	25.9	25.7	25.7	86.1	105.2	99.2	100.2	108	97
B	5.4	5.4	5.5	5.5	5.4	5.4	13.3	22	21.1	21	22.5	20.5
C	0.2	0.25	0.2	0.25	0.2	0.3	0.5	0.25	0.3	0.38	0.2	0.2
\bar{t}	76	78	76	73	76	78	38	45	43	43	45	40

To find the oxidation time \bar{t} from these graphs, it is necessary to find the central point of the oxidation process, according to the following equation:

$$O_{\text{central}} = O_s + \frac{O_e - O_s}{2}$$

where O_s is the start of oxidation and O_e is the end of oxidation.

Finally, convert this point to the axis where the oxidation time \bar{t} is located. For the C-factor, the following equation is used:

$$C\text{-factor} = \frac{\frac{O_e - O_s}{2}}{\frac{t(\text{max}) - t(\text{min})}{t(\text{max})}}$$

5. Conclusions

- At all temperatures, the oxidation rate (mass increase) ranged from 78% to 79% experimentally and from 78% to 84% mathematically, and the oxidation time decreased at higher temperatures.
- The lowest oxidation time was observed at 900 °C; furthermore, the best oxidation process was observed during the final stages of the oxidation process at 900 °C [7,8].
- At 1000 °C, the oxide powder particles were larger, which improves the oxide powder shape.
- The oxide powders formed consisted of WO_3 and Ni_2O_3 .
- The reduced powder particles consist of W, Fe, and Ni, with a particle size of 1–3 μm .
- At higher temperatures, the reduction process is more complicated and powder particles are larger and more irregular.

References

- Cotton FA, Wilkinson G. *Advances in organic chemistry*, 5th ed. Wiley; 1988.
- Sberveglieri G. Recent developments in semiconducting thin-film gas sensors. *Sens Actuators B: Chem* 1995;23:103–9.
- Sberveglieri G, Depero L, Groppe S, Nelli P. WO_3 sputtered thin films for NO_x monitoring. *Sens Actuators B: Chem* 1995;26:89–92.
- Yamazoe N, Miura N. *New approaches in the design of Gas Sensors. Gas sensors: principles, operation, and developments*; 1992.
- Yuehui H, Libao C, Baiyun H, Liaw P. Recycling of heavy metal alloy turnings to powder by oxidation-reduction process. *Int J Refract Met Hard Mater* 2003;21:227–31.
- Sikka V, Rosa C. The oxidation kinetics of tungsten and the determination of oxygen diffusion coefficient in tungsten trioxide. *Corros Sci* 1980;20:1201–19.
- Jiqiao L, Baiyun H, Zhiqiang Z. Determination of physical characterization of tungsten oxides. *Int J Refract Met Hard Mater* 2001;19:79–84.
- Warren A, Nylund A, Olofsson I. Oxidation of tungsten and tungsten carbide in dry and humid atmospheres. *Int J Refract Met Hard Mater* 1996;14:345–53.
- Lassner E, Schubert WD. *Tungsten properties, chemistry, technology of the element, alloys, and chemical compounds*. Kluwer Academic; 1999.
- Pierre GRS, Ebihara WT, Pool MJ, Speiser R. Tungsten-oxygen system. *Trans Metall Soc AIME* 1962;224:259–64.
- Yih SWH, Wang CT. *Tungsten sources, metallurgy, properties, and applications*. New York and London: Plenum Press; 1979.
- Schubert W. Kinetics of the hydrogen reduction of tungsten oxides. In: 12th international plansee seminar'89: high temperature and wear resistant materials in a world of changing technology, vol. 4; 1989. p. 41–78.

A. Alhazza

Department of Chemical Engineering, Loughborough University
Loughborough, Leicestershire, LE11 3TU, UK.

A. e-mail: cgaaa@lboro.ac.uk

Abstract—The recycling process of Tungsten alloy (Swarf) by oxidation reduction technique have been investigated. The reduced swarf was pressed under a pressure 20Kg/cm² and sintered at 50°C in dry hydrogen atmosphere. The particle size of the recycled alloy powder was 1-3 µm and the shape was regular at a reduction temperature 800°C. The chemical composition of the recycled alloy the same as the primary Swarf.

Keywords—Recycling, Swarf, Oxidation, Reduction.

I. INTRODUCTION

TUNGSTEN and tungsten alloy group represent a wide range of uses extending from every day uses (coil of an incandescent lamp) to component of nuclear fusion reactor or ion drive motors in space probes. The reason of this range of uses lies in the many outstanding properties of tungsten, high melting point, low vapour pressure, high atomic number, good electrical and thermal conductivity. [1,2]

Recently, the recycling of tungsten alloys techniques are economically viable and ecologically acceptable [2].

Scrap recycling is a very important factor on the supply of tungsten materials, where 1/3 of the total tungsten demand is supplied by tungsten alloy scrap. Furthermore, the least valuable scrap, like low-grade grinding sludge, contains about 5 times more tungsten than the average ore. Most scrap concentration. [1]

The aim of this work is to produce from a heavy metal swarf a homogenous powder by a controlled oxidation to break down the swarf, followed by a reduction process and finally pressing and sintering at certain temperature.

II. EXPERIMENTAL PROCEDURE

A. Sample Preparation

This work was carried out using heavy metal (tungsten) swarf taken from cutting machine waste. Samples for study were prepared first by washing the swarf in acetone in order to remove the oil that was used as the cooling fluid in the cutting machines. After the acetone wash, the swarf was dried at room temperature for 5 hours; it was then washed several times with distilled water to remove other possible deposits, and then dried at room temperature for 5 hours.

The swarf was mounted in cold-setting resin and polished to 6µm for 10 minutes and then etched by immersing the sample in "Nital" (Nital is an acid which removes the lighter elements from the surface of the polished samples to give two or more layers on the surface to reveal the microstructures)

chemical composition tested by Energy Dispersive Spectrometer (EDS) is listed in Table I.

For XRD analysis, the sample was ground and sieved a heavy metal powder of less than 150µm was prepared analysis.

In the final stages after the pressing and sintering pressed pallet was placed in a cold resin for mounting polishing.

TABLE I
CHEMICAL COMPOSITION OF THE PRIMARY TUNGSTEN ALLOY SWARF

composition %	W	Ni	Fe	Cu	Co	Mn
Grain	100	--	--	--	--	--
Matrix	15	36	35	8	3	0.6

B. Materials Characterization

The samples were characterised using XRD and SEM. The first characterisation was of the starting material, and subsequent characterisation was carried out after oxidation reduction, and finally after pressing and sintering

C. Oxidation Experiments

The oxidation experiments were carried out using two types of instruments according to the required analysis. Initially isothermal TGA was used with 20 mg of sample to study oxidation in a natural air environment. The experiment was carried out in order to determine the oxidation rate over a temperature range from 20°C to 1100°C. Subsequently different experiments were carried out at six different temperatures with fixed holding times. The conditions used in these experiments were 750°C, 800°C, 850°C, 900°C, 950°C and 1000°C, each with a holding time of 3 hours.

Secondly, oxidation of larger quantities (20 grams) of tungsten alloy swarf was carried out using an electric resistance Carbolite furnace to produce larger amount of oxide samples. The heavy metal swarf powder was oxidised in air at the same temperatures and for the same time determined from the TGA data. The sample was placed in ceramic boats in the furnace (the boats were inert at all temperatures, so did not react with other elements).

D. Reduction Experiment

The reduction experiments were carried out using "Vecstar Furnace" with a gas supply system. The furnace was set at an upper operating temperature of 1600°C and to accommodate gram amounts of powder. The reduction was studied at 800°C temperature for (300mg) of oxide powder.

The furnace was heated to the required temperature at

microscopy and for subsequent processing to give a sintered product.

E. Pressing and Sintering

The reduced powder was pressed into compacts using a pressure of 20 Kg/cm² in a single cylindrical die of 3.5 mm.

The compacted sample was then sintered in the same furnace used for reduction. The sintering was carried out in hydrogen gas in order to prevent the re-oxidation of the tungsten and at the same flow rate as that used for the reduction. The temperature was raised gradually at a rate of 300°C/hr to the sintering temperature. When the sintering process is completed the sample removed to be analysed in the scanning electron microscopy.

III. RESULTS AND DISCUSSION

A. Oxidation

Scanning electron micrographs show that the swarf was a composite material, with a grain size of 10 to 20 µm. Fig. 1 shows that the tungsten grains account for more than 95% of the composite swarf in the view. XRD analysis verified the EDS analysis and showed a diffraction pattern containing peaks that could be clearly related to the tungsten grains and a collection of other peaks associated with the Fe-Ni-Cu matrix alloy.

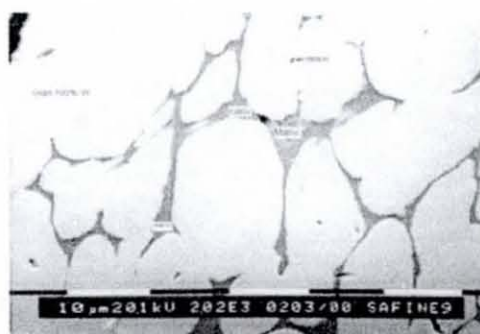


Fig. 1 Micrograph of tungsten swarf material showing tungsten grains embedded in a matrix material

The TGA data, typical examples of which are shown in Figs. 2 and 3, showed the progress of the oxidation of 20 mg samples of the swarf. The initial run using TGA, Fig. 2, was carried out to determine the temperature range over which the W-alloy oxidation took place. Subsequent TGA analyses determined the rate of oxidation at different temperatures within the range determined previously for the oxidation of the alloy.

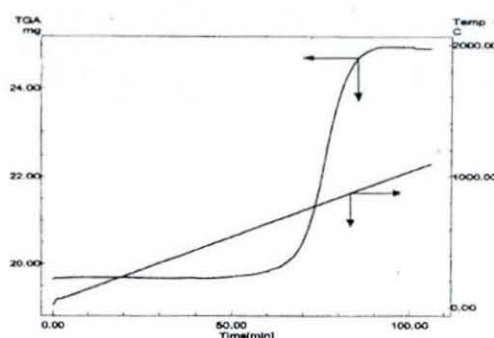


Fig. 2 Oxidation of tungsten alloy swarf in air over the temperature range from 20°C to 1100°C

It shows the trace obtained during first experiment, which was carried out over the temperature range from 20°C to 1100°C in 100 minutes. It can be observed that the oxidation process started at about 560°C (50 minutes after the start of the test). The oxidation was observed through measurement of the increase in the mass of the sample whilst being heated, since the W reacts with oxygen to form tungsten oxide. Fig. 2 shows that rapid oxidation occurs around 700°C to 870°C after 65 minutes, and the sample is fully oxidized at 960°C after 92 minutes. In order to determine the best oxidation rate, six different isothermal experiments were carried out at 750°C, 800°C, 850°C, 900°C, 950°C and 1000°C. Five temperatures were chosen in the fast oxidation region (700°C to 950°C) and the last one in the fully oxidized region in order to determine the best oxidation rate as a function of temperature.

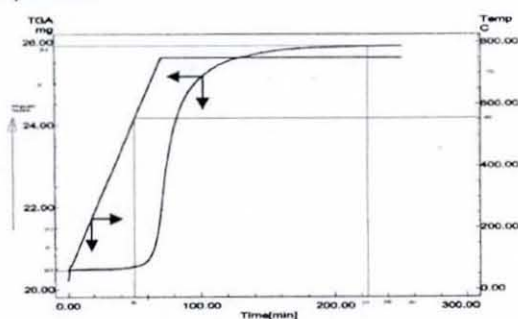


Fig. 3 Oxidation of tungsten alloy swarf in air at 750°C for 3 hours

Fig. 3 shows the oxidation of the W-alloy at 750°C over a period of three hours during which the mass changed from 20.4 mg to 25.8 mg. The results show that the oxidation starts after 50 minutes at 550°C. Above 220 minutes the alloy was fully oxidised with a mass difference of 5.4 mg in 170 minutes.

At 800°C the mass changed rapidly from 20.4 mg to 25.9 mg in 70 minutes, then the alloy was fully oxidised after 72 minutes with a maximum mass change of 5.5 mg. In the

experiment at 850°C it was found that the weight increased rapidly from 20.4 mg to 25.9 mg in slightly less than 70 minutes. The full mass change was 5.5 mg.

If the tungsten mass in the swarf is taken to be 95%, the oxidation of the tungsten part of the sample would have given a mass gain of 4.8 mg. The Fe/Ni/Cu alloy matrix would have oxidised to give the respective tungstates and a mass gain of 0.5 mg, thus giving a total mass gain of 5.3 mg. In these experiments it was observed that the oxidation starts at temperature of 550°C with full oxidation occurring at the different temperatures but taking different times as shown in Table II.

TABLE II
TIME TAKEN TO FULLY OXIDIZE SAMPLE OF THEN TUNGSTEN SWARF AT DIFFERENT TEMPERATURES

Temperature (°C)	Time to oxidise 20mg (minutes)	Time to oxidise 80 mg (minutes)
750	170	-
800	72	-
850	68	-
900	-	60
950	-	31
1000	-	29

At 750°C it was observed that the alloy took a longer time to fully oxidized [3, 4], while at the higher temperatures the oxidation was faster. However, at the higher temperatures the oxide was less friable and appeared to have a larger particle size, shown in Fig. 4. Hence larger amounts of powder (20 grams) were oxidised at 800°C, 900°C, 950°C, and 1000°C for three hours in the furnace.

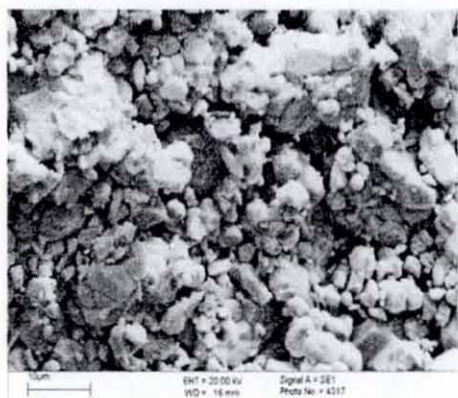


Fig. 4 SEM micrograph of the oxide after oxidation at 1000°C

Fig. 5 shows the XRD spectrum of the oxidised specimen produced at 900°C. The only peaks observed on this figure are associated with the oxide materials WO_3 , Mn_2O_3 and Fe_2O_3 , which confirmed the full oxidation of the sample. It was observed that at all temperatures the samples yielded similar results, i.e. tungsten oxide and the other metals tungstates. The tungsten content was more than 95% in the starting alloy and the matrix which comprised the remaining 5% contained 15 % of W and 85% of the other alloying elements. On this basis it is not surprising that evidence for some oxidised products could not be found as the oxides were likely to be present at a level lower than the detection limit of XRD.

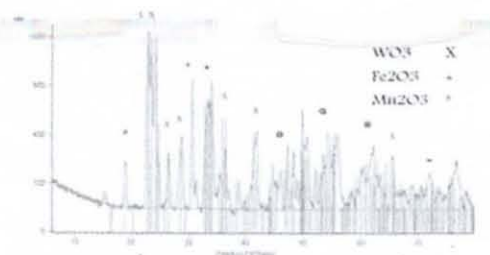


Fig. 5 XRD analysis for the tungsten alloy oxide

For all gram quantities of swarf, a 3 hour oxidation period was selected to ensure that complete oxidation occurred. The oxidation of these materials was verified by subsequent XRD analyses.

At the higher temperatures, 900°C, 950°C and 1000°C, 80 mg samples were evaluated by TGA. The mass difference was 22 milligrams, 79% of the total mass, which is the same percentage mass of the oxidised sample as in the previous lower temperature experiments, but the oxidation time is different. At 900°C, the oxidation time was 60 minutes while in 950 and 1000 it was (31 and 29 minutes respectively). The main observation in these experiments reveals that the full oxidation of the W alloy at high temperatures depends on time and temperature, and the rate of oxidation (weight gain) is constant at fully oxidation process. At higher temperatures (900°C, 950°C and 1000°C) the particle sizes are bigger, and at 1000°C not only is the oxide powder larger but the particles also have a better defined form (Fig. 5) and oxidation is faster (see Table II).

B. Reduction

The reduction experiment was carried out at 800°C for three hours in dry hydrogen atmosphere. The XRD data for a product obtained after three hours are W and a mix of Fe and Ni, and there was no evidence of any oxide in the material.

The EDS analysis data showed a tungsten peak and a very small iron peak (Fe). The quantitative analysis carried out showed 0.77% of the Fe, which is just below the claimed detection limit of the technique, and 99.23% tungsten. The Ni was not detected by EDS due to its very small concentration.

C. Pressing and Sintering

After the reduction of the oxide was completed and the XRD analysis showed the full reduction of the material, the powder was prepared for pressing and sintering. The reduced powder was pressed under a pressure of 20Kg/cm² using a 3.5mm single-action die.

Based on a previously published paper [5,6,7], a sintering temperature of 1150°C was used for all the compacted materials. The sample was placed in the furnace for three hours at a temperature 1150°C under a dry hydrogen atmosphere to prevent re-oxidation of the material.

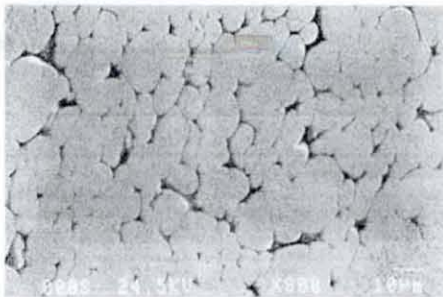


Fig. 6 Micrograph for the compacted pellet

Fig. 6 shows the compacted and sintered material obtained from the fully reduced powders. The micrograph shows that some of the grains of the tungsten have taken the same shape and size (20µm) as the un-deformed grains in the starting material Fig. 1. However, it is evident that as well as having the useful W grains present in the microstructure there seems to a rather more densified very small grained region surrounding the more round tungsten grains Fig. 6. The conclusion to be drawn here is that a massive growth and coalescence of small grains have yielded the 20µm grains during sintering.

IV. CONCLUSION

- 1) In all oxidation temperatures, the mass increasing rate was about 79% for all alloys quantities.
- 2) The lowest oxidation time and the best oxidation process was at 900°C; At 1000°C the oxide powder particles were larger which improves the oxide powder property.
- 3) The reduction sequence can be summarized as

$$\text{WO}_3 \rightarrow \text{WO}_{2.9} \rightarrow \text{WO}_{2.72} \rightarrow \text{WO}_2 \rightarrow \text{W}$$
- 4) The reduced powder particles consist of W, Fe, and Ni.
- 5) Some region of compacted and sintered pellet showed a microstructure that was very similar to that of the starting swarf. However, very fine grained regions were also observed.

REFERENCES

- [1] E. Lassner and W.D. Schubert, 1999. Tungsten Properties, Chemistry, Technology of the Element, Alloys, and Chemical Compounds, New York, Kluwer Academic.
- [2] G. D. Rieck, 1967. Tungsten and its compound, Oxford, Pergamon Press Ltd.
- [3] H. Yuehui, C. Libao, H. Baiyun and P.K. Liaw, Recycling of heavy metal alloy turning to powder by oxidation reduction process. International Journal of Refractory Metals and Hard Materials, 2003, 21, 227-231.
- [4] V.K. Sikka and C.J. Rosa, The oxidation kinetics of tungsten and the determination of oxygen diffusion coefficient in tungsten trioxide. Corrosion Science, 2003, 20, P.1201-1219.
- [5] J. N. Albiston and F. R. Sale, Thermogravimetric Studies of the Hydrogen Reduction of Nickel Tungstate, Thermochemical Acta, 103 (1986) 175-180.
- [6] P. Walkden and F. R. Sale, Silver-Tungsten contacts by the hydrogen Reduction of silver Tungstate, 28th Holm conf. On Electrical Contacts, p. 101-107.
- [7] F. R. Sale and J. N. Albiston, Production and sintering of Ag-W composites containing Ni, P/M Conf., Orlando (1988).

REDUCTION AND PRESSING OF W-OXIDE

Abdulsalam Alhazza

60 Barsby Drive, Loughborough University, Leicestershire LE11 5UJ, UK

A.A.Alhazza@lboro.ac.uk

ABSTRACT

On the basis of previously published work the reduction process in the present work was carried out at the temperature of 800°C for 3 hours. The resultant powder was characterised using X-ray diffraction analysis and scanning electron microscopy. Using the data from the characterisation study, a gram scale reduction was carried out under the same experimental conditions to produce powder for further processing. The resultant powder was pressed under a pressure 20 Kg/cm² and sintered at 1150°C for 3 hours under a dry hydrogen atmosphere to prevent re-oxidation. A microstructural study of the sintered compact has been carried out using scanning electron microscopy.

OXIDATION OF TUNGSTEN ALLOY AT HIGH TEMPERATURES IN NATURAL AIR

A. A. Alhazza¹

The purpose of this work was to produce from "heavy metal" swarf a homogenous powder for recycling. To produce such a powder a controlled oxidation process was carried out. The oxidation was achieved over the temperature range 750 to 1000°C and was studied by thermogravimetry (TGA). The oxide was characterised by X-ray diffraction analysis and scanning electron microscopy.

Keyword: Oxidation; recycling; swarf; thermogravimetry

INTRODUCTION

Tungsten and tungsten alloys have a wide range of uses extending from everyday ones (e.g. the coil of an incandescent lamp or the contact tip of an electrical switch or an automobile horn) to components of nuclear fusion reactors or ion drive motors in space probes. The reason for this range of use lies in the many outstanding properties of tungsten, notably its high melting point, low vapour pressure, high atomic number, and good electrical and thermal conductivities.

In the W-O system, there are not only the stoichiometric oxides WO_3 , $WO_{2.9}$, $WO_{2.7}$, and WO_2 , but also non-stoichiometric structure that represent the ordered or partially ordered defect structures of the oxygen-rich oxide in which the central W atom is octahedrally surrounded by six oxygen atoms. In WO_3 , neighbouring octahedra are in contact only at the corners, which increase oxygen deficiency (reduction, conversion to lower oxides), common edges and surfaces are progressively formed.

The aim of this work is to produce from a "heavy metal swarf" a homogeneous powder for recycling. The process route envisaged was a controlled oxidation to breakdown the swarf. In the first step the microstructure of the swarf was characterised using optical metallography, SEM, and XRD. This characterisation was followed by oxidation to achieve the mechanical breakdown and to give a friable oxide. In this step a TG was used to determine the temperatures for oxidation and to give some idea on the kinetics of the process. SEM and XRD were used to find the morphology and the type of the oxide. According to the TG results, temperatures were selected for oxide manufacture.

EXPERIMENTAL PROCEDURE

Sample preparation

This work was carried out using heavy metal swarf, which was taken from cutting machine waste. Samples for study were prepared first by washing the swarf in acetone in order to remove the oil that was used as the cooling fluid in the cutting machines. After washing, the swarf was dried at room temperature for 5 hours and then washed several times with

¹ Chemical Engineering Department, Loughborough University; E-mail: cgaaa@lboro.ac.uk

اندية ومدارس الطلاب السعوديين في المملكة المتحدة وايرلندا (الدورة ٢٦)



مؤتمر الإبداع العالمي

The Saudi Innovation Conference



شُكْرًا

تتقدم الملحقية الثقافية والصينة الادارية لاندية الطلاب السعوديين في المملكة المتحدة وايرلندا

ممثلة في الدورة السادسة والعشرون باسمي آيات الشكر والتقدير

للأستاذ / محمد السلام احمد المزاح

وذلك نظير جهوده المتميزة في إنجاح مؤتمر الابداع السعودي والمقام بمدينة نيوكاسل في
الفترة من 11-12 مايو 2007 والتي كان لها ابلغ الأثر في اظهار فعالياته بالشكل المأمول متمنين له

مزيجاً من التوفيق والسداد



الملحق الثقافي بالمملكة المتحدة وايرلندا

عبدالله الناصر

الرئيس العام لاندية الطلاب السعوديين

بالمملكة المتحدة وايرلندا للدورة (٢٦)

احمد بن صالح الزهراني



CERTIFICATE OF PRESENTATION

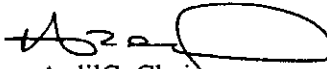
WCSET 2008

WORLD CONGRESS ON SCIENCE, ENGINEERING AND TECHNOLOGY

This certificate is awarded to

A. A. Alhazza

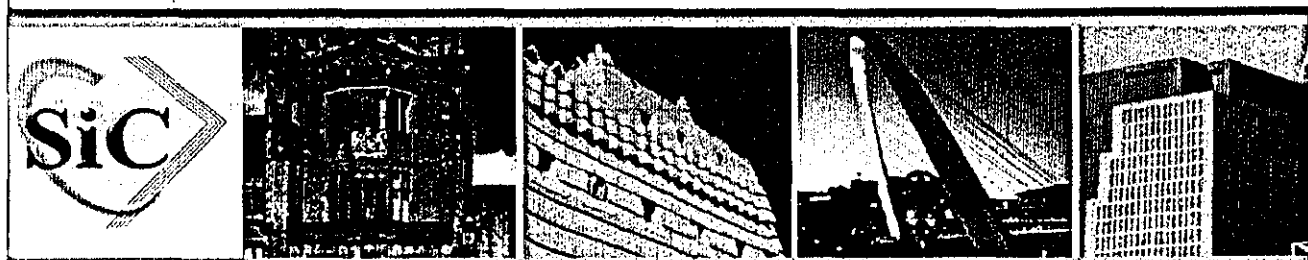
In technical presentation, recognition and appreciation of research contributions to the ICME 2008: International Conference on Manufacturing Engineering


Ardil C. Chair
WCSET 2008

Paris, France
November 21-23, 2008



SAUDI ARABIAN CULTURAL BUREAU IN LONDON
SAUDI STUDENTS CLUBS AND SCHOOLS IN THE UK
AND IRELAND TERM 26th



THE SAUDI INNOVATION CONFERENCE 2007

Proceeding of the Saudi Innovation
Conference 2007

11th-12th May 2007

Newcastle University
Newcastle upon Tyne, The United Kingdom

Edited By Ali Mesfer Al-Yami

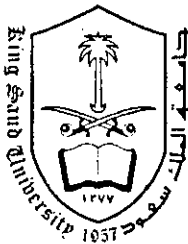
Saudi International INNOVATION CONFERENCE 2008 9 & 10 JUNE



ABSTRACTS' PROCEEDING

Editors:

Al-Shahrani, Farhan; Alalshikh, Mohammad, Al-Gharndi, Ahmed; Al-Kazemi, Basem; Al-Banyan
AbdulMajeed; Al-Shehry, Abdullah; Al-Yami, Ali

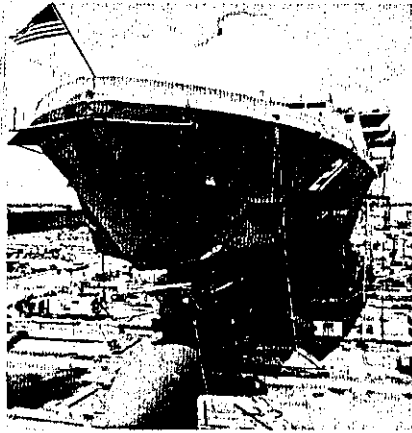


Appendix B

MATLAB Calculation for the area analysis in the tungsten alloy composite material

```
I = imread ('a8.bmp');           % to open the image file
Level = graythresh(I); % to adjust the scale
Bw = im2bw(I,level);           % to change image to black and white
SE = ones(5);
Bw2 = imdilate(bw,SE);
Increase = (bwarea(bw2)-bwarea(bw))/bwarea(bw);
```

HERE SHE IS!!!!
Made from the World Trade Center.



USS New York

It was built with 24 tons of scrap steel from the World Trade Center .

It is the fifth in a new class of warship - designed for missions that include special operations against terrorists. It will carry a crew of 360 sailors and 700 combat-ready Marines to be delivered ashore by helicopters and assault craft.

Steel from the World Trade Center was melted down in a foundry in Amite, LA to cast the ship's bow section. When it was poured into the molds on Sept 9, 2003, 'those big rough steelworkers treated it with total reverence,' recalled Navy Capt. Kevin Wensing, who was there. 'It was a spiritual moment for everybody there.'

Junior Chavers, foundry operations manager, said that when the trade center steel first arrived, he touched it with his hand and the 'hair on my neck stood up.' 'It had a big meaning to it for all of us,' he said. 'They knocked us down. They can't keep us down. We're going to be back.'

The ship's motto? 'Never Forget'

SEM analysis for oxidation at 900°C

C:\EDS\USR\abdul salam edx 26-05-06\900\2cw

Acquisition Time:11:38:55 Date:26-May-2006

kV:20.00 Tilt: 0.00 Take-off:42.25 AmpT:10.0
 Detector Type :SUTW- Resolution
 Sapphire :139.20 Lsec :30

EDAX ZAF Quantification Standardless
 Oxides
 SEC Table : Default

Element	Wt %	Mol %	K-Ratio	Z	A	F
Fe2O3	3.54	7.72	0.0278	1.1385	0.9318	1.0594
NiO	2.98	13.9	0.0295	1.172	0.9569	1.1213
W2O3	93.48	78.38	0.7555	0.9087	1.0054	1
Total	100	100				

Element	Net Inte.	Bkgd Inte.	Inte. Error	P/B
FeK	76.27	48.7	3.15	1.57
NIK	57.42	46.6	3.9	1.23
W L	467.23	44.97	0.92	10.39

SEM analysis for oxidation at 950°C

C:\EDS\USR\abdul salam edx 26-05-06\950\2cw

Acquisition Time:11:45:33 Date:26-May-2006

kV:20.00 Tilt: 0.00 Take-off:42.31 AmpT:10.0
 Detector Type :SUTW- Resolution
 Sapphire :139.20 Lsec :30

EDAX ZAF Quantification Standardless
 Oxides
 SEC Table : Default

Element	Wt %	Mol %	K-Ratio	Z	A	F
Fe2O3	3.65	7.89	0.0287	1.1376	0.9321	1.0595
NiO	3.19	14.73	0.0315	1.1709	0.9571	1.1208
W2O3	93.16	77.37	0.7521	0.9078	1.0053	1
Total	100	100				

Element	Net Inte.	Bkgd Inte.	Inte. Error	P/B
FeK	75.1	45.6	3.14	1.65
NiK	58.53	41.87	3.72	1.4
W L	443.83	39.2	0.94	11.32

SEM analysis for oxidation at 1000°C

CAEDS\USR\abdul salam edx 26-05-06\100>2gw

Acquisition Time:11:54:55 Date:26-May-2006

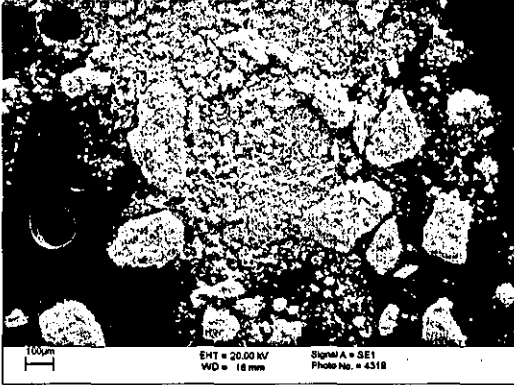
kV:20.00 Tilt: 0.00 Take-off:42.57 AmpT:10.0
 Detector Type :SUTW-Sapphire Resolution :139.20 Lsec :30

EDAX ZAF Quantification Standardless
 Oxides
 SEC Table : Default

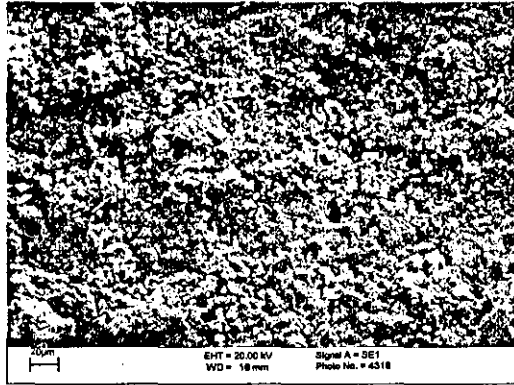
Element	Wt %	Mol %	K-Ratio	Z	A	F
Fe2O3	3.79	8.23	0.0298	1.1376	0.9324	1.0594
NiO	3.05	14.14	0.0301	1.1709	0.9572	1.121
W2O3	93.16	77.63	0.752	0.9078	1.0053	1
Total	100	100				

Element	Net Inte.	Bkgd Inte.	Inte. Error	P/B
FeK	80.7	48.23	3.01	1.67
NiK	57.9	44.07	3.81	1.31
W L	458.93	41.07	0.93	11.18

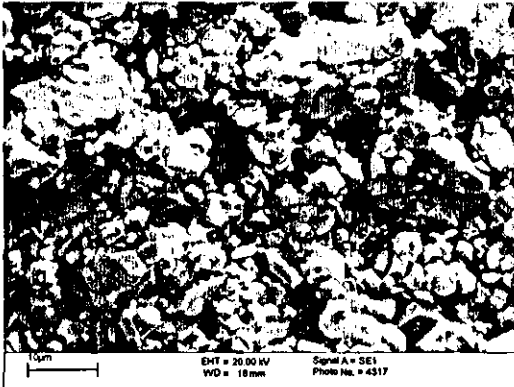
Oxide Powder Photos



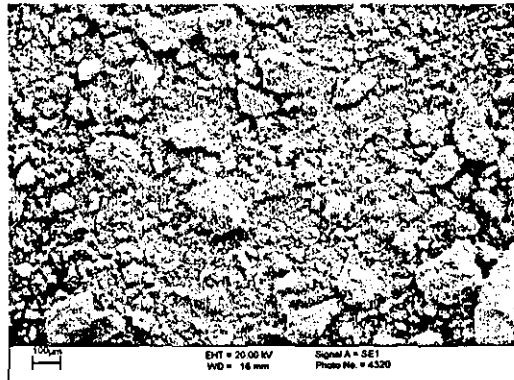
1000°C



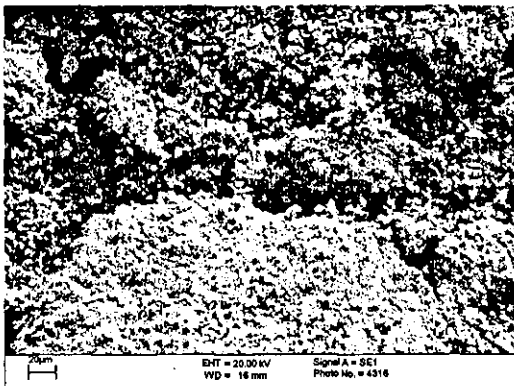
1000°C



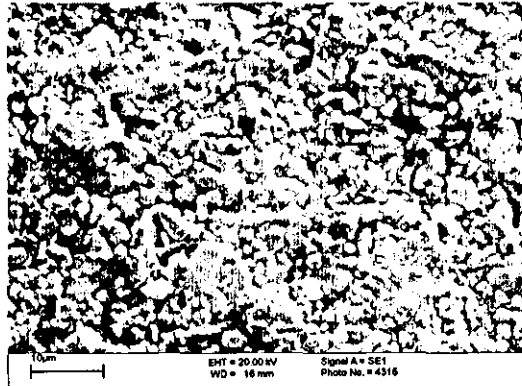
1000°C



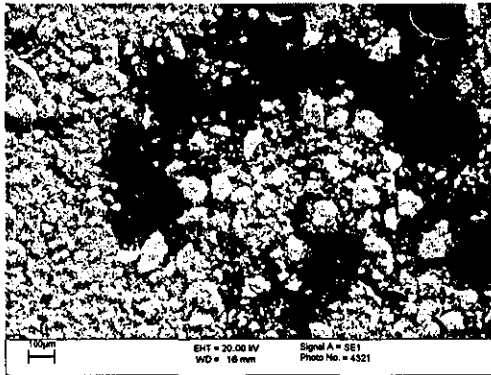
950°C



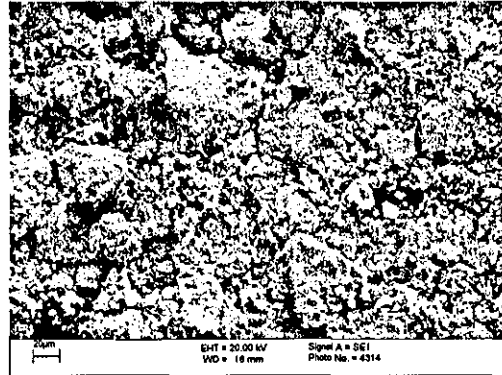
950°C



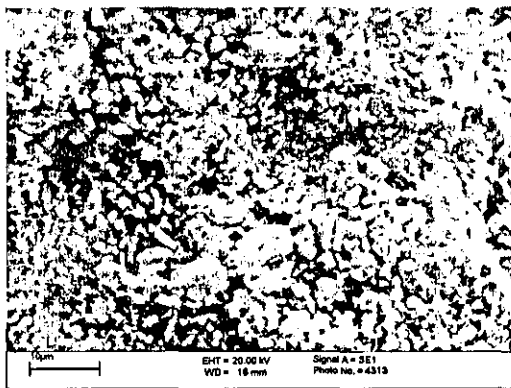
950°C



900°C

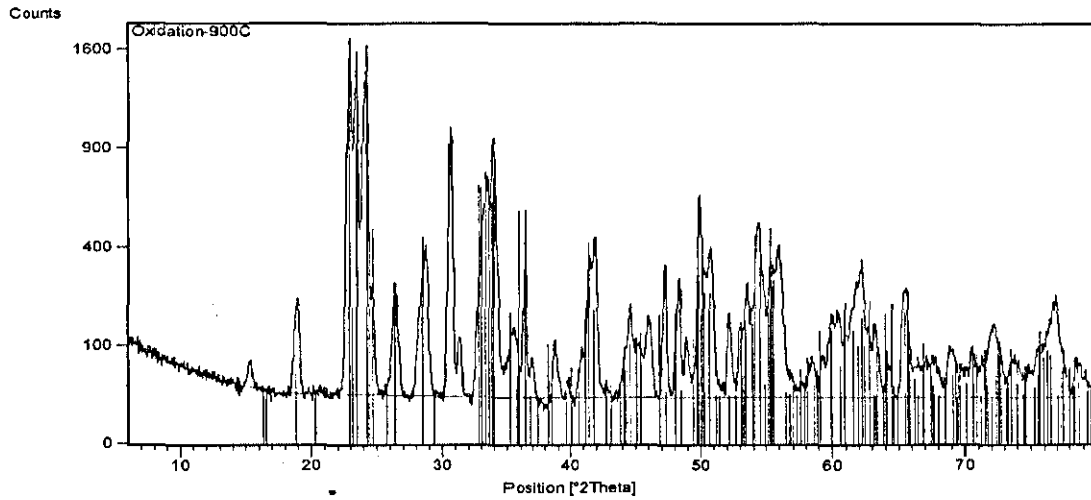


900°C



900°C

XRD for oxidation at 900°C



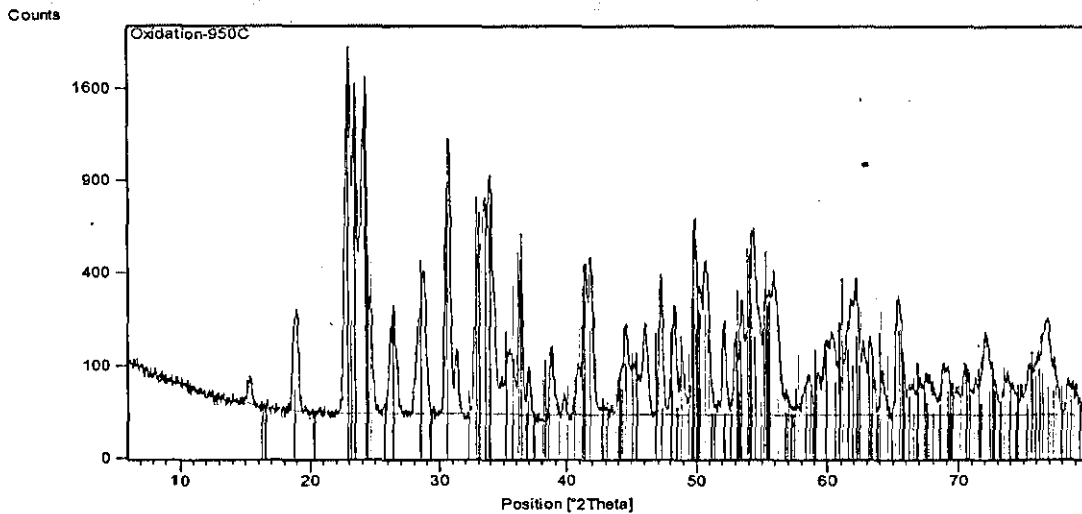
Residue + Peak List

01-071-0131	
01-084-0314	
01-084-0317	
01-084-0309	
00-031-0825	

Appendix

No.	Visible	Ref. Code	Compound Name	Chemical Formula	Score	Scale F...	SemiQu...
1	<input checked="" type="checkbox"/>	01-071-0131	Tungsten Oxide	WO ₃	58	0.878	
2	<input checked="" type="checkbox"/>	01-084-0314	Chromium Oxide	Cr ₂ O ₃	44	0.318	
3	<input checked="" type="checkbox"/>	01-084-0317	Vanadium Oxide	V ₂ O ₃	42	0.251	
4	<input checked="" type="checkbox"/>	01-084-0309	Iron Oxide	Fe ₂ O ₃	40	0.404	
5	<input checked="" type="checkbox"/>	00-031-0825	Bixbyite-ITCARG, syn	Mn ₂ O ₃	38	0.364	

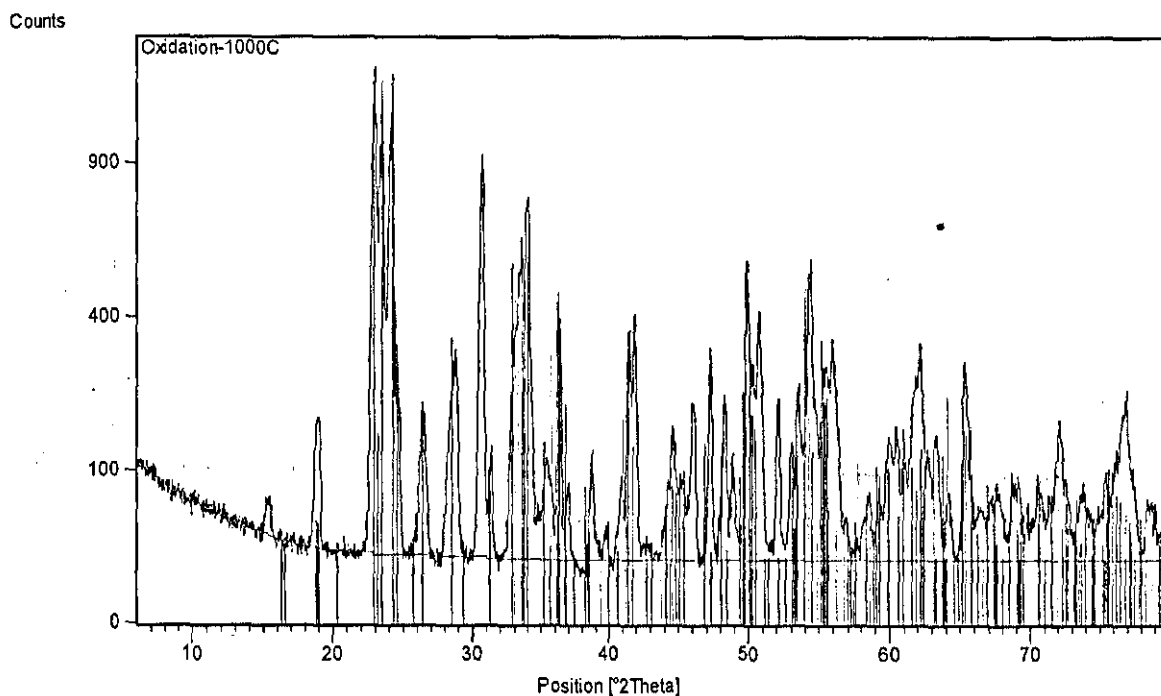
XRD for oxidation at 950°C



Residue + Peak List
01-071-0131
01-084-0317
01-084-0314
01-084-1396
00-031-0825
00-013-0534
00-035-0584

No.	Visible	Ref. Code	Compound Name	Chemical Formula	Score	Scale F...	SemiQu...
1	<input checked="" type="checkbox"/>	01-071-0131	Tungsten Oxide	WO ₃	56	0.763	
2	<input checked="" type="checkbox"/>	01-084-0317	Vanadium Oxide	V ₂ O ₃	41	0.223	
3	<input checked="" type="checkbox"/>	01-084-0314	Chromium Oxide	Cr ₂ O ₃	41	0.278	
4	<input checked="" type="checkbox"/>	01-085-1396	Karelianite chromian, low - synth...	(Cr _{0.052} V _{0.948}) ₂ O ₃	40	0.256	
5	<input checked="" type="checkbox"/>	00-031-0825	Bixbyite-ITCARG, syn	Mn ₂ O ₃	38	0.352	
6	<input checked="" type="checkbox"/>	00-013-0534	Hematite, syn	Fe ₂ O ₃	31	0.300	
7	<input checked="" type="checkbox"/>	00-035-0584	Srilankite	(Ti, Zr)O ₂	35	0.466	

XRD for oxidation at 1000°C



Residue + Peak List	
01-071-0131	
01-085-1396	
01-085-1403	
01-084-0313	
00-010-0069	
00-013-0534	
00-026-1136	

No.	Visible	Ref. Code	Compound Name	Chemical Formula	Score	Scale F...	SemiQu...
1	<input checked="" type="checkbox"/>	01-071-0131	Tungsten Oxide	W O3	54	0.859	-
2	<input checked="" type="checkbox"/>	01-085-1396	Karelianite chromian, low - synthetic	(Cr.0052 V.9948)2 O3	42	0.336	-
3	<input checked="" type="checkbox"/>	01-085-1403	Karelianite - synthetic	V2 O3	41	0.353	-
4	<input checked="" type="checkbox"/>	01-084-0313	Chromium Oxide	Cr2 O3	38	0.285	-
5	<input checked="" type="checkbox"/>	00-010-0069	Bixbyite, syn	Mn2 O3'	37	0.364	-
6	<input checked="" type="checkbox"/>	00-013-0534	Hematite, syn	Fe2 O3	28	0.394	-
7	<input checked="" type="checkbox"/>	00-026-1136	Iron Oxide	Fe3 O4	29	0.128	-
8	<input checked="" type="checkbox"/>	00-035-0584	Srilankite	(Ti , Zr) O2	33	0.594	-

Oxidation from 0- 1000°C

Appendix

Line #1	
4.68750000000000e-001	1.96658396946565e+001
1.25000000000000e+000	1.96661975190840e+001
1.87500000000000e+000	1.96664837786260e+001
2.81250000000000e+000	1.96783635496183e+001
3.59375000000000e+000	1.96787213740458e+001
4.68750000000000e+000	1.96792223282443e+001
6.25000000000000e+000	1.96799379770992e+001
8.90625000000000e+000	1.96811545801527e+001
1.14062500000000e+001	1.96822996183206e+001
1.35937500000000e+001	1.96833015267176e+001
1.68750000000000e+001	1.96848043893130e+001
1.96875000000000e+001	1.96860925572519e+001
2.10937500000000e+001	1.96867366412214e+001
2.25000000000000e+001	1.96873807251908e+001
2.42187500000000e+001	1.96767175572519e+001
2.64062500000000e+001	1.96777194656489e+001
3.00000000000000e+001	1.96793654580153e+001
3.32812500000000e+001	1.96808683206107e+001
3.50000000000000e+001	1.96816555343511e+001
3.71875000000000e+001	1.96826574427481e+001
4.06250000000000e+001	1.96842318702290e+001
4.37500000000000e+001	1.96742127862595e+001
4.64062500000000e+001	1.96868797709924e+001
4.92187500000000e+001	1.96996183206107e+001
5.01562500000000e+001	1.97114980916031e+001
5.09375000000000e+001	1.97233062977099e+001
5.18750000000000e+001	1.97237356870229e+001
5.29687500000000e+001	1.97356870229008e+001
5.40625000000000e+001	1.97476383587786e+001
5.48437500000000e+001	1.97479961832061e+001
5.57812500000000e+001	1.97598759541985e+001
5.67187500000000e+001	1.97717557251908e+001
5.79687500000000e+001	1.97837786259542e+001
5.90625000000000e+001	1.98071803435115e+001
5.98437500000000e+001	1.98189885496183e+001
6.06250000000000e+001	1.98536975190840e+001
6.12500000000000e+001	1.98768845419847e+001
6.21875000000000e+001	1.98887643129771e+001
6.31250000000000e+001	1.99120944656489e+001
6.39062500000000e+001	1.99582538167939e+001
6.46875000000000e+001	1.99929627862595e+001
6.54687500000000e+001	2.00391221374046e+001
6.60937500000000e+001	2.00852099236641e+001
6.65625000000000e+001	2.01197757633588e+001
6.70312500000000e+001	2.01543416030534e+001

Appendix

6.75000000000000e+001	2.01889074427481e+001
6.79687500000000e+001	2.02349236641221e+001
6.85937500000000e+001	2.03153625954198e+001
6.93750000000000e+001	2.03958730916031e+001
7.00000000000000e+001	2.04877624045802e+001
7.04687500000000e+001	2.05566793893130e+001
7.07812500000000e+001	2.06255248091603e+001
7.12500000000000e+001	2.07058921755725e+001
7.15625000000000e+001	2.07976383587786e+001
7.20312500000000e+001	2.08894561068702e+001
7.23437500000000e+001	2.09697519083969e+001
7.26562500000000e+001	2.10500477099237e+001
7.28125000000000e+001	2.11188215648855e+001
7.29687500000000e+001	2.11761450381679e+001
7.34375000000000e+001	2.13023139312977e+001
7.37500000000000e+001	2.13940601145038e+001
7.39062500000000e+001	2.14628339694656e+001
7.42187500000000e+001	2.15431297709924e+001
7.43750000000000e+001	2.16462547709924e+001
7.45312500000000e+001	2.17379293893130e+001
7.50000000000000e+001	2.18297471374046e+001
7.51562500000000e+001	2.18985209923664e+001
7.53125000000000e+001	2.19672948473282e+001
7.54687500000000e+001	2.20475190839695e+001
7.56250000000000e+001	2.21277433206107e+001
7.59375000000000e+001	2.22194895038168e+001
7.60937500000000e+001	2.23111641221374e+001
7.60937500000000e+001	2.23684160305344e+001
7.64062500000000e+001	2.24487118320611e+001
7.67187500000000e+001	2.25290076335878e+001
7.68750000000000e+001	2.26092318702290e+001
7.71875000000000e+001	2.27353291984733e+001
7.75000000000000e+001	2.28270753816794e+001
7.76562500000000e+001	2.29072996183206e+001
7.78125000000000e+001	2.29875238549618e+001
7.82812500000000e+001	2.31022423664122e+001
7.85937500000000e+001	2.32168893129771e+001
7.90625000000000e+001	2.33430582061069e+001
7.92187500000000e+001	2.34003816793893e+001
7.95312500000000e+001	2.35035782442748e+001
8.00000000000000e+001	2.36182967557252e+001
8.03125000000000e+001	2.37329437022901e+001
8.06250000000000e+001	2.38017891221374e+001
8.07812500000000e+001	2.38591125954198e+001
8.12500000000000e+001	2.39509303435115e+001
8.17187500000000e+001	2.40541984732824e+001
8.21875000000000e+001	2.41460162213740e+001

Appendix

8.29687500000000e+001	2.42952290076336e+001
8.34375000000000e+001	2.43641459923664e+001
8.42187500000000e+001	2.44904580152672e+001
8.50000000000000e+001	2.45824188931298e+001
8.56250000000000e+001	2.46514074427481e+001
8.64062500000000e+001	2.47090171755725e+001
8.71875000000000e+001	2.47780772900763e+001
8.79687500000000e+001	2.48127862595420e+001
8.87500000000000e+001	2.48703959923664e+001
8.98437500000000e+001	2.48937977099237e+001
9.07812500000000e+001	2.49171278625954e+001
9.14062500000000e+001	2.49403148854962e+001
9.26562500000000e+001	2.49523377862595e+001
9.35937500000000e+001	2.49527671755725e+001
9.51562500000000e+001	2.49534828244275e+001
9.60937500000000e+001	2.49539122137405e+001
9.73437500000000e+001	2.49430343511450e+001
9.81250000000000e+001	2.49548425572519e+001
9.87500000000000e+001	2.49551288167939e+001
1.00781250000000e+002	2.49560591603053e+001

Oxidation at 750°C

Line #1

1.00691913008790e+000	2.04703632887189e+001
3.16519251138286e+000	2.04703632887189e+001
5.32346589267783e+000	2.04703632887189e+001
7.48173927397279e+000	2.04703632887189e+001
9.20835797900876e+000	2.04703632887189e+001
1.18007620672105e+001	2.04818355640535e+001
1.48223448010234e+001	2.04818355640535e+001
1.74122728585774e+001	2.04818355640535e+001
2.08655102686493e+001	2.04818355640535e+001
2.34554383262033e+001	2.04818355640535e+001
2.60453663837572e+001	2.04818355640535e+001
3.07935678226062e+001	2.04818355640535e+001
3.55417692614551e+001	2.04818355640535e+001
3.98607920546928e+001	2.04933078393881e+001
4.15898867903765e+001	2.05047801147228e+001
4.37481601716715e+001	2.05047801147228e+001
4.59089095836142e+001	2.05162523900574e+001
4.85013136718159e+001	2.05277246653920e+001
5.06620630837586e+001	2.05391969407266e+001
5.28252885263491e+001	2.05621414913958e+001
5.45519072313851e+001	2.05621414913958e+001

Appendix

5.62834779977166e+001	2.05850860420650e+001
5.75858701184368e+001	2.06195028680688e+001
5.93174408847683e+001	2.06424474187381e+001
6.10564397430430e+001	2.06998087954111e+001
6.14955225112453e+001	2.07342256214149e+001
6.28003906626133e+001	2.07801147227533e+001
6.32419494614633e+001	2.08260038240918e+001
6.36785561990178e+001	2.08489483747610e+001
6.41225910285156e+001	2.09063097514340e+001
6.54348872718269e+001	2.09866156787763e+001
6.58764460706769e+001	2.10325047801147e+001
6.67595636683770e+001	2.11242829827916e+001
6.72110265898180e+001	2.12160611854685e+001
6.76575374499635e+001	2.12848948374761e+001
6.80990962488136e+001	2.13307839388145e+001
6.85480831396069e+001	2.14110898661568e+001
6.89896419384569e+001	2.14569789674952e+001
6.90094501836389e+001	2.15487571701721e+001
6.94559610437845e+001	2.16175908221797e+001
6.94708172276710e+001	2.16864244741874e+001
6.99272322104076e+001	2.18011472275335e+001
7.03836471931441e+001	2.19158699808795e+001
7.08276820226419e+001	2.19732313575526e+001
7.08425382065285e+001	2.20420650095602e+001
7.12915250973218e+001	2.21223709369025e+001
7.21696906337263e+001	2.21912045889101e+001
7.21870228482606e+001	2.22715105162524e+001
7.22068310934426e+001	2.23632887189293e+001
7.22192112466814e+001	2.24206500956023e+001
7.26582940148837e+001	2.24550669216061e+001
7.31072809056770e+001	2.25353728489484e+001
7.35636958884135e+001	2.26500956022945e+001
7.35785520723001e+001	2.27189292543021e+001
7.40349670550367e+001	2.28336520076482e+001
7.53720236048255e+001	2.30286806883365e+001
7.58259625569143e+001	2.31319311663480e+001
7.62823775396509e+001	2.32466539196941e+001
7.67338404610919e+001	2.33384321223709e+001
7.76243861507352e+001	2.34646271510516e+001
7.80733730415285e+001	2.35449330783939e+001
7.89589666698763e+001	2.36481835564054e+001
7.94054775300219e+001	2.37170172084130e+001
8.02935471890174e+001	2.38317399617591e+001
8.11865689093085e+001	2.39694072657744e+001
8.25062932445630e+001	2.40841300191205e+001
8.29627082272996e+001	2.41988527724665e+001
8.47140872388132e+001	2.43135755258126e+001

Appendix

8.55897767445699e+001	2.43709369024857e+001
8.64704183116222e+001	2.44512428298279e+001
8.73510598786745e+001	2.45315487571702e+001
8.86608800913380e+001	2.46003824091778e+001
8.95390456277425e+001	2.46692160611855e+001
9.04147351334993e+001	2.47265774378585e+001
9.25903407293286e+001	2.48068833652008e+001
9.43367676795466e+001	2.48986615678776e+001
9.60782425684691e+001	2.49674952198853e+001
9.78221934880394e+001	2.50478011472275e+001
9.99953230532209e+001	2.51166347992352e+001
1.01731845880848e+002	2.51625239005736e+001
1.04770760829195e+002	2.52428298279159e+001
1.07804723716247e+002	2.53001912045889e+001
1.10841162633946e+002	2.53690248565966e+001
1.13880077582294e+002	2.54493307839388e+001
1.17340743084309e+002	2.54837476099426e+001
1.20803884616972e+002	2.55296367112811e+001
1.24698680825894e+002	2.55755258126195e+001
1.29888441063593e+002	2.56214149139579e+001
1.33778285211219e+002	2.56443594646272e+001
1.37238950713234e+002	2.56787762906310e+001
1.41128794860861e+002	2.57017208413002e+001
1.45450293684746e+002	2.57246653919694e+001
1.50637577891797e+002	2.57590822179732e+001
1.54959076715683e+002	2.57820267686424e+001
1.58846444832662e+002	2.57934990439771e+001
1.63597122302158e+002	2.58049713193117e+001
1.69645239831080e+002	2.58279158699809e+001
1.76988321388778e+002	2.58508604206501e+001
1.82170653534534e+002	2.58623326959847e+001
1.89077128354678e+002	2.58623326959847e+001
1.95986079205469e+002	2.58738049713193e+001
2.01165935320577e+002	2.58738049713193e+001
2.07645707525758e+002	2.58967495219885e+001
2.12823087610218e+002	2.58852772466539e+001
2.20595347813527e+002	2.58967495219885e+001
2.27070167957412e+002	2.58967495219885e+001
2.31818369396261e+002	2.58967495219885e+001
2.36998225511369e+002	2.58967495219885e+001
2.48223723124751e+002	2.59082217973231e+001
2.51245305858564e+002	2.59082217973231e+001

Oxidation at 800°C

Line #1

9.21601953763139e-001	2.04316265408162e+001
-----------------------	-----------------------

Appendix

3.07915710961865e+000	2.04307189650336e+001
5.66822329664527e+000	2.04296298740945e+001
8.26636524149766e+000	2.04400092407716e+001
1.04239203973532e+001	2.04391016649890e+001
1.25905513110345e+001	2.04496625468227e+001
1.51796174980611e+001	2.04485734558836e+001
1.77686836850877e+001	2.04474843649445e+001
2.12207719344565e+001	2.04460322436923e+001
2.51134469728222e+001	2.04558670648999e+001
2.89970462533622e+001	2.04542334284913e+001
3.07230903780466e+001	2.04535073678652e+001
3.28806455339021e+001	2.04525997920826e+001
3.54697117209287e+001	2.04515107011435e+001
3.80678536657811e+001	2.04618900678207e+001
4.02254088216366e+001	2.04609824920381e+001
4.28235507664890e+001	2.04713618587152e+001
4.49901816801703e+001	2.04819227405488e+001
4.80289104140196e+001	2.05035890496856e+001
5.10585633900431e+001	2.05137869012063e+001
5.32342700615501e+001	2.05358162406561e+001
5.58505635220541e+001	2.05691325225656e+001
5.80353459513869e+001	2.06026303196317e+001
6.02292041385456e+001	2.06475965743140e+001
6.15781917790135e+001	2.07158627745417e+001
6.29090279038300e+001	2.07611920595370e+001
6.42670913021237e+001	2.08409267173809e+001
6.51845679114206e+001	2.09093744327651e+001
6.61111202785433e+001	2.09892906057656e+001
6.65880100988433e+001	2.10464513786901e+001
6.70830514347948e+001	2.11265490668471e+001
6.80368310753948e+001	2.12408706126962e+001
6.85227966535206e+001	2.13094998432369e+001
6.90269137472979e+001	2.14010659890101e+001
6.95310308410752e+001	2.14926321347833e+001
7.00351479348526e+001	2.15841982805564e+001
6.96671672084619e+001	2.16646589990264e+001
7.05846438177588e+001	2.17331067144107e+001
7.06572498803650e+001	2.18248543753403e+001
7.11432154584908e+001	2.18934836058811e+001
7.16654840679197e+001	2.20079866668867e+001
7.21786769195228e+001	2.21110212702761e+001
7.22603587399548e+001	2.22142373888220e+001
7.23329648025610e+001	2.23059850497517e+001
7.28643091698157e+001	2.24319565683735e+001
7.29187637167703e+001	2.25007673140707e+001
7.29732182637250e+001	2.25695780597680e+001
7.34954868731539e+001	2.26840811207736e+001

Appendix

7.35590171779344e+001	2.27643603240871e+001
7.40812857873632e+001	2.28788633850927e+001
7.37223808187984e+001	2.29707925611789e+001
7.42355736704015e+001	2.30738271645682e+001
7.47578422798304e+001	2.31883302255738e+001
7.48304483424366e+001	2.32800778865035e+001
7.53708684675170e+001	2.34175178627415e+001
7.54888533192522e+001	2.35666078117523e+001
7.60383492021584e+001	2.37155162456065e+001
7.61291067804162e+001	2.38302008217686e+001
7.66604511476708e+001	2.39561723403904e+001
7.71917955149255e+001	2.40821438590122e+001
7.77503671556575e+001	2.42425207504827e+001
7.82726357650864e+001	2.43570238114883e+001
7.88039801323411e+001	2.44829953301101e+001
7.93534760152473e+001	2.46319037639643e+001
8.02981798980215e+001	2.47347568521972e+001
8.12882625699246e+001	2.48949522285111e+001
8.17923796637019e+001	2.49865183742843e+001
8.31595188198214e+001	2.50777214897444e+001
8.41132984604214e+001	2.51920430355935e+001
8.54713618587152e+001	2.52717776934374e+001
8.63888384680121e+001	2.53402254088216e+001
8.81874886553027e+001	2.54312470091253e+001
8.95183247801191e+001	2.54765762941206e+001
9.17484859985809e+001	2.55674163792677e+001
9.39423441857395e+001	2.56123826339499e+001
9.65767891618950e+001	2.56686358310919e+001
9.92021583802247e+001	2.57134205706176e+001
1.04866256332404e+002	2.57798716192802e+001
1.09217669675418e+002	2.58239302981799e+001
1.13964291018300e+002	2.58219336314582e+001
1.16993943994324e+002	2.58321314829788e+001
1.20464183759344e+002	2.58536162769591e+001
1.23493836735367e+002	2.58638141284797e+001
1.26514413953565e+002	2.58625435223841e+001
1.29544066929589e+002	2.58727413739047e+001
1.32573719905612e+002	2.58829392254253e+001
1.36888830217323e+002	2.58811240738602e+001
1.39909407435521e+002	2.58798534677646e+001
1.43361495684890e+002	2.58784013465124e+001
1.47254170723255e+002	2.58882361677200e+001
1.51146845761621e+002	2.58980709889276e+001
1.54167422979819e+002	2.58968003828320e+001
1.58060098018185e+002	2.59066352040395e+001
1.60640088447385e+002	2.58940776554842e+001
1.63660665665583e+002	2.58928070493886e+001

Appendix

1.67112753914952e+002	2.58913549281365e+001
1.70564842164321e+002	2.58899028068844e+001
1.73585419382518e+002	2.58886322007888e+001
1.77037507631887e+002	2.58871800795366e+001
1.79635649576740e+002	2.58975594462138e+001
1.83519248857280e+002	2.58959258098051e+001
1.87402848137819e+002	2.58942921733965e+001
1.90854936387188e+002	2.58928400521444e+001
1.94738535667728e+002	2.58912064157357e+001
1.99916668041781e+002	2.58890282338575e+001
2.03800267322321e+002	2.58873945974489e+001
2.07270507087342e+002	2.59088793914292e+001
2.11576541641227e+002	2.58955957822478e+001
2.15891651952938e+002	2.58937806306827e+001
2.19343740202307e+002	2.58923285094305e+001
2.22364317420505e+002	2.58910579033349e+001
2.25816405669873e+002	2.58896057820828e+001
2.31426049075098e+002	2.58872460850481e+001
2.35741159386809e+002	2.58854309334829e+001
2.39202323394003e+002	2.58954472698470e+001
2.43948944736886e+002	2.58934506031254e+001
2.49127077110939e+002	2.58912724212472e+001
2.53442187422650e+002	2.58894572696820e+001
2.56031253609676e+002	2.58883681787429e+001

Oxidation at 850°C

Line #1

7.06106081276613e-001	2.02562652445326e+001
3.29571292736368e+000	2.02571582124106e+001
5.44958452189011e+000	2.02693951796271e+001
7.60759022696267e+000	2.02701393195254e+001
1.06287982140642e+001	2.02711811153830e+001
1.45090743726487e+001	2.02840133945182e+001
1.75302823597503e+001	2.02850551903758e+001
2.05514903468519e+001	2.02860969862334e+001
2.35726983339535e+001	2.02871387820910e+001
2.74571086030840e+001	2.02884782339080e+001
3.17731200132292e+001	2.02899665137046e+001
3.52217950307991e+001	2.03026499648601e+001
3.78114018768862e+001	2.03035429327380e+001
4.08284757534416e+001	2.03160775559138e+001
4.38455496299971e+001	2.03286121790897e+001
4.55678200835090e+001	2.03407003183265e+001
4.85848939600645e+001	2.03532349415023e+001
5.07387655545909e+001	2.03654719087188e+001
5.33242382901319e+001	2.03778577039150e+001

Appendix

5.46107734920832e+001	2.04012898424904e+001
5.63289098350490e+001	2.04248708090454e+001
5.84745132084832e+001	2.04600934308983e+001
6.10434495018397e+001	2.05184505353673e+001
6.23217164826987e+001	2.05648683285791e+001
6.35999834635578e+001	2.06112861217909e+001
6.48741163338708e+001	2.06691967423209e+001
6.57166480631692e+001	2.07269585348712e+001
6.65509115713754e+001	2.08077059820580e+001
6.69618421596594e+001	2.08653189466286e+001
6.78002397784117e+001	2.09345735664972e+001
6.86262350655256e+001	2.10383066683203e+001
6.94563644631858e+001	2.11305469428253e+001
6.98631609409236e+001	2.11996527347141e+001
7.02658233081153e+001	2.12802513539212e+001
7.06726197858531e+001	2.13493571458101e+001
7.10752821530448e+001	2.14299557650172e+001
7.14738104096904e+001	2.15220472115424e+001
7.18764727768821e+001	2.16026458307495e+001
7.22708669229815e+001	2.17062301045930e+001
7.22377940386126e+001	2.17981727231386e+001
7.30596552151805e+001	2.19133986522800e+001
7.34540493612799e+001	2.20169829261234e+001
7.34251105874571e+001	2.20974327173509e+001
7.33961718136343e+001	2.21778825085783e+001
7.37947000702799e+001	2.22699739551036e+001
7.41890942163793e+001	2.23735582289470e+001
7.45876224730249e+001	2.24656496754723e+001
7.49737483980322e+001	2.25922196039522e+001
7.53640084335855e+001	2.27072967051139e+001
7.53268014386705e+001	2.28107321509777e+001
7.61445285046922e+001	2.29374509074373e+001
7.60742486254082e+001	2.31328289718467e+001
7.64727768820538e+001	2.32249204183720e+001
7.72781016164372e+001	2.33861176567861e+001
7.76683616519906e+001	2.35011947579478e+001
7.76228864359833e+001	2.36276158584481e+001
7.80131464715367e+001	2.37426929596097e+001
7.84116747281822e+001	2.38347844061350e+001
7.87853983215511e+001	2.39958328165695e+001
7.96031253875729e+001	2.41225515730291e+001
7.99851172020340e+001	2.42606143288272e+001
8.07904419364174e+001	2.44218115672413e+001
8.11517631981479e+001	2.46173384596304e+001
8.19694902641697e+001	2.47440572160900e+001
8.27830832196453e+001	2.48822687998677e+001
8.36090785067593e+001	2.49860019016909e+001

Appendix

8.44392079044194e+001	2.50782421761958e+001
8.56802678903634e+001	2.52280954152714e+001
8.73777336805986e+001	2.53091405184175e+001
8.90710653602877e+001	2.54016784488817e+001
9.03451982306007e+001	2.54595890694117e+001
9.20550663524743e+001	2.55061556906032e+001
9.41924015048162e+001	2.55643639670925e+001
9.59105378477821e+001	2.55879449336475e+001
9.80602753317624e+001	2.56116747281822e+001
1.01932283269255e+002	2.56474926619538e+001
1.06671627599322e+002	2.56721154243664e+001
1.10120302616892e+002	2.56847988755219e+001
1.14867915168052e+002	2.56864359832982e+001
1.17889123155153e+002	2.56874777791558e+001
1.22632601595767e+002	2.57006077142503e+001
1.27380214146926e+002	2.57022448220265e+001
1.31696225557071e+002	2.57037331018231e+001
1.36875439249246e+002	2.57055190375791e+001
1.42486254082434e+002	2.57074538013146e+001
1.48097068915623e+002	2.57093885650502e+001
1.54139484889826e+002	2.57114721567655e+001
1.61045103146058e+002	2.57138534044400e+001
1.67087519120261e+002	2.57159369961553e+001
1.73561536235479e+002	2.57181694158502e+001
1.80035553350697e+002	2.57204018355451e+001
1.86513704576460e+002	2.57111414279218e+001
1.90398114845591e+002	2.57124808797387e+001
1.95577328537765e+002	2.57142668154946e+001
2.01619744511968e+002	2.57163504072099e+001
2.08956963909215e+002	2.57188804828641e+001
2.15862582165447e+002	2.57212617305387e+001
2.18887924263095e+002	2.57108106990781e+001
2.22340733391211e+002	2.57120013229154e+001
2.29246351647443e+002	2.57143825705899e+001
2.34425565339617e+002	2.57161685063459e+001
2.39608913142337e+002	2.57064616147836e+001
2.43920790441936e+002	2.57194427218984e+001
2.48240935962628e+002	2.57094381743768e+001
2.56872958782918e+002	2.57124147339700e+001
2.60325767911034e+002	2.57136053578073e+001
2.62052172475092e+002	2.57142006697259e+001

Oxidation at 900°C

1.10E-01	7.29E+01
4.15E+00	7.28E+01
7.60E+00	7.29E+01

Appendix

1.31E+01	7.29E+01
1.88E+01	7.28E+01
2.26E+01	7.29E+01
2.59E+01	7.30E+01
2.89E+01	7.31E+01
3.04E+01	7.33E+01
3.20E+01	7.36E+01
3.31E+01	7.39E+01
3.39E+01	7.42E+01
3.43E+01	7.44E+01
3.51E+01	7.48E+01
3.54E+01	7.52E+01
3.58E+01	7.57E+01
3.61E+01	7.60E+01
3.65E+01	7.64E+01
3.66E+01	7.69E+01
3.69E+01	7.73E+01
3.74E+01	7.79E+01
3.77E+01	7.85E+01
3.77E+01	7.90E+01
3.80E+01	7.95E+01
3.85E+01	8.01E+01
3.88E+01	8.08E+01
3.90E+01	8.13E+01
3.93E+01	8.17E+01
3.93E+01	8.22E+01
3.96E+01	8.26E+01
3.98E+01	8.30E+01
4.01E+01	8.36E+01
4.04E+01	8.40E+01
4.06E+01	8.47E+01
4.09E+01	8.52E+01
4.17E+01	8.61E+01

Oxidation at 950°C

Line #1

9.95807214636512e-001	7.81555220456423e+001
2.79342462669644e+000	7.81503576199281e+001
4.44124058775137e+000	7.81456235630234e+001
6.68826235282628e+000	7.81391680308806e+001
8.48587976488621e+000	7.81340036051664e+001
8.93582924959937e+000	7.81507237913862e+001
1.04338435097661e+001	7.81464105720324e+001
1.17820563439162e+001	7.81425286746141e+001
1.40290777341663e+001	7.81360588455834e+001
1.55270919943331e+001	7.81317456262297e+001
1.71749076805165e+001	7.81270010849406e+001

Appendix

1.86729219406833e+001	7.81226878655868e+001
2.07724644076457e+001	7.82052362482954e+001
2.42178972060292e+001	7.81953158437818e+001
2.67656826996772e+001	7.82322768157824e+001
2.79640941078106e+001	7.82288262402994e+001
2.91648280186729e+001	7.83139625546203e+001
3.06663260329331e+001	7.84425296699724e+001
3.20191838725410e+001	7.86158215521617e+001
3.29214761827345e+001	7.87461139552553e+001
3.44287804538170e+001	7.90961482951171e+001
3.50361149174350e+001	7.94044771216892e+001
3.59465359871798e+001	7.98448236390963e+001
3.62554288501289e+001	8.01983085544411e+001
3.67187681445526e+001	8.07285359274583e+001
3.70264997561372e+001	8.10377273979011e+001
3.73353926190863e+001	8.13912123132459e+001
3.77987319135100e+001	8.19214396862631e+001
3.82609099565692e+001	8.24073736143783e+001
3.85721253222473e+001	8.28494454195269e+001
3.88856631906542e+001	8.33801041144795e+001
3.90435933762222e+001	8.36897269068577e+001
3.93548087419003e+001	8.41317987120063e+001
3.96660241075783e+001	8.45738705171550e+001
4.01340084074599e+001	8.52812716697799e+001
4.04498687785958e+001	8.59005172545363e+001
4.06147664723506e+001	8.64759007163262e+001
4.12371972037067e+001	8.73600443266235e+001
4.14009336460970e+001	8.78911343435114e+001
4.14137074111062e+001	8.83783622374328e+001
4.20268481315466e+001	8.89081582885146e+001
4.20384606451913e+001	8.93510927375340e+001
4.24994774368860e+001	8.97927332207473e+001
4.29663004854031e+001	9.04558409284702e+001
4.32798383538101e+001	9.09864996234228e+001
4.35910537194881e+001	9.14285714285714e+001
4.37559514132429e+001	9.20039548903613e+001
4.40752955384723e+001	9.27560808098235e+001
4.45374735815315e+001	9.32420147379387e+001
4.51506143019718e+001	9.37718107890205e+001
4.56174373504889e+001	9.44349184967435e+001
4.59309752188959e+001	9.49655771916961e+001
4.60981954153796e+001	9.56295475432898e+001
4.71677079220568e+001	9.64238102979771e+001
4.76310472164805e+001	9.69540376709943e+001
4.83916668602086e+001	9.73948155103368e+001
4.86970759690643e+001	9.76154200909757e+001
4.91557702580301e+001	9.79684736843851e+001

4.94611793668858e+001	9.81890782650241e+001
4.99163899017581e+001	9.84092515237277e+001
5.05214018626472e+001	9.86289934604959e+001
5.09766123975196e+001	9.88491667191995e+001
5.14283391782985e+001	9.89364596431972e+001
5.21808300624753e+001	9.90671833682262e+001
5.27800357665420e+001	9.90654580804847e+001
5.36811668253710e+001	9.91514570386763e+001
5.44301739554544e+001	9.91493004289994e+001
5.65273939196879e+001	9.91432619219042e+001
5.77269665791857e+001	9.91841047913231e+001
6.17716050816360e+001	9.91724590990680e+001
6.34194207678194e+001	9.91677145577789e+001
6.47676336019695e+001	9.91638326603605e+001
6.70146549922196e+001	9.91573628313299e+001
6.92605151311053e+001	9.91065995573973e+001
7.04600877906032e+001	9.91474424268163e+001
7.15086977727199e+001	9.91444231732687e+001
7.42051234410200e+001	9.91366593784319e+001
7.67517476833035e+001	9.91293269055305e+001
7.98975776296537e+001	9.91202691448877e+001
8.34928118540539e+001	9.91099174184387e+001
8.81389785632998e+001	9.91851333282459e+001
9.32322270478668e+001	9.91704683824432e+001
9.92242840885338e+001	9.91532155050282e+001
1.05965348259284e+002	9.91338060179364e+001
1.14651508465522e+002	9.90202024558807e+001
1.23943841884014e+002	9.91706342754953e+001
1.32332721740948e+002	9.91464802471143e+001
1.34579743131198e+002	9.91400104180837e+001

Oxidation at 1000°C

Line #1

1.10318879624684e-001	7.29491139652089e+001
4.15263487934598e+000	7.28488813831499e+001
7.60039018045846e+000	7.29275478684402e+001
1.31430429430755e+001	7.29115889568313e+001
1.88331746289802e+001	7.28066118334832e+001
2.25816940334905e+001	7.29287091198047e+001
2.58796479085863e+001	7.30078069270303e+001
2.88791601830132e+001	7.31320608230286e+001
3.03818194486379e+001	7.33049213832826e+001
3.20366026430081e+001	7.35659375114052e+001
3.30933413846761e+001	7.38729723721711e+001

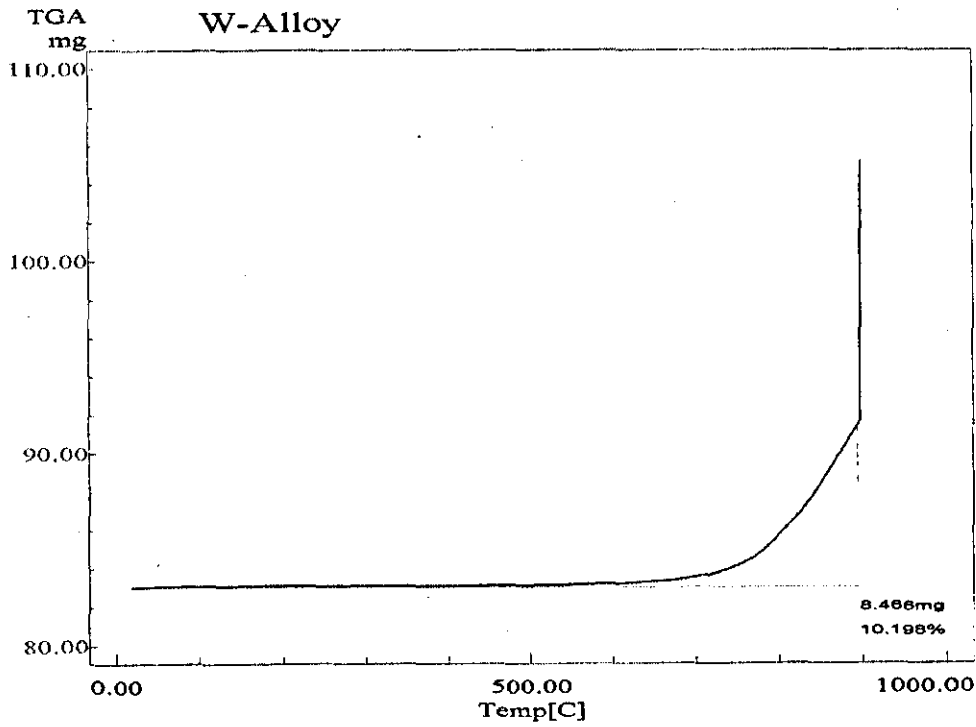
Appendix

3.38504772743108e+001	7.41808698768078e+001
3.43068490605476e+001	7.44453365804133e+001
3.50663074529113e+001	7.48418209748539e+001
3.53752003158604e+001	7.51953058901987e+001
3.58385396102840e+001	7.57255332632159e+001
3.61451099705042e+001	7.59904312887568e+001
3.64563253361823e+001	7.64325030939054e+001
3.66177392758436e+001	7.68750062209894e+001
3.69289546415217e+001	7.73170780261381e+001
3.73946164386743e+001	7.79358922889592e+001
3.77093155584458e+001	7.85108444288136e+001
3.77209280720905e+001	7.89537788778330e+001
3.80356271918619e+001	7.95287310176875e+001
3.85012889890146e+001	8.01475452805086e+001
3.88183106115150e+001	8.08110843101669e+001
3.89797245511763e+001	8.12535874372510e+001
3.92921011682189e+001	8.17399526873016e+001
3.93037136818636e+001	8.21828871363210e+001
3.96137677961772e+001	8.25806654965677e+001
3.97751817358385e+001	8.30231686236517e+001
4.00898808556100e+001	8.35981207635062e+001
4.04010962212881e+001	8.40401925686548e+001
4.05683164177718e+001	8.47041629202486e+001
4.08818542861788e+001	8.52348216152011e+001
4.16540864435516e+001	8.61185339035630e+001
4.19687855633230e+001	8.66934860434175e+001
4.24332861091112e+001	8.72680068613366e+001
4.27491464802471e+001	8.78872524460931e+001
4.32101632719418e+001	8.83288929293063e+001
4.36723413150010e+001	8.88148268574216e+001
4.42912882922637e+001	8.95660901330130e+001
4.47523050839585e+001	9.00077306162263e+001
4.52156443783821e+001	9.05379579892435e+001
4.58276238474580e+001	9.10234605954233e+001
4.62909631418817e+001	9.15536879684405e+001
4.70539052883387e+001	9.20830526975869e+001
4.73593143971944e+001	9.23036572782259e+001
4.81141277841001e+001	9.25229678930587e+001
4.93183454490559e+001	9.27409845420854e+001
5.00685138305037e+001	9.27831213773105e+001
5.11194463153494e+001	9.28686890135667e+001
5.27695845042618e+001	9.29525313620815e+001
5.45683628678264e+001	9.29916489437589e+001
5.57690967786887e+001	9.30767852580798e+001
5.68177067608054e+001	9.30737660045322e+001
5.83157210209722e+001	9.30694527851784e+001
5.95141324291056e+001	9.30660022096955e+001

Appendix

6.08623452632557e+001	9.30621203122771e+001
6.38583737835892e+001	9.30534938735696e+001
6.65547994518894e+001	9.30457300787328e+001
6.91014236941728e+001	9.30383976058315e+001
7.22472536405230e+001	9.30293398451886e+001
7.58424878649232e+001	9.30189881187396e+001
7.97373249413568e+001	9.30077737484199e+001
8.37819634438070e+001	9.29961280561648e+001
8.82760062243073e+001	9.29831883981035e+001
9.23206447267576e+001	9.29715427058484e+001
9.69644889332745e+001	9.29581717258518e+001
9.99605174536080e+001	9.29495452871443e+001

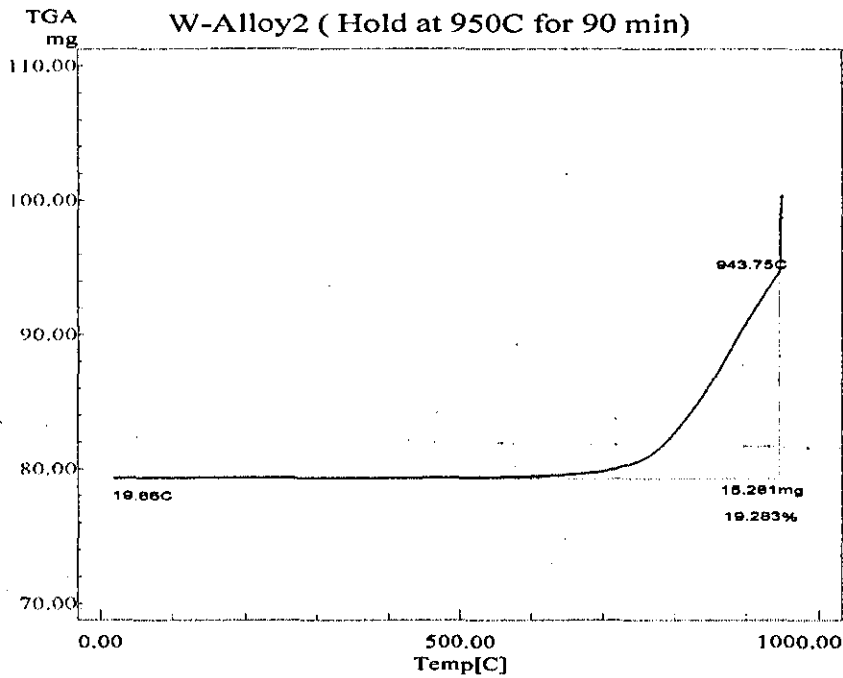
Oxidation at 900°C Weight Vs Temperature



File Name: W-ALLOY.D00
Detector Type: Shimadzu TGA-50H
Sample Name: Tungsten Alloy
Weight: 83.02[mg]
Cell: Platinum
Atmosphere: Air
Rate Flow: 40.00[ml/min]

JOB NO.
Central Analytical Lab.
Physical Chemistry

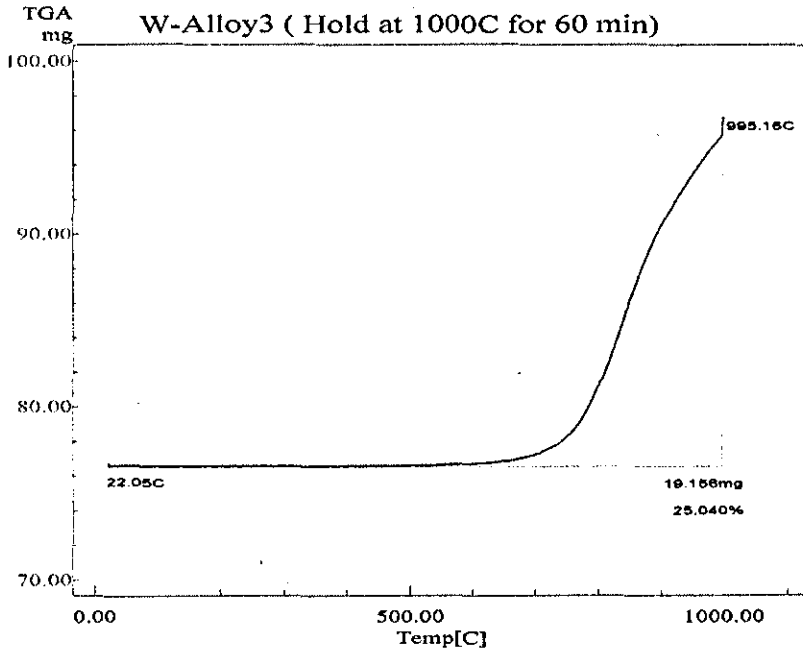
Oxidation at 950°C Weight Vs Temperature



File Name: W-ALLOY2.D00
 Detector Type: Shimadzu TGA-50H
 Sample Name: Tungsten Alloy(Hold for:1:30hr
 Weight: 79.25[mg]
 Cell: Platinum
 Atmosphere: Air
 Rate Flow: 40.00[ml/min]

JOB NO.
 Central Analytical Lab.
 Physical Chemistry

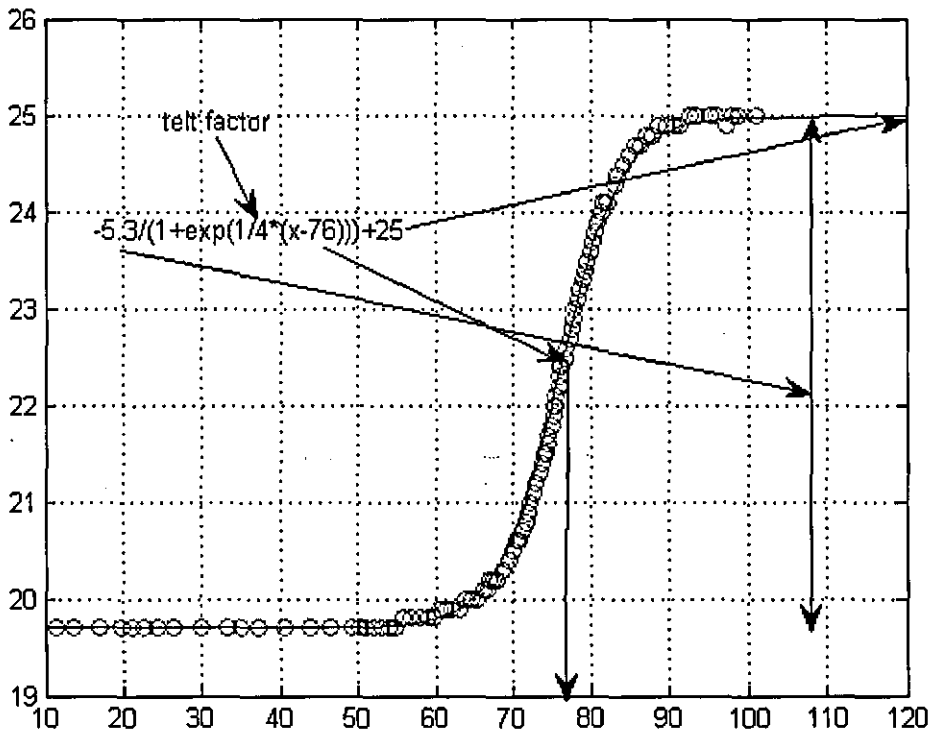
Oxidation at 1000°C Weight Vs Temperature



File Name: W-ALLOY3.D00
 Detector Type: Shimadzu TGA-50H
 Sample Name: Tungsten alloy(hold at1000C)
 Weight: 76.50[mg]
 Cell: Platinum
 Atmosphere: Air
 Rate Flow: 40.00[ml/min]

JOB NO.
 Central Analytical Lab.
 Physical Chemistry

Correlation curve equation



Oxidation curve 3 in 1

